UNIVERSITÀ DEGLI STUDI DI PISA

Master of Science dissertation in

Conservation and Evolution

Using the biomechanical characteristics of the Humerus to infer the subsistence economy of the Middle Bronze Age population from Olmo di Nogara (Verona, Italy)

Supervisors:
Prof. Damiano Marchi
Prof. Alessandro Canci

Candidate:
Giulia Medaglini

Assistant Supervisors:
Dr. Sergio Tofanelli
Dr. Marta Colombo

Academic year 2015/2016

Index

1. Introduction

1.1 Overview

The concept that bone form reflects its mechanical loading history during life is fundamental to the study of skeletal material (Evans, 1953; Fresia et al., 1990; Lieberman et al, 2004; Marchi, 2004). Particularly, it has been shown that upper limbs are variably employed during manipulation. Some of the physical activities performed by an individual are expected to affect both arms equally (e.g., maize pounding, digging) while other produce a pronounced unilateral mechanical loading (e.g. hunting) (Sladek, 2007). A consistent number of studies in the past thirty years have demonstrated that the study of diaphyseal geometric properties of long bones (cross-sectional geometry, CSG) constitutes one of the best ways to reconstruct behavioral patterns, social stratification and subsistence economy of human past populations (Ibanez-Gimeno et al., 2013; Lovejoy et al., 1976; Marchi, 2007; Marchi and Sparacello, 2006; Marchi et al., 2006, 2011; Ogilvie et al., 2011; Porcic et al., 2009; Ruff and Hayes, 1983; Ruff et al., 2006; Sparacello, 2005; Sparacello and Marchi, 2008; Sparacello et al., 2011, 2014; Stock, 2006; Stock et al., 2011; Weiss, 2009). In past populations, the more physically demanding habitual activities were generally those linked to subsistence strategies. Results of these researches suggest that changes in subsistence technology and behavior eventually led to bone remodeling to adapt to the changes in physical demands to which the skeleton was subjected (Sparacello and Marchi, 2008). Given that each temporal age was characterized by a specific economic and social situation, differences among the historical periods can be highlighted through the comparison of the CSG properties. Moreover, even internal differences of a single population can be highlighted, as they are reflected in the variation of skeletal characteristics such as the degree of robusticity, the sexual dimorphism, or the bilateral asymmetry.

In addition to the CSG properties, another humerus-specific characteristic – the humeral torsion - has been proved to be useful in the process of inferring human behavior (Rhodes, 2004, 2006; Rhodes and Churchill, 2009; Rhodes and Knusel, 2005). The humeral torsion is a measure of the degree of torsion of the humerus. Previously, it has been considered a static, phylogenetic trait that varies slightly between sexes, sides, and populations (Rhodes and Churchill, 2009). While recently, it has been shown to vary with limb function among hominoids, having mainly to do with keeping elbow flexion in a parasagittal plane (Larson, 1988). Particularly, in humans, recent studies demonstrated how the degree of humeral torsion is related with the presence in a sample of repeated throwing movements (e.g., hunting, professional baseball players, pitchers) or with a regular use of the sword during life (Rhodes, 2004, 2006; Rhodes and Churchill, 2009; Rhodes and Knusel, 2005). Moreover, humeral torsion has shown to be also influenced by the overall manipulative activity (Rhodes and Knusel, 2005), thus representing another fundamental variable to account in the process of reconstructing behavioral and activity patterns in human past populations.

In this work the CSG approach and the study of the humeral torsion have been used together to try to describe the behavioral background and subsistence economy of a Middle Bronze Age population from the Olmo di Nogara (OdN) necropolis (Verona, Italy). During the course of the Bronze Age a number of important changes took place and lend the period its characteristic appearance which distinguished it from anything that had gone before (Coles and Harding, 1979). In

particular, those changes affected both the subsistence economy and the social stratification, leading to the:

a. predominance of a subsistence economy based primarily on agriculture and pastoralism;
b. first appearance of social stratifications;
c. increase of gender perception.

The demographic expansion that characterized the European Bronze Age (Peroni, 1979) led to a rapid increase in food production that could only be faced by an intensive development of agriculture. Moreover, the increased production and improved quality of metal objects - especially those connected with extensive deforestation (e.g. axes, chisels and saws) - in addition to the rise of stable and densely populated settlements and to the general move away from grazing land to areas more suited to seed-crops, are evidence of a clear tendency towards intensive and sedentary agriculture (Peroni, 1979).

This transition from the hunter-gatherer economy of the Palaeolithic to the agriculture and pastoralism typical of the Bronze Age resulted in important modifications in the pattern of activities performed by men and women (Berelov, 2005; Gilman, 1981; Kristiansen, 2014; Macintosh et al., 2014; Peroni, 1979). This is particularly exemplified by an increase of bimanual activities performed (e.g. wheat grind, ploughing) with respect to unimanual ones (e.g. hunting) as well as by the introduction of domesticated animals - both for sustenance and work force, as in the horse case (Mercuri, 2006; Levine, 1999; Gilman, 1981).

Of all the changes that occurred during the Bronze Age in Europe, perhaps the most obvious was the rise of the privileged (Coles and Harding, 1979). The

stratification of societies in Bronze Age has been taken for granted since over a century ago (Coles and Harding, 1979; Peroni 1979). The burials - which represent the majority of the evidence - leave no doubt that some sort of *élites* emerged in the social fabric (Gilman, 1981; Pulcini, 2014). Moreover, a consistent number of studies (Gilman, 1981; Pulcini, 2014; Shennan 1975) suggested that these *élites* were in fact hereditary and represented the first step toward the more complex social stratifications that characterized the Iron Age. The rise of social stratifications led in turn to the beginning of a differentiation in everyday works and activities performed by individuals belonging to different social groups (Gilman, 1981; Peroni, 1979). Particularly, for men the processes of increasing social complexity were connected with the emergence and institutionalizing of violence and warfare, thus during this period the warrior as a new social character is thought to have appeared (Aranda-Jiménez, 2009). Clearly, a higher involvement in warlike activities as well as a use of proper weapons has a different impact on the general behavior and on the pattern of movements on the individuals belonging to the *élite* (Aranda-Jiménez, 2009; Kristiansen, 2002). However, it should be also noted that the Bronze Age is a period of changes that occurred at different times in different geographical areas, therefore each population must be considered separately.

It has been argued that in the Central Europe the intensification of economy resulted not only in changes of subsistence economy but also in changes of gender relations (Shennan, 1993). Some authors also mentioned that the transition from the Palaeolithic to the Bronze Age that led to the increase in gender perception, was more a continuous process than a drastic shift (Sladek, 2007). Nonetheless, independently from the nature of the transition the result was the same as the Bronze Age society saw the increase in the differentiation of works between sexes. A recent

study of Sladek (2007) on manipulative behavior, considered the differences between females and males as evidence of gender-specific activities. According to the author's results males might have been associated with extra-domestic agricultural labor - that resulted in asymmetrical manipulative loading - and females with domestic labor - with symmetrical manipulative loading.

Given the amount of changes that characterized the Bronze Age in Europe and the repercussions they had on the behavior of individuals, the general assumption of the present work is that they should be visible in the morphology and shape of the upper limbs. Therefore, the use of the CSG approach could be of extreme usefulness both in outlining the social and economic background of the population in exam and in corroborating results of previous palaeobiological analysis (Pulcini, 2014, Salzani, 2005).

The choice of the humerus as the object of this study is due to the great amount of information that can be extrapolated from the analysis of this bone. Many researchers in recent years have shown how the morphology of the humerus is strictly related to the behaviour and the social organisation of a population, as well as to the subsistence economy (Ibanez-Gimeno, 2013; Marchi and Sparacello, 2006; Marchi et al., 2006; Ogilvie, 2011; Sladek, 2007; Sparacello et al., 2011; Trinkaus, 1980). Particularly, importance of the humerus resides in two peculiar characteristics that differentiates it from the bones of the lower limb. Not only is the humerus largely free from weight bearing activities – since it belongs to the upper limb – but also it can widely be employed both unimanually and bimanually in a wide variety of ways (Macintosh, 2014). Moreover, a significant amount of studies has shown the existence of a correlation between the degree of humeral torsion and the amount of repeated throwing-like movements performed by an individual during life (Osbahr,

2002; Pieper, 1998; Reagan, 2002; Rhodes, 2004, 2006; Rhodes and Knusel, 2005). This freedom from constrictions and versatility are what makes the morphology of the humerus so strictly correlated to the behaviour and pattern of activities performed by an individual, making it the most informative bone in the process of inferring social organization and subsistence economy of a population (Ibanez-Gimeno, 2013; Macintosh, 2014; Marchi and Sparacello, 2006; Ogilvie, 2011; Sladek, 2007).

However, interpreting morphology in the context of cultural change in the past could be challenging. A single dominant activity has the potential to obscure the presence of multiple less-dominant behaviours. Moreover, the habitual performance of multiple less-dominant behaviours, without a dominant one can also drive bone morphological change (Macintosh, 2014). That is the reason why each biomechanical analysis needs to be supported by an as much as possible accurate knowledge of the archaeological background against which results can be confronted/corroborated.

1.2 Archaeological background

The Olmo di Nogara necropolis – dated to the Middle Bronze Age and the first phase of the Late Bronze Age (~1700 BC – ~1350 BC) – is located in the western plain of Veneto, a few hundred meters from the city of Nogara and around 30 km south from Verona (Fig. 1.1). The first tombs were accidentally discovered in 1936-1937, during the implantation of a vineyard nearby Corte Serraglio. However, the whole complex became object of systematic studies only in 1987 when it was brought back to the attention of the scientific community thanks to a series of excavations done by the *Soprintendenza per i Beni Archeologici del Veneto* under the

direction of the doctor Luciano Salzani. Researches then proceeded seamlessly until 1997, with only two additional interventions in 2002 and in 2009.

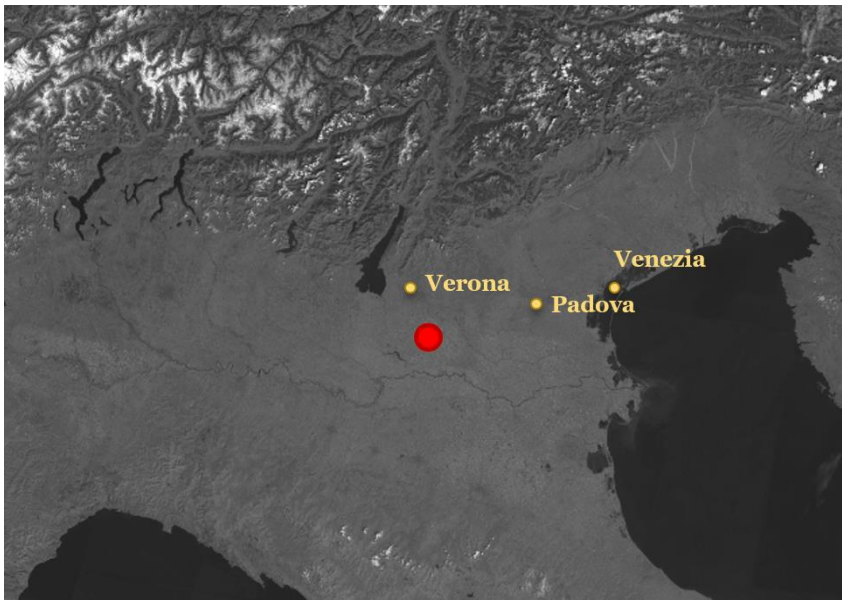

Fig. 1.1 - Geographical location of the Olmo di Nogara Necropolis (image modified from Salzani, 2005).

The whole complex of the necropolis is located on the right bank of the Tartaro palaeochannel and is divided into six areas (from A to F, Fig. 1.2). The palaeochannel of the river is a small valley with a width of 380 meters and a depth of 4 meters from the banks. Outcomes of the excavations revealed signs of a frequentation of the area prior and after the foundation of the necropolis, both for residential and funerary use. Proved frequentations date back to the Neolithic, the Copper Age, the Roman era and the Medieval Age, as well as of course the Bronze Age (Pulcini, 2014; Salzani, 2005).

The Bronze Age necropolis is composed by three big nuclei corresponding with the areas A, B and C. These nuclei are located beside a 400 meters sepulchral road and are aligned on a NW-SE direction. All individuals that are comprised in the

sample here studied are from these three different areas: 3 from the A area, 24 from the B area and 13 from the C area (see Table 1.1 for details).

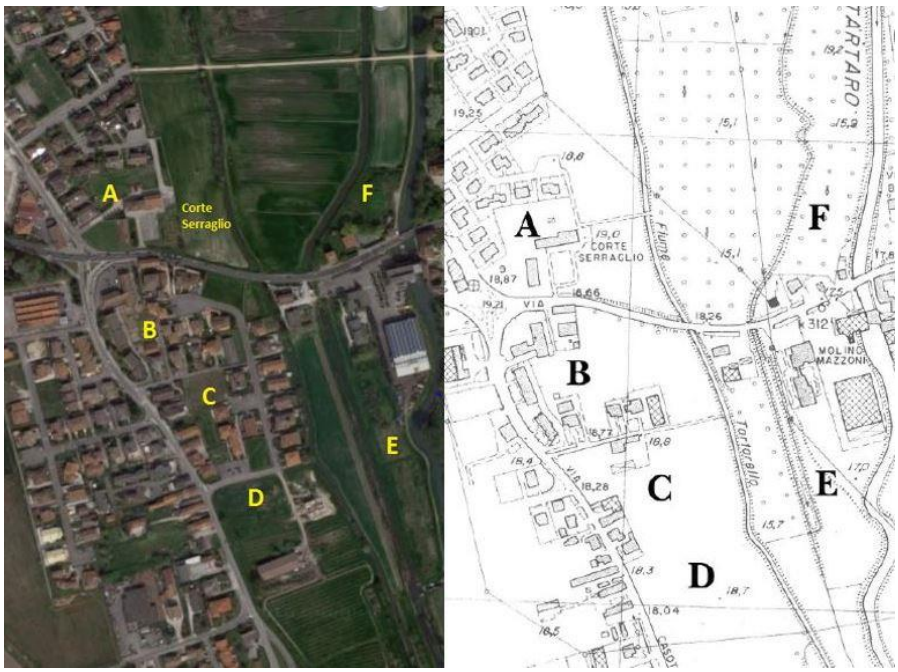

Fig. 1.2 - Satellite view and planimetry of the Olmo di Nogara necropolis complex. The six areas are indicated with letters from A to F. Corte Serraglio represents the location of the first finding of the tombs (satellite view modified from Google maps; planimetry modified from Pulcini, 2014).

- The area A has undergone a series of agricultural interventions, root canal treatments and previous archaeological excavations that damaged it, therefore is considered incomplete. It is composed of 33 burial tombs, 9 of which are completely disarranged.
- The B area, on the contrary, is more studied. It is composed of 123 tombs, 108 of which are burial tombs while the other 15 are incineration tombs.
- The C area is the most studied of the three as well as the amplest - with an extension of 6.240 square meters - and is composed of two groups of tombs located at N and S respectively. Signs of agricultural interventions from the medieval and the modern era can be found in all the area. Furthermore, in the 80s the area was leveled leading to the destruction of some infant tombs and

incineration tombs – generally located nearer the surface. However, this still remains the richest area in terms of archaeological material - with a totality of 377 tombs, 318 of which are burial tombs while 47 are incineration tombs.

To sum up, the whole Bronze Age Necropolis is composed of 471 burial tombs and 62 incineration tombs, for a totality of 533 individuals (Pulcini, 2014; Salzani, 2005).

Of all the 471 burial tombs - either females, males or infants - 34% is characterized by the presence of grave goods (Pulcini, 2014). For males, grave goods mainly consist of weaponry and generally comprise a sword positioned either on the shoulder/arm or on the body. In addition, other offensive and defensive weapons can be found (e.g. daggers or studs from a helmet). The study of musculoskeletal stress markers (MSM) and CSG properties of the upper limb on a sample of armed males from the necropolis highlighted the possibility of a common use of shields in battle (Riga, 2008). However, no sign of shield were found in the tombs.

Table 1.1 - Additional information on area and grave goods for each individual of the sample analyzed in this study.

ID	Area	Sex[1]	Age[2]	Grave goods
1	**A**	M	30-40	absent
8	**A**	M	40-50	absent
16	**A**	F	55-65	present
25	**C**	M	45-55	present
28	**C**	M	35-45	present
43	**C**	M	35-45	absent
87	**C**	M	35-45	present
89	**C**	F	40-50	present
94	**C**	F	35-45	present
98	**C**	F	20-25	absent
99	**C**	M	30-40	present
109	**C**	M	40-50	absent
110	**C**	F	30-40	present
148	**C**	M	45-55	absent
159	**C**	F	40-50	absent
189	**C**	F	50-60	absent
202	**C**	M	30-35	present
223	**C**	F	20-25	absent
225	**C**	F	20-25	absent
244	**C**	F	25-30	present
287	**C**	F	35-45	present
295	**C**	F	45-55	present

297	**C**	F	50-60	present
301	**C**	F	35-45	absent
316	**C**	F	50-60	present
321	**C**	F	35-45	absent
360	**C**	F	45-55	absent
391	**B**	M	30-40	present
411	**B**	F	50-60	present
413	**B**	M	20-25	absent
417	**B**	M	40-50	present
418	**B**	M	40-50	absent
421	**B**	M	30-35	absent
439	**B**	F	50-60	absent
475	**B**	M	35-45	present
476	**B**	M	>55	absent
479	**B**	M	18-21	absent
484	**B**	M	40-50	present
486	**B**	M	35-45	present
500	**B**	M	35-45	present

[1] Estimated sex (after Pulcini, 2014): M = male, F = female.
[2] Estimated age at death. After Pulcini (2014).

On the other hand, female grave goods mainly comprise one or two bronze cloak pins – which become three in the richer tombs. Other ornamental objects – both in amber and bronze – can also be present (e.g. necklaces and bracelets) (Pulcini, 2014). For the specific grave goods and details on the burial of every individual of the sample in exam see Appendix I.

The concentration of male and female tombs with grave goods in some areas of the Necropolis suggests a sort of social stratification, characterized by the presence of an *élite* of males and females. This hypothesis is furthermore supported by the discovery of an individual (OdN 410) with a much reduced ability to use his arms due to a possible lesion of the brachial plexus but buried with a sword, therefore unable to use it during war (Pulcini, 2014). In this case the presence of weaponry in grave goods can only be attributed to a social status instead of an effective participation in warlike activities. Moreover, in at least one case two armed males from spatially close tombs show the presence of the hidden cleft spine, a skeletal

alteration with a certain degree of heredity that suggests the presence of possible relations between the members of the *élite* (Canci et al. in Salzani, 2005).

However, despite the appearances, the *élite* of warriors doesn't seem to be the only one involved in battles. Pulcini's analysis of inflicted traumas on males revealed the use of improper or casual weapons during warlike activities (Fig. 1.3), thus suggesting the involvement of unspecialized warriors – presumably those buried without grave goods - in addition to the warrior *élite*. Such evidence leads to the hypothesis of a uniform pattern of stresses for the entire male population of the Necropolis without regard for social differences. Moreover, observing injuries and fractures allowed to highlight the presence of a somewhat ample medical activity in the population, suggesting that individuals in need were taken care of by the community (Pulcini, 2014).

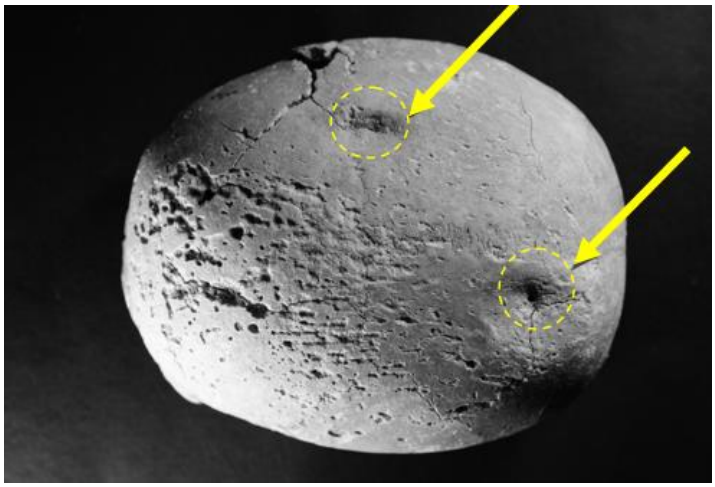

Fig. 1.3 - Superior view of the skull of the individual OdN 95 showing elliptic injuries, probably inflicted by an improper weapon (modified from Pulcini, 2014).

It should be also noted that the analysis of inflicted traumas revealed the presence of 13 injuries caused by weapons – however, they do not include all the superficial injuries that were not deep enough to reach the bone, thus are not visible

on it. Of the 13 traumas, eight have been found on armed males and five on unarmed males (Pulcini, 2014). In particular, three injuries are located on the skulls of two individuals and have been presumably inflicted with a downward movement - indicating a higher position of the opponent - whereas two of the injuries are located on the left ulna and femoral diaphysis of another individual and have been inflicted with an upward movement - indicating a higher position of the warrior compared to the opponent (Fig. 1.4). As suggested by Pulcini (2014), the injuries inflicted from above could provide evidence of the use of horses during battles thus supporting the

Fig. 1.4 - Lateral view of the distal epiphysis of the left femur with a cutting wound (photograph modified from Pulcini, 2014).

hypothesis of the presence of a horse-riding activity in the population. Further support to this hypothesis is found in the results of the study of occupational stress markers of the lower libs. In particular, for the femurs a wide distribution of all the skeletal alterations that can be related to the so-called “horseman syndrome” is observed in males. In fact, a higher use of the pelvis, tight and calf muscles could be

related to the necessity of balancing on a horse without a saddle (Pulcini, 2014). However, contrary to the expectations, a quite high percentage of stress markers related to horse-riding activity was found even in females thus suggesting a use of the horse not only for military purpose but also for other working activities. As for health, results of Pulcini (2014) and Salzani (2005) analysis showed a quite good health status for the whole population, with evidences of the same diet and the same work involvement for all the individuals, independently of their social position.

Interestingly, with regard to the activities pattern, outcomes of the palaeopathological analysis are of extreme usefulness. Not only a similar amount of stressful activities is suggested for all the individuals of the population but also no substantial differences were found between males and females. Particularly, useful information was obtained from the study of the skeletal column (Pulcini, 2014; Salzani, 2005). In addition to the great amount of osteoarthritis' signs located on the vertebral columns of the observable adults, 12 cases of spondylolysis were found on a sample of 169 adults, 11 of which are females and represent the 13,7% of the observable females. The spondylolysis is a serious fracture of the *pars interarticularis* (a portion of the lumbar spine) due to a great amount of biomechanical stresses (Fig. 1.5). This fracture is a skeletal indicator of reiterated and strenuous actions at the expense of the vertebral column and is generally caused by recurring combinations of flexions, extensions and rotations of the column. Some working activities connected with these movements are: habitual carriage of heavy objects and prolonged works performed standing with curved back and extended legs, just like all the activities related to arduous domestic works (Pulcini, 2014).

The significant predominance of spondylolysis in females compared to males strongly contrasts with the traditional archaeological descriptions which report a

higher involvement of males in arduous works - sometimes even double compared to females. Therefore, for the OdN sample sexual division of work has been hypothesized in which females were involved in highly laborious domestic activities. Coherently with the palaeobiological analysis, the presence of spondylolysis has been observed in females both with and without grave goods, suggesting a similar pattern of activities not correlated with the social status.

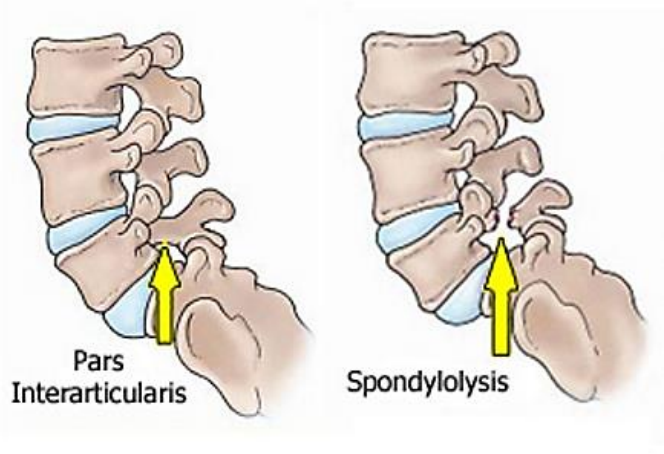

Fig 1.5 - Illustration of a vertebral column with (right) and without (left) the fracture of the pars interarticularis (image modified by http://orthoinfo.aaos.org/topic.cfm?topic=a00053).

1.3 Beam Theory

Biomechanics is the discipline that applies mechanical principles to biological systems such as, in this case, the skeleton. Much of the development of skeletal biomechanics was carried out by anatomists and orthopedists in the 1800s and early 1900s (Evans, 1953). However, soon anthropologists became interested in the biomechanical interpretation of bone form. Most of the early works on the subject focused on the interpretation of the functional significance of the orientation of the trabeculae (von Meyer, 1867; Roux, 1885, in Evans, 1953) while only more recently stresses (forces applied to the bone) and strains (deformations due to the forces

applied) have also been studied (Evans, 1953). One of the first works on the functional significance of the orientation of trabeculae was the one of Julius Wolff. His work is currently known as "Wolff's law" and, to say it with Wolff's words: "is the law according to which alterations of the internal architecture clearly observed and following mathematical rules, as well as secondary alterations of the external form of the bone following the same mathematical rules, occur as a consequence of primary changes in the shape […] of the bone" (Wolff, 1986; quote in Ruff et al., 2006). In the past, the term "Wolff's law" was widely used in relation with the phenomenon of bone adaptation to mechanical loadings, however more recently many authors started to question at least portions of the law (Bertram and Swartz, 1991; Demes et al., 1998; Lovejoy et al., 2003). The main critique was at Wolff's mathematical handling of bone remodeling, as it included both engineering and biological misconceptions (Ruff et al., 2006). One of the premises of the law that have been considered false is Wolff's model of bone as a homogeneous, solid and isotropic structure subjected to static applied loads, which is instead incorrect (Cowin, 2001, Ruff et al., 2006). The main characteristic of the bone, in fact, is its biphasic nature. Bony tissue is composed by minerals (calcium and phosphate) and collagen, a peculiar composition that gives it both strength and elasticity. It should be noted, however, that none of the critiques to the Wolff's law was meant to deny the importance of mechanical loading in the development of bone form (Cowin, 2001). The general concept that bone adapts to its mechanical environment during life, thus differences in morphology can be used to investigate differences in past mechanical enviroments, is still accepted among bioarchaeologists and anthropologists (Ruff et al., 2006). Nonetheless, recent authors suggested to discard the term "Wolff's law" in favour of a more appropriate and less confusing term, *bone functional adaptation*

(Roux, 1881; as referenced in Ruff et al., 2006). In Fig. 1.6 a schematic diagram of the modern concept of *bone functional adaptation* is represented. The bone modelling and remodelling stimulus is based on strain - the actual physical deformation of the bone tissue - and acts through a series of feedback loops. Increased strain (e.g. through an increase in activity level) leads to deposition of more bone tissue, which then reduces strain to its original "optimum customary level". On the other hand, decreased strain (e.g. through inactivity) leads to resorption of bone tissue, which again restores the original strain levels (Ruff et al., 2006). It is generally acknowledged by authors the existence of the "customary" strain level window, above which bone deposition is stimulated and below which resorption is stimulated. However, this "customary strain level", to which bone tissue is adapted, is apparently not constant but varies by skeletal location (Ruff et al., 2006).

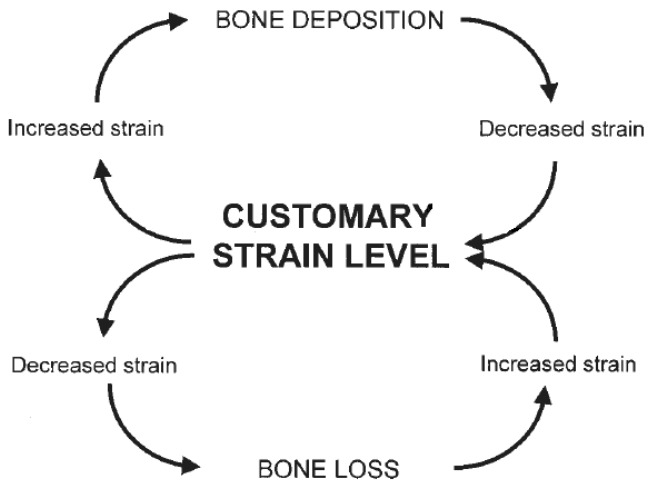

Fig. 1.6 - Feedback model of bone functional adaptation (image modified from Lanyon, 1982; in Ruff, 2006).

The high adaptability of bone – due to its biphasic nature - makes it capable to respond to mechanical loadings deposing bone tissue on the direction in which is

most needed to provide the necessary resistance. The modern and widely accepted *bone functional adaptation* has its roots in the *Beam Theory*, an engineering theory which is, in turn, the natural extension of the *Saint Venant's principle* for hollow beams. In the engineering field, a beam is defined as a structural element with fairly straight long axes whose length is several times greater than their width and depth (Lieberman et al., 2004). According to the *Saint Venant's principle* the beam model can be applied to every elastic object as long as it has a shape that is similar to a hollow beam and the sections are taken not too near the beam ends (Nunziante et al., 2011). Thanks to their elongated shape, long bones are typically considered as hollow cylindrical beams which can be subjected to different kind of forces applied to their ends. More in detail, the different loadings to which every beam can be subjected are: compression, tension, bending, shear or torsion (see Fig. 1.7). However, what characterizes the bone is that during life it does not experience a single loading at a time but a combination of the above mentioned ones. Particularly, when a bone is subjected to mechanical loadings the forces applied to it are equally applied in each one of its cross sections. The *cross-sectional geometric* (CSG) analysis (or *Beam Theory* analysis) mainly pivots on this assumption. A common goal of all osteological studies is to reduce the complex morphology of bones to quantifiable and interpretable variables (Ruff, 1992). To do so, CSG analysis is very useful in that directly relates form and function of skeletal elements in a readily interpretable way.

In the CSG analysis, cross sections are taken perpendicular to the long axis of the long bone and certain geometric properties are determined from the amount and distribution of material (i.e. bone tissue) in the section. These properties are direct measures of the mechanical characteristics of the bone at that section – that is, they

reflect how strong the bone is at that location for resisting mechanical forces placed upon it (for a detailed explanation of the geometric properties studied see paragraph 2.2.4). These loadings are due to the action of gravity and muscles on the bone and can vary owing to a number of factors (e.g. body mass, habitual postures and activity types and levels) (Ruff, 1992).

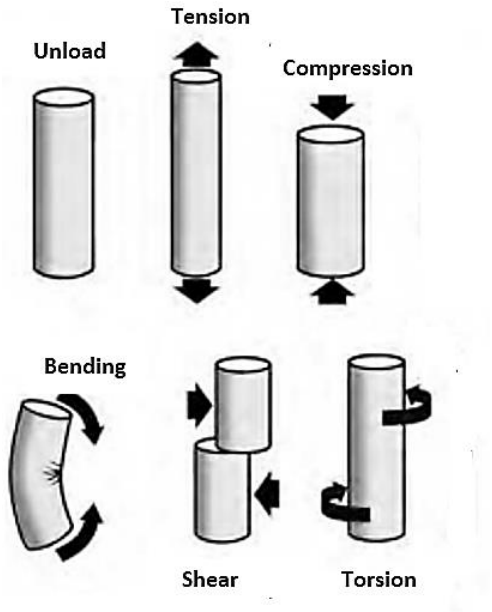

Fig. 1.7 – Different types of mechanical loadings that a beam can be subjected to (image modified from Bankoff, 2007).

1.3.1 Humeral torsion

Humeral torsion can be defined as a difference in the relative position of the long axes of the proximal and distal ends of the bone (Krahl, 1947; in Rhodes and Churchill, 2009). In other words, it is a measurement of humeral architecture that describes the angle formed between the proximal and distal articular surfaces (Rhodes, 2006) (for further explanation on how the angle is determined see paragraph 2.2.5). Historically, the degree of humeral torsion was considered to

distinguish between late archaic and early modern humans, while now it is viewed as an adaptive change rather than a taxonomic variation (Rhodes, 2006).

Based on the orientation of the humeral head in quadrupeds and non-human primates, humeral retroversion is seen to be the primitive condition in primates - in which the humeral head faces posteriorly -, while humans exhibit increased torsion, resulting in a more medially placed humeral head. Since the degree of torsion can be quantified in different ways a terminology explanation is fundamental. An increased torsion (= decreased retroversion) refers to changes in the orientation of the humeral head such that it faces more medially, while a decreased humeral torsion (= increased retroversion) involves a more posterior orientation of the humeral head.

Although body shape and overall activity have been shown to contribute to variation in humeral torsion (Churchill, 1994, 1996; Larson, 2007), there is also strong evidence that regular throwing – or more in general a movement of the limb that keeps the elbow on a para-sagittal plane - results in greater retroversion of the humerus of the throwing limb. A consistent number of studies have documented a significant bilateral asymmetry in both professional handball players (Pieper, 1998) and professional and college-level baseball players (Reagan et al., 2002). Recently, some studies performed on bioarchaeological material, particularly on warrior samples in which the use of the sword is thought to have influenced the humeral torsion as well as on hunter-gatherer populations (Rhodes, 2006; Rhodes and Churchill, 2009). However, results of these studies are not so consistent with expectations, since humeral torsion is highly influenced by both activities performed prior to skeletal maturity and repeated subsistence related behaviours. Therefore, an archaeological and biomechanical background is fundamental for the interpretation of a humeral torsion data.

1.4 The Humerus

The humerus is the largest bone of the upper limb as well as the only skeletal component of the arm. Together with the forearm - ulna and radius, with which it articulates at the level of the elbow – it forms the upper limb. All the movements that can be performed by the upper limb depend on the articulations and connections of the three bones even though each one of them is a functionally distinct element. In particular, the ulna is hinged tightly to the humerus at the level of the elbow joint to provide strength and stability to the forearm, while the radius pivots against the humerus and ulna to supply hand rotation (Steele, 2012).

Like all the long bones the structure of the humerus is similar to the one of an elongated tube that ends in joint structures and comprises three parts:

a. a proximal epiphysis;

b. a diaphysis – or shaft – the tubular part of the bone;

c. a distal epiphysis.

In the proximal epiphysis we can distinguish some elements that are important both for articulation and muscular insertions (White et al., 2012) (Fig. 1.8):

- the *humeral head* is a hemispherical articulation that faces medially and articulates with the scapula – which in turn forms the pectoral girdle together with the clavicle;
- th*e anatomical neck* is a sort of groove that encircle the humeral head and where the ligaments of the shoulder joint capsule are attached;
- the *lesser* and *greater tubercles* are blunt eminences that provides insertions for the rotator cuff muscles: subscapularis muscle and supraspinatus on the lesser tubercle, infraspinatus and teres major muscles on the greater tubercle. The

rotator cuff muscles aid in medial and lateral rotation of the arm as well as in its adduction and abduction. The two eminences are separated by an *intertubercular groove* which is the sulcus that hosts the bicipital tendon.

Generally, in a bone an area called *surgical neck* can be identified where fractures most often separate an expanded end from the shaft (Steele, 2012). In the humerus this can be found between the humeral head and the diaphysis and is identified as a constriction of the shaft right under the greater and lesser tubercles.

Fig. 1.8 - Anterior (left) and posterior (right) views of a proximal humerus (right side). a. humeral head b. greater tubercle c. lesser tubercle d. intertubercular groove e. anatomical neck f. surgical neck (images modified from White et al., 2012).

Distal to the proximal epiphysis starts the diaphysis. It is a long shaft that connects the two epiphyses and provides robustness and length to the humerus, making it the longest and heaviest upper limb bone (Steele, 2012). Its shape is similar to the one of a cylinder with a round cross section near the proximal end and a somewhat triangular one when approaching the distal end due to the flattening of the epiphysis (Fig. 1.9). Generally, the shaft has a semi-smooth surface and it appears

to be twisted – with a slightly difference among individuals – due to the presence of the deltoid tuberosity, the place of insertion of the deltoid muscle. The tuberosity is recognizable as a rough surface with a shape somewhat similar to a "V" and located on the lateral surface of the shaft (White et al., 2012). Since the deltoid muscle is a major abductor of the arm that plays a big role in its movement it is not unlikely to find the tuberosity to be prominent in those individuals that had a higher usage of the upper limb.

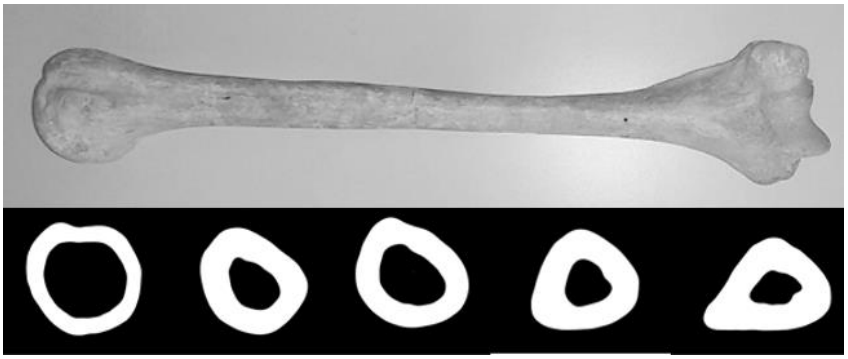

Fig. 1.9 - Changes in the shape of the cross section of a humerus from the proximal epyphisis (on the left) to de distal epiphysis (on the right).

When we move from the shaft to the distal epiphysis the cylindrical form of the bone flattens dorsally. The distal epiphysis is extremely important as it comprises all the elements that articulates with the forearm (Fig.1.10):

- the *lateral* and *medial epicondyles* are non-articular elements, located laterally and medially to the epiphysis, respectively. The *lateral epicondyle* provides attachment for the *radial collateral ligament* of the elbow and for the common tendon of origin of the *supinator* and the *extensor muscles* in the forearm. The *medial epicondyle* provides attachment to the *ulnar collateral ligament*, to many of the *flexor muscles* in the forearm, and to the *pronator teres muscle*;
- the *lateral* and *medial epicondylar ridges* are located above the correspondent epiphysis and form the borders of the distal humerus;

- the *trochlea* is located medially and articulates with the ulna;
- the *capitulum* is the small round-shaped articulation that is located laterally and articulates with the radius;
- the *oleocranon fossa* is the largest among the three hollows of the distal epiphysis, it is posteriorly located and receives the oleocranon process of the ulna when the elbow is extended. Occasionally the *fossa* can be perforated forming a septal aperture;
- the *coronoid* and *radial fossae* are the other two hollows of the distal epiphysis. They are both located in the anterior face of the epiphysis and they receive the coronoid process of the ulna and the radial head, respectively, during maximum flexion of the forearm.

Fig. 1.10 - Anterior (left) and posterior (right) views of the humeral distal epiphysis. a. capitulum b. trochlea c. coronoid fossa d. radial fossa e. lateral epicondyle f. oleocranon fossa g. medial epicondyle (image modified by White et al., 2012).

The humerus develops during uterine life first in cartilage (Steele, 2012). Around the second or third month the primary center of ossification for the diaphysis appears and starts to ossify until birth time, when we find it completely formed. The centers of ossification for both the epiphysis starts to appear between the second week and the twelve year of life. In particular, right after birth three proximal centers are formed – one for the head and two for the tuberosities - while the four distal ones appear lately: one for the capitulum and the lateral part of the trochlea, one for the medial part of the trochlea and two in both the epicondyles (Steele, 2012). Nonetheless, the fusion of the epiphysis is precocious for the distal end while it happens only at the end of the puberty proximally (Platzer, 2007).

In a bioarchaeological context, the level of ossification of the epiphysis could be of great help to determine the age of sub-adult individuals. In this study sub adult individuals were not included (see explanation in paragraph 2.1). However, some young adults with a not-yet-complete fusion of the proximal epiphysis to the diaphysis may be present due to the late fusion of this epiphysis.

1.5 Aims of the study

In this study a biomechanical analysis was conducted on both CSG properties and torsion of the humerus. Variables have been analyzed within the sample in order to corroborate previously obtained palaeobiological hypothesis on the subsistence economy and behavioral pattern of the Olmo di Nogara population (Pulcini, 2014). A diachronic analysis has then been performed for the CSG variables. The aims of this study are:

(1) To demonstrate if there are differences between individuals buried with and without grave goods for both humeral torsion and CSG variables. According to Pulcini (2014), the presence of grave goods in the burials (mainly weaponry for males and ornamental objects for females) should be the index of the belonging to a social *élite*. However, results for the palaeopathological analysis suggests a similar lifestyle for all the individuals, without regard of their social status. If the explanation provided by Pulcini (2014) is correct, we would expect to find no differences in both humeral torsion and CSG variables between individuals buried with and without grave goods;

(2) To corroborate the palaeobiological hypothesis that horses were used by both sexes. Analysis of war injuries and occupational stress markers suggest not only the use of the horse in war but also for other working activities (Pulcini, 2014; Salzani, 2005). Since the act of keeping reins (or the horse main) could be considered a movement that keeps the elbow on a para-sagittal plane, should the palaeobiological hypothesis be true, we would expect to find the same degree of humeral torsion bilateral asymmetry in both males and females;

(3) To test the presence of a correlation between humeral torsion and CSG variables. A previous study on activity-related skeletal changes (Rhodes and Knusel, 2005) suggested the presence of a correlation between humeral torsion and CSG variables. Since humeral torsion other than by the repeated throwing-like movements is affected also by the overall activity - like the CSG variables – some sort of correlation is expected to be present. Moreover, since CSG variables are strictly related one to another, the same correlation would be expected to be found between humeral torsion and each one of them;

(4) To validate the results of the palaeopathological analysis about different activities performed by males and females but similar amount of stresses for both sexes. Skeletal column alterations and pathologies suggest a high involvement of females in stressful activities at a level comparable to that of males (Pulcini, 2014). Should the hypothesis be true, no significant differences in sexual dimorphism for CSG variables are expected to be present for the humerus;

(5) To highlight differences in sexual dimorphism and CSG variables between our sample and the Iron Age comparative samples. The transition towards Iron Age was viewed as a significant shift in social organization associated with an increase in gender perception (Childe, 1930; Gilman, 1981; Sladek et al., 2007). According to this assumption, higher levels of sexual dimorphism are expected to be found in the Iron Age samples. Significant differences in the CSG properties should also be present as a result of the changes in subsistence economy and social stratification.

2. Materials and Methods

2.1 Materials

The total sample analyzed in this study is composed of 40 individuals, 19 females and 21 males – for a total of 80 humeri – all dating back to the Middle Bronze Age (from a non-initial phase of the Middle Bronze Age to the initial phase of the Recent Bronze Age), and coming from the Olmo di Nogara necropolis, Italy (Pulcini, 2014; Salzani, 2005) (Fig. 2.1). Only adult individuals, with completely

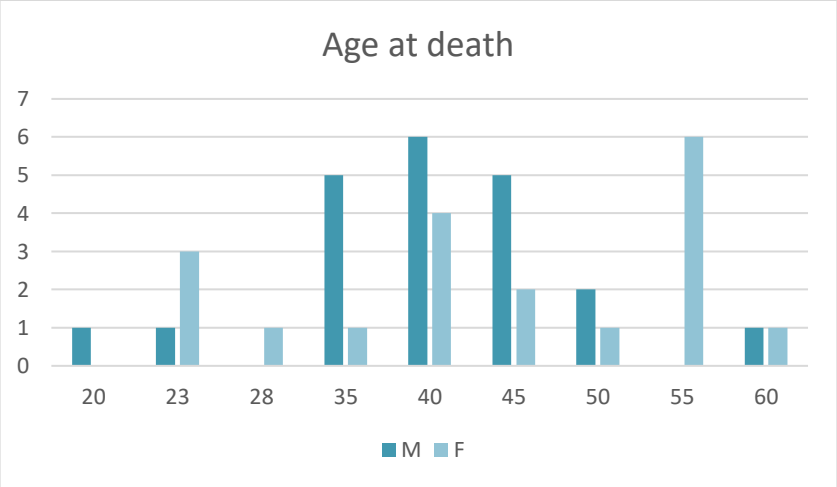

Fig.2.1. - Average distribution of both male and female estimated age at death in the studied sample. Data from Pulcini, 2014.

fused epiphyses, were included in this study (Tab. 2.1) due to the different responses that sub adult bones show when subjected to mechanical loadings (Ruff et al., 1994). During adolescence, periosteal apposition of bone tissue is higher compared to that of adult age. Sub adult individual long bones are more plastic - due to the growth process - resulting in higher remodeling rate than the one showed by an adult bone under the same load environment. Thus sub adults and adult individuals cannot been pooled in the same sample when trying to elucidate subsistence patterns from bone

morphology (Bertram and Swartz, 1991; Ruff, 2000; Ruff et al., 1994; Ruff et al., 2006; Sparacello and Marchi, 2008).

Sex and age used in the present study are from a Ph.D. thesis conducted in the past on the same necropolis (Pulcini, 2014). I referred to Pulcini's work also for other information useful to interpret biomechanical results, such as grave goods, epigenetic traits, bone modification and so on.

The left and right humeri of each individual have been selected to analyze lateralization. Effort have been put toward choosing bones with complete epiphyses, given that they are fundamental in measuring the retroversion angle. Unfortunately, some of them still have damaged epiphysis (Fig. 2.1), thus some measures were not taken. In general, the sample is in a good state of preservation. Only individuals without any sign of serious pathologies (e.g. tuberculosis, osteomas, arthrosis, etc.) or fractures were taken because such changes can lead to modification in the posture of the body and potentially different patterns of stress applied to the limbs that could not be easily interpreted. Furthermore, particular attention has been put in choosing humeri from individuals which presented at least one femoral head intact – a fundamental information in order to calculate the index of body mass thus standardize the data (see paragraph 2.2.6 for further details).

Among the individuals included in the present study, five have minor pathologies (Pulcini, 2014) (Table 2.1). More in detail, two show the presence of the hidden cleft spine, a closure defect of the vertebral spine:

- Individual (Ind.) 475 (Male, 35-45 years old)
- Ind. 16 (Female, 55-65 years old)

However, contrary to the more dangerous form of the pathology – the cleft spine or spondyloschisis –, which damages the spinal cord, the hidden cleft spine does not have any medical relevance. Thus the three pathological individuals were included in the sample.

Other two individuals show the presence of spondylolysis, a stress fracture commonly located at the level of the fifth or fourth lumbar vertebra:

- Ind. 223 (Female, 20-25 years old)
- Ind. 244 (Female, 25-30 years old)

In the total sample of the necropolis a significant number of females show the presence of spondylolysis, thus indicating their involvement in stressful activities (Pulcini, 2014). Finally, one individual shows the presence of sinus infection, Ind. 500 (Male, 35-45). However, no signs of additional periostitis have been found in the rest of the skeleton thus meaning that the infection did not spread.

Table 2.1 - Additional information for each individual of the total sample. L (left), R (right). Grave goods, pathologies and trauma from Pulcini, 2014.

ID	Sex est.	Age est.	Grave goods	Pathologies	Inflicted traumas	Damaged epiphysis
1	M	30-40	absent			
8	M	40-50	absent			
16	F	55-65	present	hidden cleft spine		
25	M	45-55	present			L and R proximal
28	M	35-45	present			R proximal
43	M	35-45	absent			
87	M	35-45	present		vertebra T11	
89	F	40-50	present			
94	F	35-45	present			
98	F	20-25	absent			
99	M	30-40	present			
109	M	40-50	absent			
110	F	30-40	present			
148	M	45-55	absent			
159	F	40-50	absent			
189	F	50-60	absent			R distal
202	M	30-35	present			
223	F	20-25	absent	spondylolysis		L proximal
225	F	20-25	absent			

244	F	25-30	present	spondylolysis		
287	F	35-45	present			
295	F	45-55	present			
297	F	50-60	present			L distal and proximal
301	F	35-45	absent			
316	F	50-60	present			
321	F	35-45	absent			
360	F	45-55	absent			
391	M	30-40	present			L distal and proximal
411	F	50-60	present			
413	M	20-25	absent			
417	M	40-50	present			
418	M	40-50	absent			
421	M	30-35	absent			
439	F	50-60	absent			
475	M	35-45	present	hidden cleft spine	L femur and ulna	
476	M	>55	absent			
479	M	18-21	absent			R proximal
484	M	40-50	present			
486	M	35-45	present			L proximal and distal
500	M	35-45	present	sinus infection		R proximal and distal

2.1.2 Comparative samples

For the aim of this study, four samples from Central Italy – kindly provided by Vitale Stefano Sparacello - have been included in order to perform a diachronic statistical analysis for the variables of CSG (Sparacello, 2004, 2013) (Tab. 2.2). All the four comparative samples belong to the Samnites, a term used by Greek historians to identify numerous Oscan ethno-linguistic groups who migrated into central Italy probably during the Bronze Age (Sparacello, 2013) and inhabited the territory through all the European Iron Age (from 1000 BC to the Roman Conquest, depending on the population in exam).

More specifically, the samples belong to a series of necropoles located within the Abruzzo region and are divided in:

- an Orientalizing-Archaic (O-A) sample (800-500 BC);

- a Hellenistic (HELL) sample (400-27 BC);
- a sample from the 5th century (V SEC);
- an undetermined Iron Age sample (IRON).

For every sample 20 individuals (10 females and 10 males) were randomly chosen in order to have a coherency in the sample size during the statistical analysis (see Table 2.2 for further details).

Table 2.2 - List of comparative sample used in this study.

Group	N	N females	N males	Data source
V SEC	20	10	10	*Sparacello, 2013*
O-A	20	10	10	*Sparacello, 2013*
IRON	20	10	10	*Sparacello, 2013*
HELL	20	10	10	*Sparacello, 2013*

2.2 Methods

The first part of the analysis consisted in the re-attachment of fragments from broken humeri and the measurement of the femoral head breadth with a sliding caliper. Whereas in the second step of the study, which is the most substantial one, medical CT scans of the humeri were performed and analyzed using *Avizo 6.3* (Visualization Sciences Group, Mérignac, France) and *Image J* software (http://rsb.info.nih.gov/ij/).

2.2.1 Computed Tomography

All the humeri included in the study were complete. Some of them were found broken during the excavation and were fixed. However, during the transport from the University of Padua to the University of Pisa some of them happened to lose a correct alignment. Using acetone, the glue was removed and the fragments re-

attached in alignment with a water based glue. The CT scans used in this study were taken at the University Hospital Santa Chiara of Pisa.

The acronym CT stands for *Computed Tomography,* a technique developed in the 1970's (Fig. 2.2). Although CT scan studies have a large number of applications – from the reconstruction of molecular structures to the reconstruction of maps of radio emission from celestial objects – one of the best-known applications is in the field of diagnostic medicine (Herman, 2009). Taking as an example a long bone, what happens during a CT scan is the scanning of the element by an X-ray beam along a large number of lines through the length of the bone. More in detail, a CT scanner is composed by an X-ray source and a group of X-ray detectors opposite to it

Fig. 2.2 - Nov. 9, 2010 photo released by the University of Vermont. A mummy is seen before a CT scan at Fletcher Allen Health Care in Burlington.

and arranged in an arc (Hughes, 2011). When the X-ray beam passes through an object – e.g. patient or archaeological artifact - it loses intensity (attenuation) and this loss is recorded by a detector and then processed by a computer, giving as a result a two-dimensional image on the screen (Natterer, 2001). Every time we deal with a complex object we also need to take into account the differences of density that characterize the various materials of which it is composed. This difference is the basis on which the CT process works: the X-ray beam is differently absorbed by the

object depending on the material that stands between the ray and the detector. In particular, the greater is the density the greater is the attenuation of the X-ray beam (Hughes, 2011). It is possible to see this in the black and white output image: white areas are those in which the attenuation is maximum – and so the density is higher – while darker areas are those in which there is less attenuation due to a minor density of the material. The black areas are therefore the areas where there is no material at all because the X-ray is not attenuated.

Generally, the source of X-ray and the detectors move on a ring so that each detector is in the same position as the source (Fig. 2.3), however this is just the current modern model. In the past, first generation scanners possessed an X-ray source that rotated around a stationary object while the absorption pattern was used to generate a 2D image often printed on a film. This was an extremely long process given the high amount of calculation necessary to reconstruct an image from all these data. With the increasing processing power of computers, the CT technique had undergone important developments. In particular, the use of computers has reduced considerably the waiting time for the process and has allowed a three-dimensional reconstruction, surely more detailed than the two dimensional one.

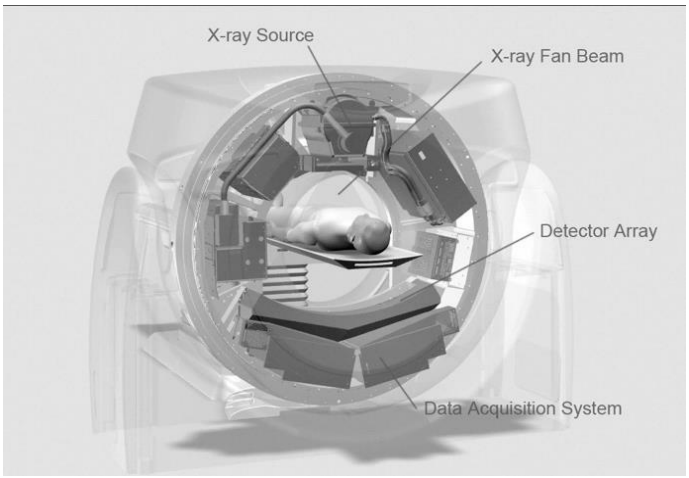

Fig. 2.3 - Structure of a CT scan machine provided by *Analogic.com*

Summarizing, the CT process can be divided in two fundamental phases:

1) the acquisition of raw data from the attenuation of the X-ray source;

2) the reconstruction of a tomographic image through a rendering software.

The second step is the most complex yet easiest for us considering that it is entirely performed by a computer. A specific software can reconstruct a volume by using mathematic algorithms having as a starting point only the pack of raw data from the X-ray scanning - for example, in the present study I have used the program *Avizo.* The whole process can be compared to a piling action of all the single-slice images that come as an output from the scanning in order to obtain a 3D reconstruction of the object. Of course the quality and resolution of the image obtained depends on the raw data, thus on the type of CT scan machine used; the more are the slices obtained during the scanning process the higher the resolution of the 3D reconstruction, as in the case of multi-slice computed tomography (MSCT) in which multiple detectors placed next to each other allow to collect multiple slice data at the same time, resulting in a higher-quality reconstruction.

However, even when using high-resolution machines for CT the image obtained can contain artifacts – e.g. grain on the images or streaks – (Herman, 2009) thus it may require some sort of graphic correction if it then needs to be used for analysis such as cross-sectional geometry (CSG) analysis. Luckily, rendering software generally provide us with tools to overcome these problems.

2.2.2 *Avizo Analysis*

The computer-based analysis of this study pivots on the use of a specific 3D modeling software that allows us to work on a 3D image of our bones acquired from a CT scan. As previously mentioned, in this study the *Avizo 6.3* software was used.

Avizo is a 2D and 3D analysis software for scientific and industrial data distributed by the FEI Visualization Sciences Group, Mérignac, France. It allows the user to explore materials structures and properties through both simple functions - like visualization and measurement - and more complicated ones such as image processing, quantification, analysis and reporting.

The first step in the computer analysis is to provide the software with the necessary data to reconstruct the bone. A CT scan output is composed of a series of files with a "dicom" format, each one of them representing a slice of the image acquired. By dragging them to the pool, Avizo is able to read the complete volume of the data and reconstruct a 3D rendering of our bone (Fig. 2.4). Once the volume of the bone is uploaded in Avizo and a 3D rendering created, it is possible to perform many actions on it: zoom, rotation on single axis, measure of lengths or angles, change of color and so on.

In this study, three fundamental steps compose the general protocol applied for every bone:

1) segmentation;

2) positioning;

3) determination of cross sections.

1) As previously pointed out, even with high definition CT scans the possibility to have artifacts in reconstructed images is concrete. Moreover, ancient bones can be filled with sand or dirt and the software is not able to discriminate between different

materials with only slight different densities. During the segmentation, the operator manually gives a value to every pixel of an image so that pixels with the same value share certain characteristics. In other words, we label the shades of gray of the image as white or black, were white means material (in our case bone) and black absence of material (in our case air). We lose information, but we gain in clarity of representation.

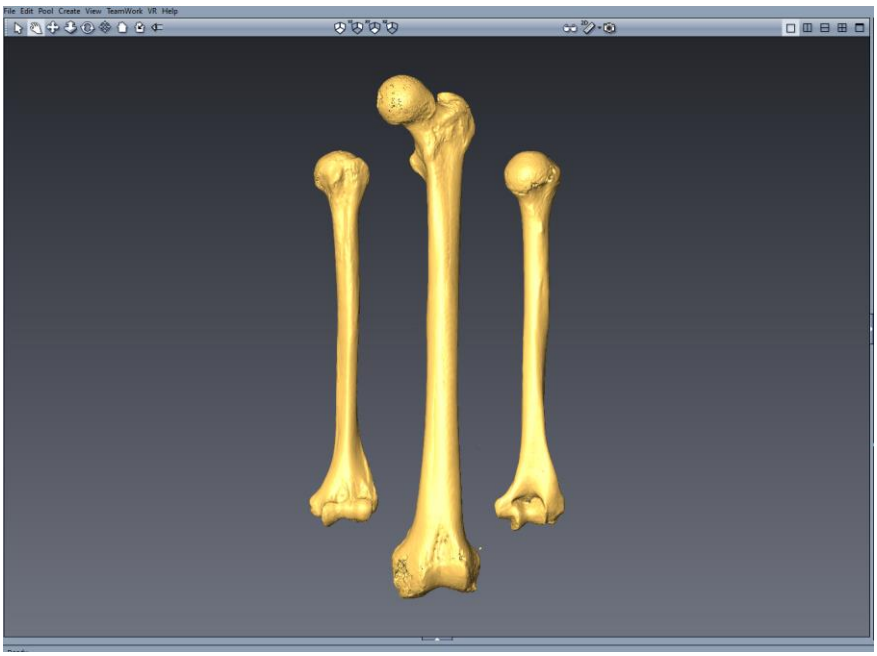

Fig. 2.4 - Example of a 3D rendering of two humeri (left and right) and one femur (center) performed by the Avizo 6.3 software.

To do so we use the "Labelling" function: first we determine a threshold – on the basis of one selected pixel – on which the software automatically perform an initial differentiation. Then with the aid of a graphic tablet we manually delete all that is not bone tissue along all the three axes and in all the slices (Fig. 2.5). The result of this process should be a reconstructed 3D image of the bone as similar as possible to the original.

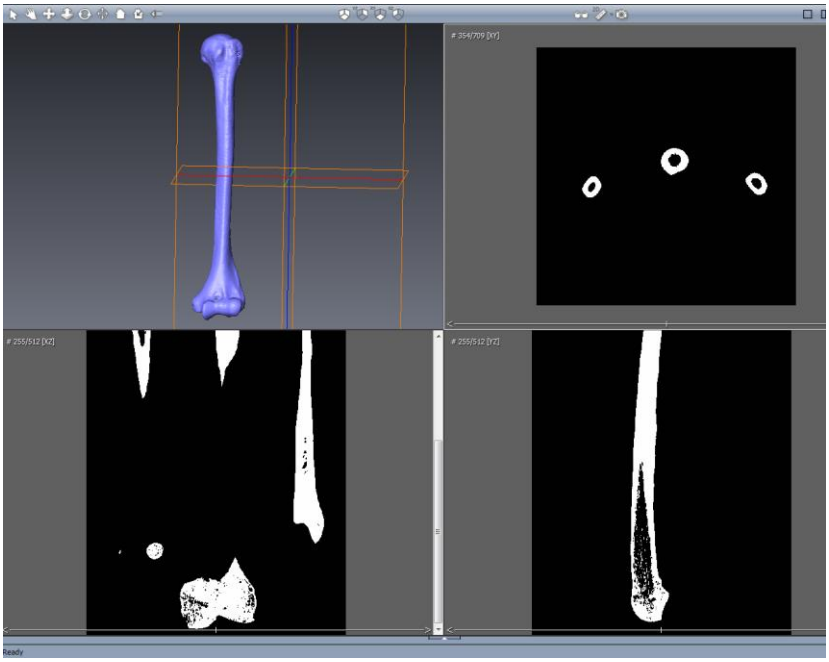

Fig.2.5 - Example of the view along the three axis on which the segmentation needs to be performed. (Image obtained on Avizo 6.3)

2) Once a bone is reconstructed its extension changes into “stl” which is a smaller and easier file format to manage. On this file we proceed with the positioning of the bone in the so-called “anatomical position”. Anatomical position refers to the position that a bone has in the body of a standing human body with palms facing forwards. Because of the sensitivity of many cross sectional properties to bone positioning error, it is vital in this kind of analysis to define bone reference axes as precisely and consistently as possible. In this study, indications given by Ruff (2002) for bone positioning were used to position the bone with respect to standardized global axes. More specifically, in a positioned humerus the coronal plane is parallel to the M–L axis through the centers of the trochlea and capitulum and contains the A–P midpoints of the diaphysis just proximal to the olecranon fossa and just distal to the humeral head (i.e., the surgical neck). While the sagittal plane is taken perpendicular to this through the M–L midpoint of the proximal shaft and the lateral lip of the trochlea. Since cross-sectional images are obtained in the transverse plane of each bone, i.e., perpendicular to both coronal and sagittal planes, it is evident why

the positioning step has such an importance in the whole analysis. In the Avizo software each humerus had to be positioned in all the three geometrical planes (XY, XZ, YZ) (Figs 2.6, 2.7).

- XY plane: the line that joins the midpoints of the two maximum diameters of the distal articulations (capitulum and trochlea) is positioned parallel to the horizontal plane.
- XZ plane: the line that joins the midpoint of the shaft – just under the surgical neck – and the external part of the trochlea is positioned perpendicular to the horizontal plane.
- YZ plane: the line that joins the two midpoints of the shaft – just under the surgical neck and just above the epicondylar ridge – is positioned perpendicular to the horizontal plane.

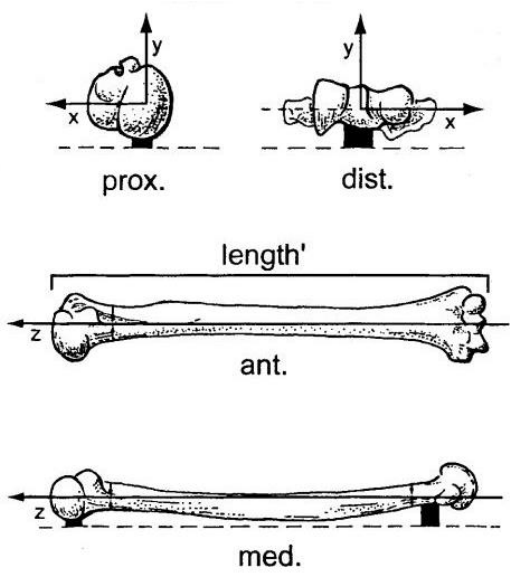

Fig.2.6 - Anatomically positioned humerus according to Ruff (image modified after Ruff, 2002)

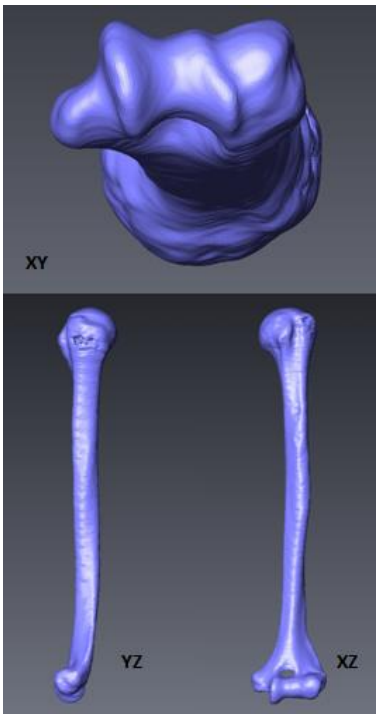

Fig.2.7 - An example of a positioned humerus in the three planes on Avizo 6.3 program.

Once a humerus is positioned its file is saved in “stl” extension. This step is advisable to have a more easy-to-process file that can be used for future elaboration without the need to re-open the entire network of work.

3) The third and last part of the computer-based analysis is the acquisition of the cross sections. First, we measure the mechanical length of the humerus, which is the distance between the postcranial point of the humeral head and the most distal point of the capitulum (Fig. 2.8). The mechanical length is used to define the 20% and 80% levels (from distally) of the diaphysis, which delimitate the part of the shaft from where the cross sections are going to be extrapolated.

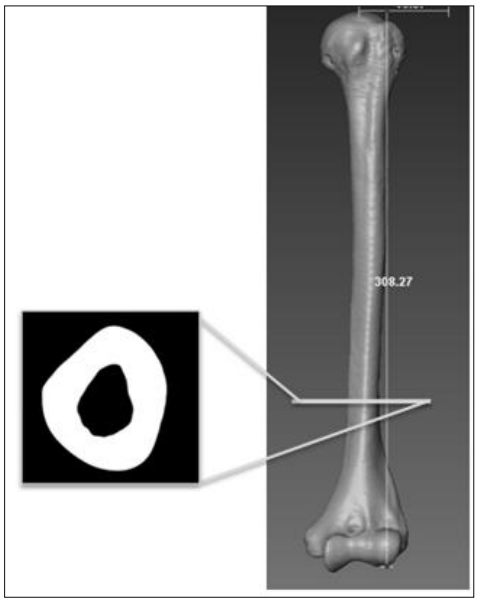

Fig. 2.8 - View of a cross section at the 35% of the mechanical length.

The *Avizo* software has a function that allow us to choose specifically the number of cross sections required and their resolution. In this case, 61 cross sections have been extrapolated for each humerus – saved by the program with the “bmp” extension – and the ones necessary for the CSG analysis have been selected.

For the humerus, the cross section selected is at the 35% level, which falls right under the deltoid tuberosity (Marchi and Sparacello, 2006, 2008; Sparacello et al., 2014). Moreover, at the 35% of the diaphysis there are no muscular insertions – meaning no direct muscular activity that could influence the remodeling of the bone – and it is generally the level at which the bone experiences minimal longitudinal changes in shape and area. Thus, the cross section at this level is thought to be a good representative of the mechanic of the whole bone (Sparacello et al., 2014).

Even though we tried to select complete humeri, some of them are lightly damaged and may lack part of the epiphysis. Missing some articular landmarks may create problem in the positioning of humeri. However, *Avizo* allows us to overcome this problem. If only one of the humeri of a pair was damaged, the function "mirroring" allows using the complete bone to position the incomplete one. For some of the humeri, the damage was such that the mechanical length could not be measured. For those bones, regression lines have been built to find a correlation between the mechanical length and other measurements (Tab. 2.3). The r squares of each regression line have been confronted to select the best correlation. The estimated mechanical length was then used to locate the cross section at the 35% level.

Table 2.3 - Table of individuals that required the use of a regression line in order to calculate the mechanical length.

		ML-L1		**ML-L2**		**ML-DEML**	
		Regression eq.	**r^2**	**Regression eq.**	**r^2**	**Regression eq.**	**r^2**
ID	**Side**	y = 1,254x + 2,427	0,943	y = 0,991x + 7,877	0,992	y = 5,274x - 3,753	0,657
99	R			X			
189	R			X			
479	R	X					
500	L			X			
500	R	X					

ML (mechanical length), L1 (length from the capitulum to the surgical neck), L2 (length from the distal point of the epicondylus to the most proximal point of the humeral head), DEML (distal epiphysis medio-lateral breadth). When L2 was not available the second best fitting regression line was used (hence L1).

2.2.3 ImageJ

The second step of the computer based analysis was performed on the *ImageJ* "Image processing and analysis in Java" program. *ImageJ* was developed by the National Institute of Health and is a public domain image processing program (http://rsb.info.nih.gov/ij/) that supports a vast amount of file formats and can perform logical, arithmetical and geometrical operations on images – as well as other functions for a large amount of necessities. Furthermore, *ImageJ* is designed with an open architecture that provides extensibility via Java plugins that make it possible to solve almost any image processing or analysis problem. In particular, in this study the Moment Macro 1.3 (http://www.hopkinsmedicine.org/FAE/mmacro.html) plugin was used to obtain the variables required for the CSG analysis. Thanks to this plugin, the program – which works on our ".bmp" images obtained from *Avizo* – is able to automatically place the minor and major axis on the cross section and then calculates a series of variables from which we can select the ones that we need. In this case the selected variables for the statistical analysis are: CA (cortical area), %CA, I_x and I_y, I_{max} and I_{min}, I_x/I_y, I_{max}/I_{min} and J, see below.

2.2.4 Cross-Sectional Geometry variables

In this study the Cross-Sectional Geometry method was used to reconstruct the influence of activity patterns on humeral morphology. The cross-sectional variables analyzed are described below.

The cortical area (CA) is the parameter that indicates the resistance of the cross section to compressive or tensile loadings. It is an appropriate dimension for evaluating internal resistance to pure axial loads, that is, loads applied perpendicular to the cross section surface with the force resultant passing through the centroid.

Nonetheless, pure axial loads are rather uncommon in long bones due to the bone curvature and the muscle action. Moreover, CA is less mechanically informative as it does not provide information about the bone distribution nor is it useful to investigate the adaptation of the bone to bending and torsion (Ruff and Hayes, 1983; Marchi 2004; Ogilvie and Hilton, 2011). Since the distribution of the material within the cross section is important to determine the strength and stiffness of a bone, other geometric properties need to be studied.

Second moments of areas (SMAs) are the most important parameters for evaluating bone strength and rigidity under bending. The SMA variables are calculated as the sum of the products of small unit areas of the cross section and their squared distance from either the centroid or an axis running through the centroid (Ruff and Hayes, 1983; Ogilvie and Hilton, 2011).

In this study, I_x, I_y, I_{max} and I_{min} have been used. I_x and I_y are proportional to bending rigidity in the AP (anteroposterior) and ML (mediolateral) planes, respectively. Mathematically, they are quantified by the following formulae:

$$I_x = \int_A X^2 \, dA = \sum_i X_i^2 \, \Delta A_i$$

and

$$I_y = \int_A Y^2 \, dA = \sum_i Y_i^2 \, \Delta A_i$$

Where I_x and I_y = antero-posterior (AP) and medio-lateral (ML) bending moments respectively, X and Y = perpendicular distance from the neutral axis to the unit area for I_y and I_x respectively, dA = infinitesimal area of the cross-section. I_{max}

and I_{min} are the maximum and minimum SMAs and indicate the greatest and least bending rigidity of the cross section in relation to the principal axes. The two axes define the directions of greatest and least bending rigidity and their orientation is given by the angle θ as depicted in Fig. 2.9. In this study the statistical analysis was conducted also on the I_{max}/I_{min} and I_x/I_y ratios, which are an index of the biomechanical shape of a section. A ratio near to 1.0 is related to a circular shape of the section while one higher than 1.0 means a strongly defined direction of greatest bending rigidity (Ruff and Hayes, 1983).

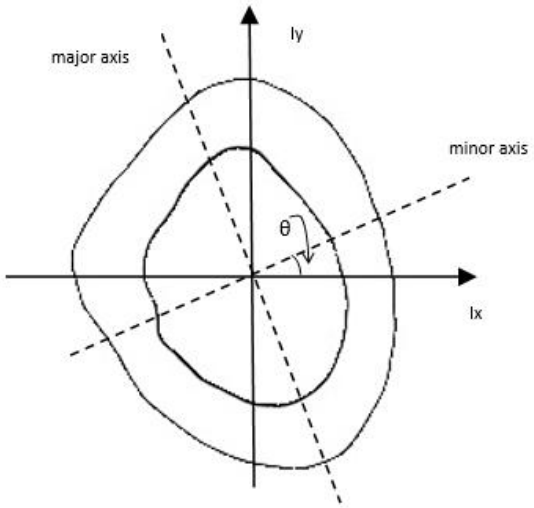

Fig 2.9 - Cross-sectional geometric properties on a left humeral cross section at the 35% level of the diaphysis. All variables explained in text.

Since stress within a cross section under bending is a function of distance from the neutral axis, greater tensile and compressive stresses will be found in more distant fibers of the cross section. This is mathematically quantified by the "flexure formula":

$$\sigma_z = \frac{M_x y}{I}$$

Where σ_z = normal compressive or tensile stress in unit area; M_x = externally applied bending moment about the x axis; y = perpendicular distance from the neutral axis to unit area; I = second moment of area.

Maximum stress occurs in the outermost fibers of the cross section in the plane of bending, where y = ymax. In this case, ymax is often denoted c and the I/c ratio is called section modulus, or Zp. The section modulus is the direct measure of the strength of a bone and depends on the location of the neutral axis, which is the axis that divides the cross section such that the compression force from the area in compression (A_C) equals the tension force from the area in tension (A_T) (Gere, 2001). Z_p can be calculated as the sum of the areas of the cross section on each side of the neutral axis multiplied by the distance between the two centroids and the neutral axis itself (Megson, 2005):

$$Z_p = A_C y_C + A_T y_T$$

The SMA parameter used to evaluate the torsional strength is calculated referring to the centroid of the cross section and is denoted polar moment of area (J). Torsion produces sheer stress in circular cross sections according to the formula:

$$T_{xy} = \frac{T_z \rho}{J}$$

Where T_{xy} = shear stress in unit area; T_z = externally applied torque about longitudinal (z) axis; ρ = radial distance from section centroid to unit area; J = polar moment of area. J is the parameter that better evaluates differences in torsional strength and rigidity. It is an index of the resistance of the bone to the torsion and is

given by the sum of I_{max} and I_{min}. Since its accurateness as a measure of torsional rigidity decreases in non-circular cross sections, some caution must be exercised when using this parameter in areas departing significantly from circularity. However, this is not a concern when studying the humerus, given the tubular form that characterizes the shaft.

2.2.5 *Humeral Torsion*

The humeral torsion angle is formed by the proximal mid-humeral axis and the distal articular axis (Rhodes, 2006, 2009; Rhodes and Knusel, 2005) (Fig. 2.10). The proximal mid-humeral axis is the line that divides the humeral head into an anterior and a posterior half – passing generally between the insertion sites of the muscles supraspinatus and infraspinatus – while the distal articular axis passes between the center of both the trochlea and the capitulum.

When measuring the humeral torsion there are two angles that are formed by the two axis: the obtuse angle (torsion angle) and the acute one (retroversion angle). The statistical analysis of this study was conducted on the retroversion angle, from

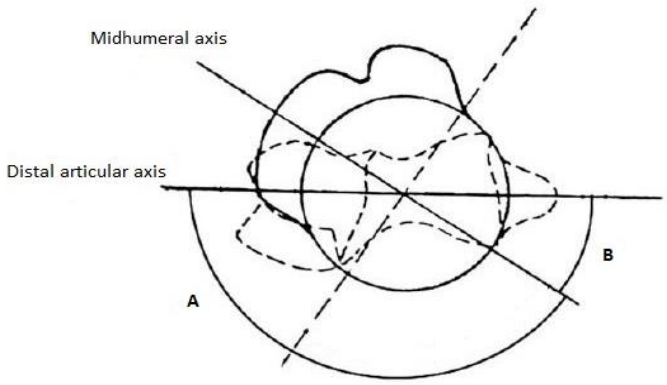

Fig. 2.10 - Humeral torsion (A) and humeral retroversion (B)angles. (Image modified after Rhodes, 2009).

now on referred as humeral torsion (HT).

The retroversion angle was measured according to Rhodes (2006, 2009) although she used a laser torsiometer on the humerus positioned on the osteometric board while in this study the measurements was taken on the *Avizo* software on the 3D renderings of previously positioned bones. The positioned bones were re-orientated in order to have the distal articular axis parallel to the horizontal line. The retroversion angle was measured using the *Avizo* tool for 2D angles measurements as the angled formed by the mid-humeral axis and the horizontal line – now parallel to the distal articular axis (Fig. 2.11).

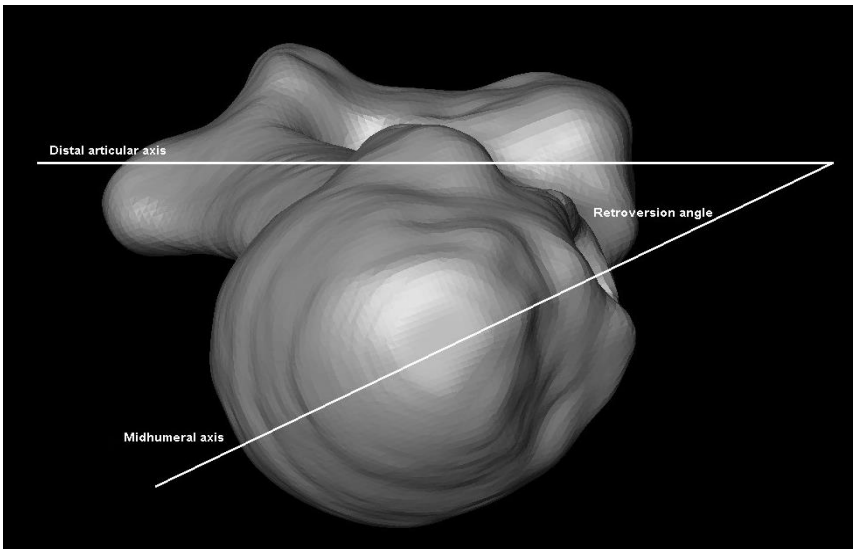

Fig. 2.11 - Example of a retroversion angle measured on the Avizo 6.3 software

2.2.6 Statistical analysis

The robustness of long bones is related to physical activity, bone length and body mass (Ruff ,1997, 2000b). To identify behaviourally significant differences, activity effects need to be isolated, therefore it is necessary to control for the effects of body size. To do so, prior to the statistical analysis all the data have been standardized by the index of body mass estimation (BME). Particularly, CA was

divided by BME, while J and SMAs were scaled by the product of BME and the square of humeral mechanical length (ML). Body mass was estimated from supero-inferior femoral head breadth (FHSI) using previously published sex-specific formulae for raw data (Ruff et al., 1997).

$$BM = 2.741 \times FHSI - 54.9 \quad \textit{(males)}$$

$$BM = 2.426 \times FHSI - 35.1 \textit{ (females)}$$

I_x/I_y and I_{max}/I_{min} ratios were obtained using non-standardized data. Likewise, percentage of cortical area (%CA) was calculated as $(CA/TA) \times 100$ using non-standardized data.

Statistical analysis of differences between individuals with or without grave goods (both females and males) as well as of sexual dimorphism – both for HT and CSG variables – consisted in a Mann Whitney U-test. A non-parametric test was preferred to prevent the effects of poor sample size due to the lack of some measurements for some individuals. In addition to this a Levene test was performed in order to analyze the homogeneity of variances. As for what concerns the correlation between CSG variables (J, %CA, I_x/I_y, I_{max}/I_{min}) and HT, an analysis of correlation was performed to obtain the Pearson p-values and its related r-squares.

Additionally, a diachronic analysis was performed for CSG measures in order to highlight possible changes between the Olmo di Nogara (OdN) sample and the other comparative samples. Variables included in the diachronic analysis are: J, CA, %CA, I_x, I_y, I_{max}, I_{min}, I_x/I_y, I_{max}/I_{min}. Statistical analysis for temporal differences of CSG properties - between the OdN group and each comparative sample - consisted in a Kruskal-Wallis ANOVA test for each variable considered in this study. A non-parametric test was preferred due to the small sample size of some group in which not all the variables are available for all individuals.

On the other hand, statistical analysis of temporal differences in sexual dimorphism consisted in a Mann-Whitney U-test between sexes within groups for each variable considered in this study. Again, a non-parametric test was preferred due to the low number of females data available for some group.

In addition to these tests a descriptive statistical analysis was performed for all the variables considered. Graphics not shown in text can be found in Appendix II. Non parametric statistical analysis have been carried out with *Statistica 7* (Statsoft Inc. 2004) whereas, for the descriptive statistic both *Statistica 7* and *SPSS 23* (IBM 2015) have been used.

3. Results

Not shown graphs and tables are found in Appendix II.

3.1 Humeral torsion variability

The presence or absence of a sword in the male grave goods is not significantly related neither with humeral torsion - for both right and left side - nor with bilateral asymmetry (Table 3.1; Figs. II.1 and II.2). Furthermore, even if a

Table 3.1 - Differences in humeral torsion values in males buried with and without sword.

	Sword (*n*)		**No-Sword (*n*)**		**p-value[a]**	**p Levene[b]**
	Mean	**SD**	**Mean**	**SD**		
HT med[c]	18.65 *(10)*	11.72	18.33 *(8)*	11.33	0.85	0.73
HT BA[d]	5.54 *(6)*	5.43	4.77 *(5)*	3.82	1	0.38
HT right	22 *(7)*	13.01	19.8 *(7)*	12.47	0.85	0.85
HT left	16.37 *(7)*	10.57	17.11 *(9)*	11.11	0.96	0.32

[a] p-values obtained through Mann-Whitney U-test between "sword" and "no- sword" groups.
[b] p-values to test the homogeneity of variances obtained through a Levene test.
[c] Humeral torsion (HT) mean value between left and right arm.
[d] Humeral torsion bilateral asymmetry (HT BA) between left and right arm. Bilateral asymmetry calculated as (max-min).

slightly higher variance in both HT bilateral asymmetry and HT mean value - for males buried with a sword - is observed (Table 3.1, Figs. 3.1, 3.2), the Levene test of the homogeneity of variances shows no statistical significance between the variances of both groups for all of the values observed (Table 3.1). No significant correlation has been found even for females between humeral torsion and presence/absence of grave goods - i.e. presumably belonging to different social classes (Pulcini, 2014) (Table 3.2, Figs. II.3, II.4).

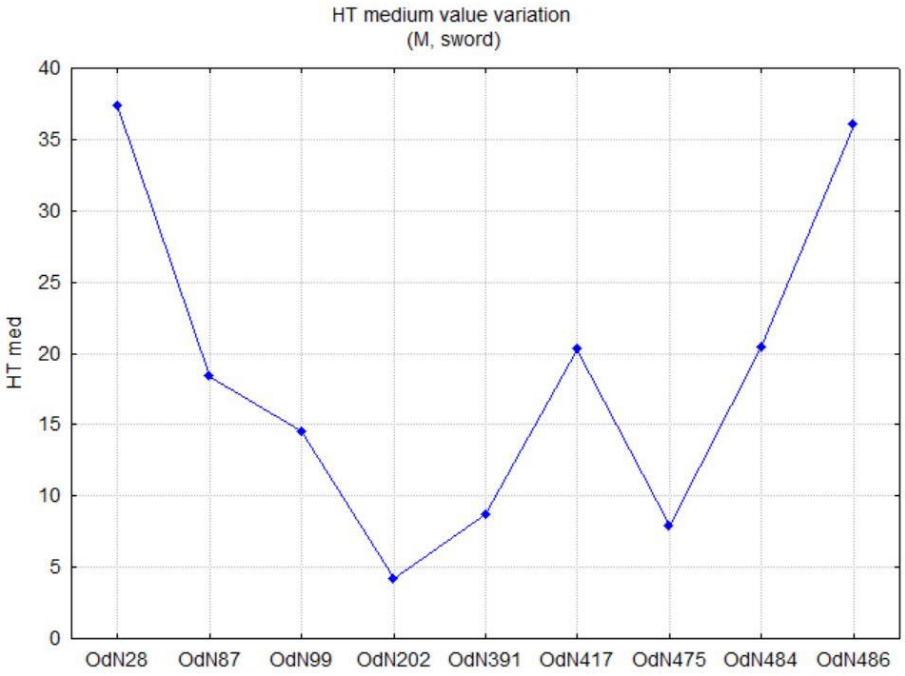

Fig. 3.1 - Variation of humeral torsion mean value in males buried with a sword. BA = Bilateral asymmetry; HT = humeral torsion.

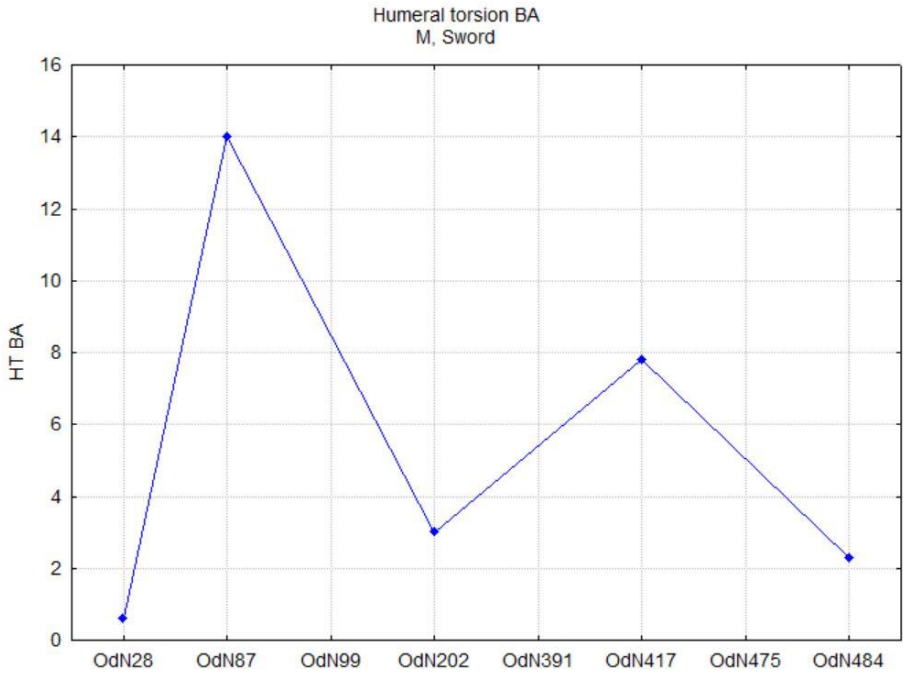

Fig. 3.2 - Variation of humeral torsion bilateral asymmetry in males buried with a sword. BA = Bilateral asymmetry; HT = humeral torsion.

Table 3.2 - Differences in humeral torsion (HT) values in females buried with and without grave goods.

	Grave goods (*n*)		No-grave goods (*n*)		p-value[a]	p Levene[b]
	Mean	**SD**	**Mean**	**SD**		
HT med[c]	18.55 (*10*)	8.61	18.86 (*9*)	8.39	0.74	0.84
HT BA[d]	5.38 (*8*)	4.84	7.76 (*7*)	5.71	0.45	0.37
HT right	20.67 (*9*)	8.15	22.48 (*8*)	8.01	0.56	0.79
HT left	17.13 (*9*)	10.03	14.98 (*8*)	8.67	0.92	0.99

[a] p-value obtained through Mann-Whitney U-test between "grave goods" and "no- grave goods" groups.
[b] p-value to test the homogeneity of variances obtained through a Levene test.
[c] Humeral torsion (HT) mean value between left and right arm.
[d] Humeral torsion bilateral asymmetry (HT BA) between left and right arm. Bilateral asymmetry calculated as (max-min).

Females show higher bilateral asymmetry than males (Table. 3.3, Fig. II.5), no difference is present neither in HT mean value between sexes nor in left and right values (Fig. II.6). However, statistical significance is never reached. Although a higher variance of HT bilateral asymmetry values for females is observable, no significant difference is present according to the Levene test for homogeneity of variances (Table 3.3).

In Table 3.4 results of the Pearson test for correlation – and its associated r-squares – are summarized. Scatterplots for males right and left side show no correlation between HT and J (Figs. 3.3, 3.4). No significant correlations are found between humeral torsion and all the diaphyseal geometric properties (J, I_{max}/I_{min}, I_x/I_y, %CA) neither for left and right values nor for bilateral asymmetry. In females, significant correlation is observed between HT and J on the right side ($p < 0.05$) (Fig.

3.5; Table 3.4). For both I_x/I_y and %CA for the left side an almost significant correlation is observed ($0.05 < p < 0.06$), while for bilateral asymmetry none of the p-values reach statistical significance (Table 3.4, Figs. II.7, II.8).

Table 3.3 - Sexual dimorphism in humeral torsion (HT) values.

	Males (n)		Females (n)		p-value[a]	p Levene[b]
	Mean	SD	Mean	SD		
HT med[c]	18.49 *(18)*	11.18	18.7 *(19)*	8.27	0.738	0.12
HT BA[d]	5.12 *(11)*	4.39	6.49 *(15)*	5.22	0.364	0.75
HT right	20.9 *(14)*	12.3	21.52 *(17)*	7.89	0.87	0.086
HT left	16.79 *(16)*	10.52	16.12 *(17)*	9.19	0.96	0.26

[a] p-value obtained through Mann-Whitney U-test between sexes.
[b] p-value to test the homogeneity of variances obtained through a Levene test.
[c] Humeral torsion (HT) mean value between left and right arm.
[d] Humeral torsion bilateral asymmetry (HT BA) between left and right arm. Bilateral asymmetry calculated as (max-min).

Table 3.4 - Correlation matrix of humeral torsion (HT) values and cross-sectional geometric variables for males and females.

	HT-J[a]		HT-I_{max}/I_{min}[b]		HT-I_x/I_y[c]		HT-%CA[d]	
	r^2	p-value	r^2	p-value	r^2	p-value	r^2	p-value
Males								
Right	0.069	NS[e]	0.048	NS	0.032	NS	0.13	NS
Left	0.039	NS	0.045	NS	0.049	NS	0.021	NS
BA[f]	0.27	NS	0.016	NS	0.0003	NS	0.002	NS
Females								
Right	0.34	*	0.18	NS	0.19	NS	0.012	NS
Left	0.18	NS	0.079	NS	0.23	°	0.24	°
BA	0.0096	NS	0.22	NS	0.005	NS	0.012	NS

[a] Correlation between humeral torsion (HT) and polar moment of area (J).
[b] Correlation between humeral torsion (HT) and maximum and minimum second moments of area ratio (I_{max}/I_{min}).
[c] Correlation between humeral torsion (HT) and antero-posterior and medio-lateral second moments of area ratio (I_x/I_y).
[d] Correlation between humeral torsion (HT) and percentage of cortical area (%CA).
[e] * $p<0,05$; ° = $0.05 < p < 0.06$; NS = non-significant. p-values were obtained through a Pearson test of correlation; associated r^2 are shown in table.
[f] BA (Bilateral Asymmetry) calculated as [(max-min)/min] x100.

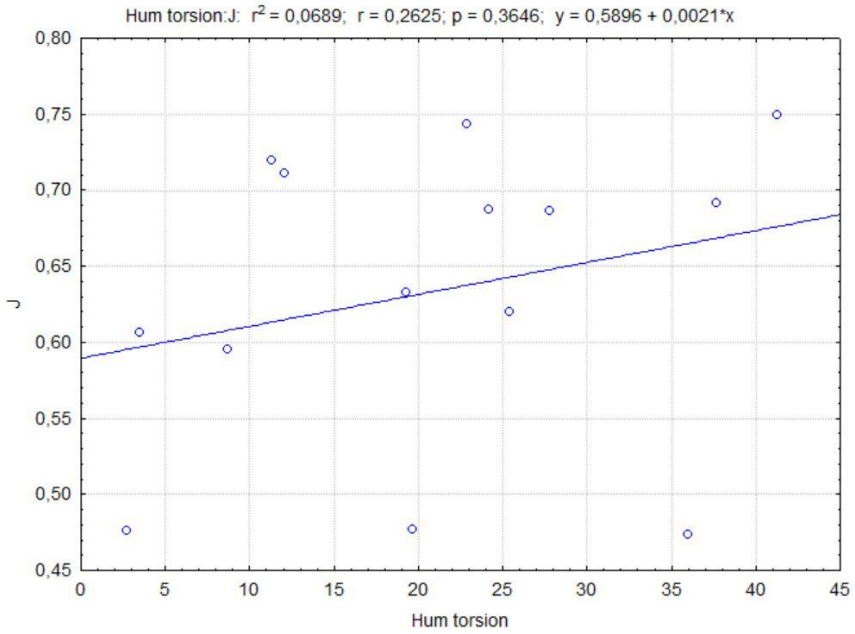

Fig. 3.3 - Scatterplot of the regression line showing the correlation between humeral torsion (HT) and J: males right values. J= polar moment of area (see text for explanation).

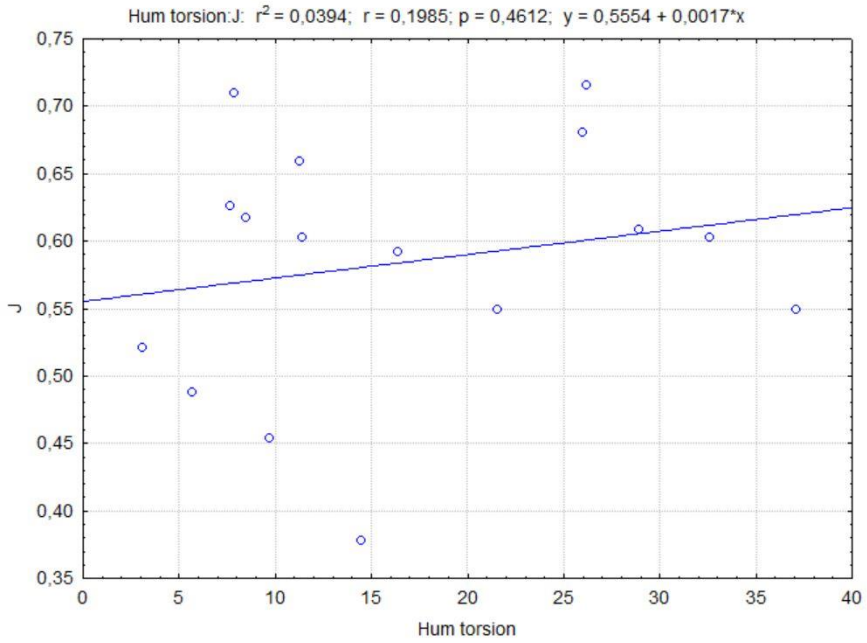

Fig. 3.4 - Scatterplot of the regression line showing the correlation between humeral torsion (HT) and J: males left values. J= polar moment of area (see text for explanation).

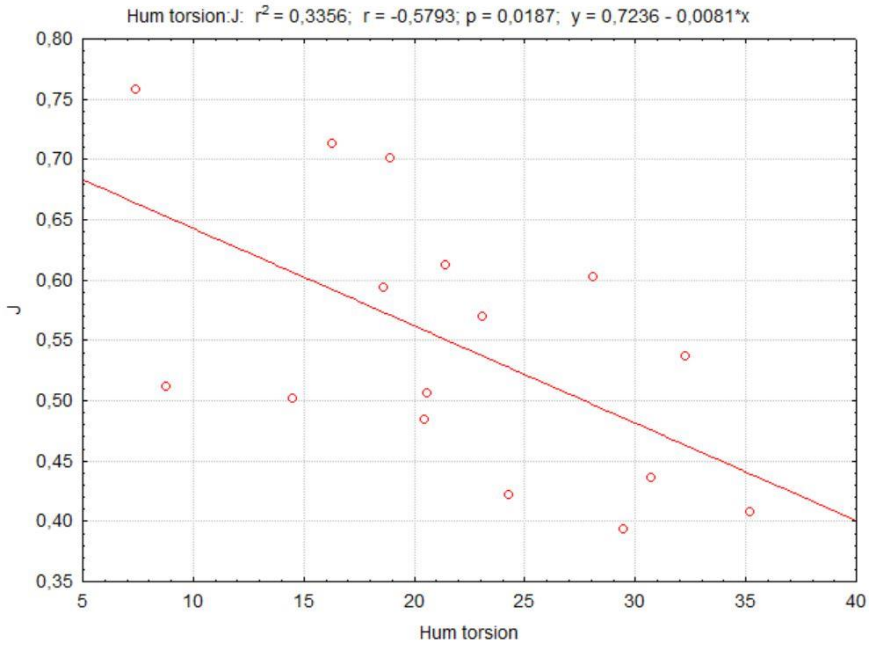

Fig. 3.5 - Scatterplot of the regression line showing the correlation between humeral torsion (HT) and J: females right values. J= polar moment of area (see text for explanation).

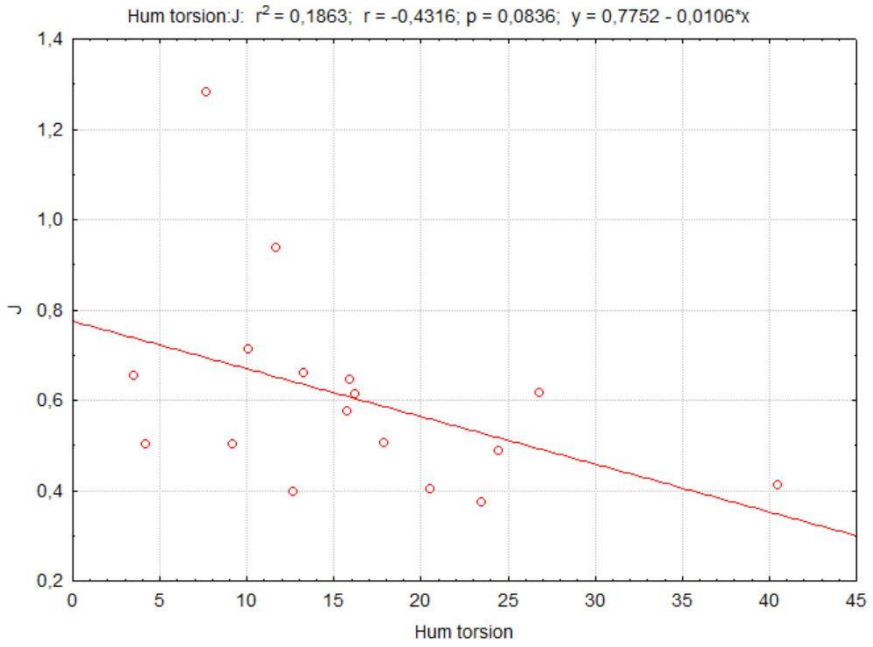

Fig. 3.6 - Scatterplot of the regression line showing the correlation between humeral torsion (HT) and J: females left values. J= polar moment of area. (see text for explanation).

3.2 CSG intra-sample variability

The presence or absence of a sword in male grave goods is not significantly related with diaphyseal geometric properties (Table 3.5). For right and left side, as well as bilateral asymmetry, p-values fail to reach statistical significance for each one of the variables accounted. The same results can be observed for the Levene test of homogeneity of variances (Table 3.5).

In females no statistical differences are observed between those buried with and without grave goods (Table 3.6), with the only exception of the CA bilateral asymmetry ($p < 0.05$). On the contrary, the Levene test for homogeneity of variances is significant for I_y, I_{max}, I_{min} and J for the right side and I_x for the left side ($p < 0.05$), and for I_x ($p < 0.01$), I_{max}, I_{min} and J bilateral asymmetry ($p < 0.05$) (Table 3.6), indicating a significant difference between the variances of these variable between the two groups.

Sexual dimorphism of CSG variables is summarized in Tables 3.7 and 3.8.
Males show significant higher values of %CA than females both for right and left side ($p < 0.01$) (Table 3.7, Figs. II.9, II.10). Higher J values than females are also shown on the right side (Fig. II.11) though the difference does not reach significance (Table 3.7). No difference between sexes is present for I_x/I_y and I_{max}/I_{min} – on both right and left side - and for J on the left side (Fig. II.12). The Levene test shows statistical significance for %CA both for left ($p > 0.01$) and right side ($p > 0.001$) (Table 3.7).

Females show higher values of bilateral asymmetry for I_{max}/I_{min} and %CA than males, while males show higher values for J (see Figs. II.13 - II.15). However, statistical significance is not reached for any of the variables accounted (Table 3.8).

Table 3.5 - Differences in cross-sectional geometric variables in males buried with and without sword.

	Sword		No-sword		p-value[a]	p Levene[b]
	Mean (n)	SD	Mean (n)	SD		
Right						
I_x[c]	0.32 (10)	0.065	0.35 (9)	0.049	NS	NS
I_y	0.29 (10)	0.053	031 (9)	0.044	NS	NS
I_{max}	0.33 (10)	0.063	0.37 (9)	0.056	NS	NS
I_{min}	0.27 (10)	0.049	0.29 (9)	0.039	NS	NS
CA	3.49 (11)	0.574	3.59 (10)	0.469	NS	NS
J	0.61 (10)	0.110	0.66 (9)	0.089	NS	NS
I_x/I_y	1.13 (11)	0.148	1.17 (10)	0.106	NS	NS
I_{max}/I_{min}	1.23 (11)	0.083	1.27 (10)	0.124	NS	NS
%CA	85.52 (11)	4.682	82.95 (10)	5.554	NS	NS
Left						
I_x[d]	0.29 (9)	0.062	0.33 (10)	0.051	NS	NS
I_y	0.25 (9)	0.048	0.27 (10)	0.041	NS	NS
I_{max}	0.29 (9)	0.062	0.34 (10)	0.057	NS	NS
I_{min}	0.24 (9)	0.039	0.26 (10)	0.034	NS	NS
CA	3.3 (11)	0.489	3.39 (10)	0.395	NS	NS
J	0.54 (9)	0.100	0.59 (10)	0.087	NS	NS
I_x/I_y	1.18 (11)	0.169	1.21 (10)	0.125	NS	NS
I_{max}/I_{min}	1.26 (11)	0.097	1.29 (10)	0.129	NS	NS
%CA	86.04 (11)	4.484	82.26 (10)	5.130	NS	NS
Bil. Asymm.[d]						
I_x[d]	14.03 (9)	8.706	11.43 (9)	6.733	NS	NS
I_y	17.68 (9)	13.770	13.87 (9)	11.423	NS	NS
I_{max}	15.29 (9)	8.814	11.05 (9)	8.702	NS	NS
I_{min}	16.02 (9)	13.397	13.01 (9)	8.862	NS	NS
CA	6.74 (11)	4.910	6.94 (10)	3.945	NS	NS
J	14.23 (9)	11.639	11.83 (9)	8.402	NS	NS
I_x/I_y	7.89 (11)	6.123	7.97 (10)	6.745	NS	NS
I_{max}/I_{min}	6.56 (11)	5.807	4.65 (10)	3.573	NS	NS
%CA	2.90 (11)	2.475	1.89 (10)	1.415	NS	NS

[a] NS = non-significant. P-values obtained through Mann-Whitney U-test between groups.

[b] p-values to test the homogeneity of variances obtained through a Levene test.

[c] I_x, I_y = AP and ML second moments of area respectively; I_{max}, I_{min} = maximum and minimum second moments of area respectively; CA = cortical area; J = polar moment of area; I_x/I_y = AP and ML second moments of area ratio; I_{max}/I_{min} = maximum and minimum second moments of area ratio; %CA = percentage of cortical area. All variables are explained in text.

[d] Bilateral asymmetry calculated as [(maximum – minimum)/minimum] x 100

Table 3.6 - Differences in cross-sectional geometric variables in females buried with and without grave goods.

	Grave goods		No-grave goods		p-value[a]	p Levene[b]
	Mean (n)	**SD**	**Mean (n)**	**SD**		
Right						
I_x[c]	0.31 (10)	0.722	0.26 (8)	0.036	NS	NS
I_y	0.28 (10)	0.103	0.25 (8)	0.045	NS	*
I_{max}	0.33 (10)	0.094	0.28 (8)	0.037	NS	*
I_{min}	0.26 (10)	0.083	0.24 (8)	0.042	NS	*
CA	3.4 (10)	0.718	3.22 (9)	0.537	NS	NS
J	0.59 (10)	0.174	0.52 (8)	0.078	NS	*
I_x/I_y	1.17 (10)	0.180	1.1 (9)	0.122	NS	NS
I_{max}/I_{min}	1.28 (10)	0.127	1.22 (9)	0.089	NS	NS
%CA	73.35 (10)	8.027	80.01 (9)	7.377	NS	NS
Left						
I_x	0.34 (10)	0.109	0.28 (9)	0.045	NS	*
I_y	0.31 (10)	0.166	0.25 (9)	0.062	NS	NS
I_{max}	0.36 (10)	0.150	0.29 (9)	0.051	NS	NS
I_{min}	0.29 (10)	0.126	0.24 (9)	0.056	NS	NS
CA	3.39 (10)	0.983	3.25 (9)	0.659	NS	NS
J	0.65 (10)	0.273	0.53 (9)	0.105	NS	NS
I_x/I_y	1.18 (10)	0.189	1.15 (9)	0.164	NS	NS
I_{max}/I_{min}	1.28 (10)	0.169	1.26 (9)	0.140	NS	NS
%CA	70.76 (9)	9.837	79.48 (9)	7.987	NS	NS
Bil. Asymm.[d]						
I_x	10.24 (10)	12.927	8.20 (8)	4.133	NS	**
I_y	12.96 (10)	14.730	8.49 (8)	4.837	NS	NS
I_{max}	9.68 (10)	11.820	7.75 (8)	5.395	NS	*
I_{min}	14.17 (10)	14.873	7.93 (8)	4.132	NS	*
CA	8.82 (10)	6.441	3.14 (9)	3.518	*	NS
J	10.48 (10)	13.413	7.36 (8)	4.464	NS	*
I_x/I_y	9.21 (10)	6.704	6.45 (8)	6.287	NS	NS
I_{max}/I_{min}	8.8 (10)	5.380	6.07 (8)	3.695	NS	NS
%CA	33.53 (10)	84.892	3.29 (8)	2.708	NS	NS

[a] * $p < 0.05$; ** $p < 0.01$; NS= non-significant. P-values obtained through Mann-Whitney U-test between groups.

[b] p-values to test the homogeneity of variances obtained through a Levene test.

[c] I_x, I_y = AP and ML second moments of area respectively; I_{max}, I_{min} = maximum and minimum second moments of area respectively; CA = cortical area; J = polar moment of area; I_x/I_y = AP and ML second moments of area ratio; I_{max}/I_{min} = maximum and minimum second moments of area ratio; %CA = percentage of cortical area. All variables are explained in text.

[d] Bilateral asymmetry calculated as [(maximum – minimum)/minimum] x 100.

The Levene test for homogeneity of variances results in a significant p-value for the %CA bilateral asymmetry ($p < 0.05$) (Table 3.8).

Finally, Table 3.9 shows the results of a comparison of I_x and I_y within sexes. Males show significantly higher anteroposterior (I_x) than mediolateral bending rigidity (I_y) for both the right ($p < 0.05$) and the left side ($p < 0.01$) (Figs II.16, II.17). Females show a non-significant difference between anteroposterior and mediolateral bending rigidity for both sides (Table 3.9).

Table 3.7- Sexual dimorphism of cross-sectional geometric variables.

	Males			**Females**				
	Mean	**SD**	***n***	**Mean**	**SD**	***n***	**p-value[a]**	**p Levene[b]**
Right								
%CA[c]	84.3	5.154	*21*	76.51	8.25	*19*	**	**
J	0.633	0.102	*19*	0.563	0.142	*18*	NS	NS
I_{max}/I_{min}	1.250	0.104	*21*	1.251	0.112	*19*	NS	NS
I_x/I_y	1.134	0.127	*19*	1.127	0.156	*18*	NS	NS
Left								
%CA	84.24	5.06	*21*	75.12	9.78	*19*	**	***
J	0.578	0.096	*19*	0.595	0.214	*19*	NS	NS
Imax/Imin	1.277	0.112	*21*	1.268	0.152	*19*	NS	NS
Ix/Iy	1.194	0.152	*19*	1.165	0.173	*19*	NS	NS

[a] ** $p < 0.01$; *** $p < 0.001$; NS = non-significant. P-values obtained through a Mann-Whitney U-test between sexes.

[b] p-value to test the homogeneity of variance obtained through a Levene test.

[c] %CA = percentage cortical area; J = polar moment of area; I_{max}/I_{min} = maximum and minimum second moments of area ratio; I_x / I_y = AP and ML second moment of areas ratio. All variables are explained in text.

Table 3.8 - Sexual dimorphism in the bilateral asymmetry of cross-sectional geometric variables.

	Males			Females			p-value [a]	p Levene [b]
	Mean	**SD**	***n***	**Mean**	**SD**	***n***		
I_{max}/I_{min} [c,d]	5.65	4.85	*21*	7.5	4.74	*19*	NS	NS
I_x/I_y	7.93	6.26	*21*	7.9	6.48	*19*	NS	NS
%CA	2.42	4.85	*21*	19.21	4.74	*19*	NS	*
J	13.03	9.92	*18*	9.09	10.29	*18*	NS	NS

[a] * $p < 0.05$; NS = non-significant. P-values obtained through a Mann-Whitney U-test between sexes.
[b] p-value to test the homogeneity of variance obtained through a Levene test.
[c] Bilateral asymmetry calculated as [(max-min)/min] x 100.
[d] All variables are explained in text. %CA = percentage cortical area; J = polar moment of area; I_{max}/I_{min} = maximum and minimum second moments of area ratio; I_x / I_y = AP and ML second moment of areas ratio.

Table 3.9 Olmo di Nogara cross-sectional geometric bilateral asymmetry within sexes.

	Ix[a]			Iy[a]			
	Mean	**SD**	***n***	**Mean**	**SD**	***n***	**p-value[b]**
Males							
Right	105 x 10^{-5}	18 x 10^{-5}	*19*	93 x 10^{-5}	16 x 10^{-5}	*19*	*
Left	97 x 10^{-5}	17 x 10^{-5}	*19*	82 x 10^{-5}	15 x 10^{-5}	*19*	**
Females							
Right	101 x 10^{-5}	19 x 10^{-5}	*18*	92 x 10^{-5}	27 x 10^{-5}	*18*	NS
Left	109 x 10^{-5}	29 x 10^{-5}	*18*	99 x 10^{-5}	44 x 10^{-5}	*18*	NS

[a] I_x and I_y are scaled by (body mass x humeral mechanical length^2).
[b] * $p < 0.05$; ** $p < 0.01$; NS = non-significant. Significance levels were obtained through a T-test for independent samples within sex and side.

3.3 CSG diachronic comparison

Tables 3.10 and 3.11 summarize the results of the diachronic comparison between the OdN sample and the comparative samples in males and females respectively. Nonsignificant differences are observed between OdN and the comparative samples for the left side of males for all the variable analyzed. For the right side, statistically significant difference was found between the OdN and the Orientalizing-Archaic (O-A) sample for I_x, I_y, I_{max}, I_{min} and J, and between the OdN

and the Iron Age (IRON) sample for I_y, I_{max}, I_{min} and J (Table 3.10). For females, non-significant difference is observed for all the variables in each comparison for both left and right side (Table 3.11). Both females and males show no significant difference in bilateral asymmetry for all the variables analyzed, with the only exception of I_{max}/I_{min} bilateral asymmetry between OdN and Hellenistic (HELL) group ($p < 0.05$) (Table 3.12).

Almost all Iron Age groups – with the exception of the Fifth Century (V CEN) group - show an overall significance in sexual dimorphism (Table 3.13). Olmo di Nogara individuals do not show significant sexual dimorphism for any of the variable analyzed for both the right and left side (Table 3.13).

Finally, table 3.14 summarizes sexual dimorphism values for bilateral asymmetry. Olmo di Nogara individuals show among the lowest differences between sexes in all variables and significance is not reached for any of the comparisons. For Iron Age groups statistical significance is reached for I_y in O-A ($p < 0.01$), V CEN and HELL groups ($p < 0.05$), for I_x/I_y in IRON group ($p < 0.05$), for I_{min} in O-A and V CEN groups ($p < 0.05$) and for J in the O-A group ($p < 0.01$).

Table 3.10 - Temporal differences in humeral cross-sectional geometric variables: males.

	OdN - O-A[a]	**OdN - V CEN**	**OdN - HELL**	**OdN - IRON**
Right				
I_x[b,c]	*[d]	NS	NS	NS
I_y	**	NS	NS	*
I_x/I_y	NS	NS	NS	NS
I_{max}	*	NS	NS	*
I_{min}	***	NS	NS	*
I_{max}/I_{min}	NS	NS	NS	NS
J	**	NS	NS	*
%CA	-	-	-	-
CA[e]	-	-	-	-
Left				
I_x	NS	NS	NS	NS
I_y	NS	NS	NS	NS
I_x/I_y	NS	NS	NS	NS
I_{max}	NS	NS	NS	NS
I_{min}	NS	NS	NS	NS
I_{max}/I_{min}	NS	NS	NS	NS
J	NS	NS	NS	NS
%CA	-	-	-	-
CA	-	-	-	-

[a] OdN = Olmo di Nogara; O-A = Orientalizing Archaic; V CEN = fifth century; HELL = Hellenistic; IRON = Iron Age.

[b] I_x, I_y = AP and ML second moments of area; I_{max}, I_{min} = maximum and minimum second moments of area; CA = cortical area; J= polar moment of area; I_x/I_y= AP and ML second moments of area ratio; I_{max}/I_{min} = maximum and minimum second moments of area ratio; %CA = percentage of cortical area. All variables explained in text.

[c] I_x, I_y, I_{max}, I_{min}, J are scaled by (body mass x humeral mechanical length^2).

[d] * $p < 0.05$; ** $p < 0.01$; *** $p < 0.001$; NS= non-significant. Empty cells mean there are no sufficient data to perform an analysis. Significance levels are determined from Kruskal-Wallis ANOVA test between Olmo di Nogara and each temporal group within sex.

[e] CA is scaled by body mass.

Table 3.11 - Temporal differences in humeral cross-sectional geometric variables: females.

	OdN - O-A[a]	**Odn - V CEN**	**OdN - HELL**	**OdN - IRON**
Right				
I_x[b,c]	NS[d]	NS	NS	NS
I_y	NS	NS	NS	NS
I_x/I_y	NS	NS	NS	NS
I_{max}	NS	NS	NS	NS
I_{min}	NS	NS	NS	NS
I_{max}/I_{min}	NS	NS	NS	NS
J	NS	NS	NS	NS
%CA	-	-	-	-
CA[e]	-	-	-	-
Left				
I_x[a,b]	NS	NS	NS	NS
I_y	NS	NS	NS	NS
I_x/I_y	NS	NS	NS	NS
I_{max}	NS	NS	NS	NS
I_{min}	NS	NS	NS	NS
I_{max}/I_{min}	NS	NS	NS	NS
J	NS	NS	NS	NS
%CA	-	-	-	-
CA[c]	-	-	-	-

[a] OdN = Olmo di Nogara; O-A = Orientalizing Archaic; V CEN = fifth century; HELL = Hellenistic; IRON = Iron Age.

[b] I_x, I_y = AP and ML second moments of area; I_{max}, I_{min} = maximum and minimum second moments of area; CA = cortical area; J= polar moment of area; I_x/I_y= AP and ML second moments of area ratio; I_{max}/I_{min} = maximum and minimum second moments of area ratio; %CA = percentage of cortical area. All variables explained in text.

[c] I_x, I_y, I_{max}, I_{min}, J are scaled by (body mass x humeral mechanical length^2).

[d] * $p < 0.05$; ** $p < 0.01$; *** $p < 0.001$; NS= non-significant. Empty cells mean there are no sufficient data to perform an analysis. Significance levels are determined from Kruskal-Wallis ANOVA test between Olmo di Nogara and each temporal group within sex.

[e] CA is scaled by body mass.

Table 3.12 - Temporal differences in bilateral asymmetry of cross-sectional geometric variables.

	OdN[a]		O-A		V CEN		HELL		IRON	
	Mean	**(n)**	**Mean**	**(n)**	**Mean**	**(n)**	**Mean**	**(n)**	**Mean**	**(n)**
Males										
I_x[b,c]	12.06	*(18)*	20.83	*(9)*	32.14	*(7)*	16.18	*(10)*	15.93	*(10)*
I_y	14.78	*(18)*	28.00	*(9)*	36.82	*(7)*	23.97	*(10)*	27.84	*(10)*
I_x/I_y	8.22	*(18)*	10.44	*(9)*	16.91	*(7)*	15.38	*(10)*	18.37	*(10)*
I_{max}	12.50	*(18)*	18.70	*(9)*	30.56	*(7)*	16.65	*(10)*	15.70	*(10)*
I_{min}	13.41	*(18)*	30.10	*(9)*	37.84	*(7)*	24.04	*(10)*	27.21	*(10)*
I_{max}/I_{min}	5.88	*(18)*	10.96	*(9)*	8.38	*(7)*	14.53 *[d]	*(10)*	11.75	*(10)*
J	12.32	*(18)*	23.58	*(9)*	33.73	*(7)*	18.76	*(10)*	20.35	*(10)*
%CA	5.44	*(21)*	-		-		-		-	
CA[e]	6.84	*(21)*	-		-		-		-	
Females										
I_x	10.18	*(18)*	14.25	*(9)*	13.31	*(8)*	13.49	*(9)*	17.85	*(10)*
I_y	12.06	*(18)*	10.73	*(9)*	20.90	*(8)*	11.03	*(9)*	13.31	*(10)*
I_x/I_y	7.52	*(18)*	9.67	*(9)*	12.65	*(8)*	12.29	*(9)*	6.52	*(10)*
I_{max}	9.52	*(18)*	12.73	*(9)*	12.74	*(8)*	10.32	*(9)*	13.32	*(10)*
I_{min}	12.21	*(18)*	12.57	*(9)*	21.57	*(8)*	13.69	*(9)*	19.67	*(10)*
I_{max}/I_{min}	7.33	*(18)*	9.36	*(9)*	10.80	*(8)*	8.73	*(9)*	8.73	*(10)*
J	10.19	*(18)*	12.42	*(9)*	16.26	*(8)*	10.50	*(9)*	15.71	*(10)*
%CA	5.49	*(19)*	-		-		-		-	
CA	6.13	*(19)*	-		-		-		-	

[a] OdN = Olmo di Nogara; O-A = Orientalizing Archaic; V CEN = fifth century; HELL = Hellenistic; IRON = Iron Age.

[b] Bilateral asymmetry calculated as [(max-min)/min]*100. I_x, I_y = AP and ML second moments of area; I_{max}, I_{min} = maximum and minimum second moments of area; CA = cortical area; J= polar moment of area; I_x/I_y= AP and ML second moments of area ratio; I_{max}/I_{min} = maximum and minimum second moments of area ratio; %CA = percentage of cortical area. All variables explained in text.

[c] I_x, I_y, I_{max}, I_{min}, J are scaled by (body mass x humeral mechanical length^2).

[d] *p < 0.05; ** p < 0.01; *** p < 0.001; NS = non-significant. Empty cells mean that there are insufficient data to perform the analysis. Significance levels are determined from Kruskal-Wallis ANOVA test between Olmo di Nogara and each temporal group within sexes.

[e] CA is scaled by body mass.

Table 3.13 - Temporal differences in sexual dimorphism of humeral cross-sectional geometric variables.

	OdN[a]	**O-A**	**V CEN**	**HELL**	**IRON**
Right					
I_x[b,c]	NS[d]	**	NS	NS	**
I_y	NS	***	NS	**	***
I_x/I_y	NS	*	NS	**	NS
I_{max}	NS	**	NS	*	**
I_{min}	NS	***	NS	**	**
I_{max}/I_{min}	NS	*	NS	*	NS
J	NS	***	NS	**	**
%CA	NS	-	-	-	-
CA[e]	NS	-	-	-	-
Left					
I_x[a,b]	NS	NS	NS	NS	**
I_y	NS	*	NS	*	***
I_x/I_y	NS	NS	NS	NS	NS
I_{max}	NS	NS	NS	NS	**
I_{min}	NS	*	NS	*	**
I_{max}/I_{min}	NS	NS	NS	*	NS
J	NS	NS	NS	*	**
%CA	NS	-	-	-	-
CA[c]	NS	-	-	-	-

[a] OdN = Olmo di Nogara; O-A = Orientalizing Archaic; V CEN = fifth century; HELL = Hellenistic; IRON = Iron Age.

[b] I_x, I_y = AP and ML second moments of area; I_{max}, I_{min} = maximum and minimum second moments of area; CA = cortical area; J= polar moment of area; I_x/I_y= AP and ML second moments of area ratio; I_{max}/I_{min} = maximum and minimum second moments of area ratio; %CA = percentage of cortical area. All variables explained in text.

[c] I_x, I_y, I_{max}, I_{min}, J are scaled by (body mass x humeral mechanical length^2).

[d] *$p < 0.05$; **$p < 0.01$; *** $p < 0.001$; NS= non-significant. Empty cells mean that there are insufficient data to perform the analysis. Significance levels are determined from Mann-Whitney U-test between sex within groups.

[e] CA is scaled by body mass.

Table 3.14 - Sexual dimorphism in bilateral asymmetry of cross-sectional geometric variables.

	OdN[a]		O-A		V CEN		HELL		IRON	
	Sex. Dim.	**p-value[b]**	**Sex. Dim.**	**p-value**	**Sex. Dim.**	**p-value**	**Sex. Dim.**	**p-value**	**Sex. Dim.**	**p-value**
Bil. Asymm.										
I_x[c,d,e]	18.51	NS	46.11	NS	141.55	NS	19.93	NS	-10.78	NS
I_y	22.47	NS	160.99	**	76.20	*	117.29	*	109.16	NS
I_x/I_y	4.563	NS	7.98	NS	33.67	NS	25.12	NS	181.78	*
I_{max}	31.35	NS	46.89	NS	139.84	NS	61.33	NS	17.83	NS
I_{min}	9.8	NS	139.38	*	75.41	*	75.56	NS	38.31	NS
I_{max}/I_{min}	-19.80	NS	17.04	NS	-22.41	NS	66.50	NS	34.50	NS
J	20.91	NS	89.90	**	107.40	NS	78.78	NS	29.52	NS
%CA	-0.79	NS	-	-	-	-	-	-	-	-
CA[f]	11.49	NS	-	-	-	-	-	-	-	-

[a] OdN = Olmo di Nogara; O-A = Orientalizing Archaic; V CEN = fifth century; HELL = Hellenistic; IRON = Iron Age.

[b] *p < 0.05; **p < 0.01; ***p < 0.001; NS= non-significant. Empty cells mean that there are insufficient data to perform the analysis. Significance levels are determined from Mann-Whitney U-test between sex within groups [c] I_x, I_y = AP and ML second moments of area; I_{max}, I_{min} = maximum and minimum second moments of area; CA = cortical area; J= polar moment of area; I_x/I_y= AP and ML second moments of area ratio; I_{max}/I_{min} = maximum and minimum second moments of area ratio; %CA = percentage of cortical area. All variables explained in text.

[d] I_x, I_y, I_{max}, I_{min}, J are scaled by (body mass x humeral mechanical length^2).

[e] Sexual dimorphism calculated as [(males mean value- females mean value)/females mean value]x100.

[f] CA is scaled by body mass.

4. Discussion

The general aim of this study was to infer behavioral pattern, social stratification and subsistence economy of the OdN population – by both corroborating palaeobiological results and providing new ones. Particularly, the specific aims were:

(1) to demonstrate if there are differences between individuals buried with and without grave goods for both humeral torsion and CSG variables;

(2) to corroborate the palaeobiological hypothesis that horses were used by both sexes for military purposes as well as other working activities;

(3) to test the presence of a correlation between humeral torsion and CSG variables;

(4) to validate the results of the palaeopathological analysis about different activities performed by males and females but with similar amount of stresses for both sexes;

(5) to highlight differences in sexual dimorphism and CSG variables between our sample and the Iron Age comparison samples.

The results obtained are in general accordance with previous studies (Pulcini, 2014; Rhodes, 2004; Salzani, 2005; Sladek, 2007), proving the usefulness of the biomechanical approach in characterizing past population behavior.

4.1 *Differences between individuals with and without grave goods*

For OdN male individuals no statistical correlation was found between presence of the sword and HT – for both mean value and bilateral asymmetry. As suggested by the evidence of the use of occasional weapons in addition to swords (Pulcini, 2014), the similarity of HT values for armed and unarmed males is coherent with the hypothesis of a participation of all the males to warlike episodes - without regard for

social status. Following Rhodes (2006), this lack of bilateral asymmetry could be due to a sort of variety of weapons that were used in addition to the sword and that stressed the arms in different ways. Moreover, a variety of studies on professional handball, tennis and baseball players demonstrated how the degree of HT is highly influenced by pre-adolescence activity (Crockett et al., 2002; Osbahr et al., 2002; Pieper, 1998; Reagan et al., 2002). Since young males belonging to the *élite* were usually buried with a dagger, this has been hypothesized to be the first weapon given to a young warrior in training (Pulcini, 2014; Salzani, 2005). The lack of an early training with the sword could also be the reason of the low degree of HT and its bilateral asymmetry, both for armed and unarmed males.

Similar results are observed for females. According to Pulcini's (2014) palaeopathological analysis, the presence of spondylolysis is observed in females without regard of their social status. Our results corroborate this hypothesis, in that no difference is observed between HT of females buried with and without grave goods.

Measuring the humeral torsion requires an intact humeral head with the lesser and great tubercles intact. Therefore, obtaining accurate measurements for all the bones could be challenging even in a good preserved sample - as the OdN is. Because of preservation state problems, in this study the number of individuals for which HT could be reliably measured was low. Caution must be taken therefore in drawing conclusions for the whole population. Further studies with the inclusion of a larger number of individuals or devising new methods to obtain HT from fragmentary humeri are necessary to obtain provide interpretations.

4.2 *Use of the horse and humeral torsion*

Pulcini's (2014) study of the occupational stress markers of the lower limb resulted in a wide distribution of skeletal alterations related to the horse-riding activity both in males and females. Even if no archaeological evidences were found to support the use of horses in the OdN necropolis (Salzani, 2005), the

Fig. 4.1 – Image of a correct position of arms in keeping rains (photograph modified from the web).

anthropological results were considered sufficient enough to hypothesize not only a use of the horse by males but also by females. Consequently, horses were thought to be used for other working activities in addition to warlike ones. Evidence of the introduction in the agriculture of the draught horse in the Bronze Age has been found in Italy (Peroni, 1979). Humeral torsion has proven to be related to a series of movements of the upper limb that keeps the elbow on a parasagittal plane during flexion (Rhodes, 2006; Rhodes and Churchill, 2009, Rhodes and Knusel, 2005). During horse-riding keeping reins - or the main of horses - could have reproduced a parasagittal plane movement of the elbow similar the one described as responsible for the increase of HT (Fig. 4.1).

Results of the statistical analysis on the sexual dimorphism of humeral torsion show low levels of bilateral asymmetry with no significant difference between sexes.

Although this could be related to the effective use of horses by both sexes, no conclusions can be drawn from this output alone as no comparison sample is available to highlight the presence of an effective higher value of HT in our population. Moreover, the amount of movements that could have influenced the low difference of the torsion between sexes is too high to attribute the results only to horse-riding activity. However, this study is useful as it pinpoints the necessity of more specific comparisons with both other Bronze Age and attested horse-riding samples.

4.3 *CSG variables and HT correlation*

As hypothesized by Rhodes and Knusel (2005) because J is a measure of resistance to torsional forces in circular sections and given that the section of the humerus is almost circular, a relationship may be expected between J and HT. Humeral torsion angle, as a measure of architecture, was found to be correlated with measures of diaphyseal loading and robusticity (Rhodes and Knusel, 2005). Results of our study overall did not show any significant correlation between HT and CSG variables, the only exception being the correlation between J and HT in the female right side.

Changes in HT were demonstrated to relate to specific behavioral patterns and may be seen as a form of adaptation to strenuous activity (Rhodes and Knusel, 2005). However, in samples of past populations and recent humans the evidence for a correlation between humeral torsion and measures that reflect habitual upper limb activity is unclear, and it appears that not only activity levels but also variation in body shape (especially thoracic shape) and in the age at which the activity is started may all be contributing to variation in humeral torsion (Churchill, 1996; Rhodes and Churchill, 2009; Rhodes, 2006). Humeral torsion, has been demonstrated to be

highly influenced by activities performed prior to skeletal maturity (Pieper, 1998; Rheagan et al., 2002). On the contrary, CSG variables depend strictly from the pattern of mechanical loadings placed upon the bone during the whole life. These loadings are due to the action of muscles on the humerus and can vary owing to a number of factors (e.g. body mass and activity types and levels) (Ruff, 1992). We suggest that the lack of correlation between J and HT could be the reflection of a different response of the two variables to mechanical loadings. Further studies are needed in order to clarify this matter as a single sample is not enough to draw general conclusion.

4.4 *Sexual dimorphism*

Comparative studies of sexual dimorphism in overall body size and skeletal robusticity indices (Frayer, 1980; Trinkaus, 1980; Hamilton, 1982) in human populations have been fairly common in the past. However, body size and skeletal robusticity indices are relatively imprecise measures of sexual dimorphism in skeletal structure (Ruff, 1992). More precise reconstructions of behavioral differences between sexes can be obtained from bone shape characteristics (Ruff, 1992). For the OdN sample, archeological evidences brought Pulcini (2014) and Salzani (2005) to suggest a comparable amount of stresses on both males and females. However, due to the increase in gender perception that occurred in the transition toward Iron Age, activities performed by the two sexes are expected to be different. In this work sexual dimorphism of CSG variables and HT has been studied in order to test the results obtained by the archaeological investigation. For HT and almost all the CSG variables (%CA, J, I_{max}/I_{min} and I_x/I_y) no statistically significant results were found between males and females. This confirms the hypothesis of a

comparable amounts of mechanical loadings for both sexes and of a high involvement of women in strenuous works. In particular, as previously suggested by Ruff (1992) the change in the upper limb in females can be attributed to increased mechanical loads due to wheat grind.

When analyzing anteroposterior and mediolateral SMA, males showed a significant higher value of I_x for both left and right arm. I_x and I_y represents directions of bending rigidity relatively to the anteroposterior and mediolateral planes, respectively, thus the presence of substantial difference between them may be interpreted as the presence of a preferential direction of application of loads. Males show a higher anteroposterior bending rigidity in the humerus, while the lack of difference in I_x and I_y observed in females suggests an equal distribution of loads in both the anteroposterior and mediolateral planes. Since the mechanical properties of a cross section are directly related to the patterns of activities performed during life (Evans, 1953; Ruff, 1992; Ruff et al., 2006), the differences between I_x and I_y within sexes suggest different types of mechanical loadings – i.e. different activities performed.

Overall, the biomechanical analysis - on both CSG variables and HT – corroborates Pulcini's (2014) and Salzani's (2005) hypothesis of a similar engagement of males and females in highly strenuous activities. However, our results on I_x and I_y suggest that the typology of works performed by both sexes may have been slightly different, thus confirming previous studies on the gender division of works in the Bronze Age (Coles and Haring, 1979; Gilman, 1981; Kristiansen, 2014; Levy, 1979; Macintosh et al. 2014; Peroni, 1979; Sladek, 2007).

4.5 *Bronze Age and Iron Age diachronic comparison*

The transition to Iron Age has always been viewed as a significant shift in social stratification and military organization associated to an increase in gender perception (Childe, 1930; Gilman, 1981; Sladek et al., 2007). Results of the diachronic comparison show an overall significant difference for CSG variables between OdN and two of the Iron Age groups (O-A and IRON), but only for the right side. As suggested by Sladek et al. (2007) the transition toward the Iron Age can be seen more as a continuous process - that probably affected only a limited part of human activities - than a substantial change. Coherently with this observation, the variability observed in the results for the diachronic analysis support the hypothesis of a gradual transition that placed the Bronze Age in the middle of a consistent re-shaping of the society and economy (Peroni, 1979). As for females, the lack of difference observed in all the comparisons suggests a similar pattern of activities through periods with changes that, if present, were not so consistent to produce observable differences in the humeral diaphyseal structure.

The variability in the asymmetry of humeri and in CSG variables has also proved to be of great usefulness in revealing differences in manipulative tasks between males and females (Bridges, 1991; Fresia et al., 1990; Sladek et al., 2007; Weiss, 2003). Iron age males show significantly different humeral characteristics from females coherently with the hypothesis of an increase in gender perception in this period. However, despite the changes that characterized the Bronze Age (Berelov, 2005; Gilman, 1981; Kristiansen, 2014; Macintosh, 2014; Peroni, 1979) the OdN sample sexual dimorphism is found to be non-significant for both bilateral asymmetry and left and right side, supporting the Sladek's (2007) suggestion of a gradual transition.

Pulcini's (2014) palaeobiological analysis – supported by our results – showed an unusual high level of mechanical loadings for females similar to males. Since a coeval sample of comparison is not available, it is not possible to determine whether this characteristic is really unusual in the Bronze Age or not. The lack of a comparative Bronze Age sample from Europe is the main limitation of this study as it prevents us to draw more solid conclusions. Nonetheless, we are confident that this work will be useful for future studies as it proved the necessity of an increase of biomechanical studies to better evaluate the changes that characterized the Bronze Age society.

5. Conclusions

The aim of this study was to use a biomechanical approach to infer the subsistence economy and general behavior of a population of the Middle Bronze Age from the necropolis of Olmo di Nogara, northern Italy. Our results are in general accordance with previous studies. In particular:

- for both females and males, the hypothesis of an exposure to comparable amount of stresses has been demonstrated;
- the social stratification (i.e. the observed presence of an *élite* in the population) proposed by the archaeological investigation is not reflected in an actual division of works inside the OdN society as it may be gleaned from the biomechanical analysis of the humerus;
- previous hypotheses of a gradual transition to the more complex society of the Iron Age have been supported, since Bronze Age and Iron Age differences are not constant for all the variables.

In addition to the evidence in support to previous studies outlined above, new pieces of evidence emerged from the biomechanical analysis of the individuals buried in the OdN necropolis. Although both sexes were probably involved in comparable amount of stresses, the different distribution of load in the humeral cross section suggests a different pattern of activities for males and females. The presence of a preferred anteroposterior direction of loadings in males supports the hypothesis of a sexual division of labor inside the society providing further evidence to one of the actual changes that re-shaped the society during the Bronze Age.

Concerning humeral torsion relation with behavioral pattern, our results are in agreement with previous studies, yet they also highlight the necessity of more

specific studies to better evaluate the correlation between humeral torsion and CSG variables. Moreover, the lack of difference in humeral torsion between sexes could provide partial evidence to our assumption that horse-riding activity affects the degree of humeral torsion (e.g. keeping reins or horse mane). Since this is the first study looking for horse-riding evidence in past population using humeral torsion no comparison samples are available to test the hypothesis. We hope this study will stimulate further studies to test the hypothesis.

To our best knowledge. Only a previous study investigated the biomechanics of the humerus in a European Bronze Age sample (Sladeck et al., 2007). Moreover, studies combining biomechanical and palaeobiological approaches to reconstruct the subsistence economy of a population are also rare. One of the main limitations of this study is the lack of a coeval comparison sample with which our results could be compared. Nonetheless, the strength of this work is in the combination of the palaeobiological and the biomechanical approaches to better understand the numerous changes that happened with the onset of the Bronze Age in Europe. Therefore, we hope that these results could be of inspiration for other researchers in addition to providing a comparison sample to further studies on this topic.

6. Bibliography

Aranda-Jiménez G, Montòn-Subìas S and Jiménez-Brobeil S (2009). Conflicting evidence? Weapons and skeletons in the Bronze Age of south-east Iberia. Antiquity. 83: 1038–1051.

Bankoff ADP (2012). *Biomechanical Characteristics of the Bone*. In: Human Musculoskeletal Biomechanics. Goswami T, editor. InTech, DOI: 10.5772/19690

Berelov I (2006). Signs of sedentism and mobility in an agro-pastoral community during the Levantine Middle Bronze Age: Interpreting site function and occupation strategy at Zahrat adh-Dhra in Jordan. J. Anthropological Archaeology. 25: 117- 143.

Bertram JE, Swartz SM (1991). The ‘‘law of bone transformation’’: a case of crying Wolff? Biol. Rev. Cambridge Philosophic Soc. 66:245–273.

Bridges PS (1991). *Skeletal evidence of changes in subsistence activities between the Archaic and Mississippian time periods in northwestern Alabama*. In: Powell ML, Bridges PS, Mires AMW, editors. What mean these bones? Studies in southeastern bioarchaeology. Tuscaloosa: University of Alabama Press.

Childe VG (1930). The Bronze Age. Cambridge University Press, Cambridge.

Churchill SE (1994). Human upper body evolution in the Eurasian Later Pleistocene. Ph.D. Dissertation, University of New Mexico, Albuquerque.

Churchill SE (1996). Particulate versus integrated evolution of the upper body in late Pleistocene humans: a test of two models. Am. J. Phys. Anthropol. 100: 559–583.

Coles JM, Haring AF (1979). The Bronze Age in Europe: an introduction to the prehistory of Europe c.2000-700 BC. Methuen publishing, London.

Cowin SC (2001). *The false premis in Wolff 's law*. In: SC Cowin, editor. Bone biomechanics handbook, 2nd ed. CRC Press, Boca Raton.

Crockett, HC, Gross, LB, Wilk KE, Schwartz ML, Reed J, O'Mara J, Reilly MT, Dugas, JR, Meister K, Lyman S, Andrews JR (2002). Osseous adaptation and range of motion at the glenohumeral joint in professional baseball pitchers. Am. J. Sports Med. 30: 20–26.

Demes B, Stern JT, Hausman MR, Larson SG, McLeod KJ, Rubin CT (1998). Patterns of strain in the macaque ulna during functional activity. Am. J. Phys. Anthropol. 106: 87–100.

Evans FG (1953). Methods of studying the biomechanical significance of bone form. Am. J. Phys. Anthropol. 11:413–434.

Frayer DW (1980). Sexual dimorphism and cultural evolution in the late Pleistocene and Holocene of Europe. J. Human evol. 9: 399-415.

Fresia AE, Ruff CB, Larsen CS (1990). *Temporal decline in bilateral asymmetry of the upper limb on the Georgia coast*. In: Larsen CS, editor. The archaeology of Mission Santa Catalina de Guale, Part 2: Biocultural interpretations of a population in transition. Anthropological Papers of the American Museum of Natural History, New York.

Gere JM (2001). Mechanics of materials. Fifth edition. Brooks/Cole, Pacific Grove, CA.

Gilman A (1981). The Development of Social Stratification in Bronze Age Europe. Curr. Anthropology. 22: 1-23.

Hamilton ME (1982). *Sexual dimorphism in skeletal samples*. In: Hall RL, editor. Sexual dimorphism in Homo sapiens. Praeger, New York.

Herman GT, (2009). Fundamentals of Computerized Tomography: Image Reconstruction from Projections. Second edition. Springer, London.

Hughes S (2011). *CT Scanning in Archaeology*. In: Saba L., editor. Computed Tomography - Special Applications. InTech, DOI: 10.5772/22741.

Ibanez-Gimeno P, De Esteban-Trivigno S, Jordana X, Manyosa J, Malgosa A, Galtés I (2013). Functional plasticity of the human Humerus: shape, rigidity and muscular Entheses. Am. J. Phys. Anthropol. 150: 609-617.

Krahl, VE (1947). The torsion of the humerus: its localization, cause, and duration in man. Am. J. Anat. 80: 275‑319.

Kristiansen K (2002). The tale of the sword – swords and swordfighters in Bronze Age Europe. Oxford Journal of Archaeology. 21: 319-332.

Kristiansen K (2014). *The Decline of the Neolithic and the Rise of Bronze Age Society*. In: Fowler C, Harding J, Hofmann D, editors. The Oxford Handbook of Neolithic Europe. Oxford Handbooks Online.

Lanyon LE (1982). *Mechanical function and bone remodeling*. In: Sumner-Smith G, editor. Bone in clinical orthopaedics. Saunders, Philadelphia.

Lanyon LE, Goodship AE, Pye CJ, MacFie GH (1982). Mechanically adaptive bone remodeling. J Biomechanics. 15: 141-154.

Larson SG (2007). Evolutionary transformation of the hominin shoulder. Evol. Anthropol. 16: 172–187.mer

Levine MA (1999). Botai and the Origins of Horse Domestication. Journal of Anthropological Archaeology. 18: 29–78.

Levy JE (1979). Evidence of Social Stratification in Bronze Age Denmark. Journal of Field Archaeology. 6: 49-56.

Lieberman DE, Polk JD, Demes B (2004). Predicting long bone loading from Cross-Sectional Geometry. Am. J. Phys. Anthropol. 123: 156-171.

Lovejoy CO, Burstein AH, Heiple KG (1976). The biomechanical analysis of bone strength: a method and its application to Platycnemia. Am. J. Phys. Anthropol. 44: 489-506.

Lovejoy CO, McCollum MA, Reno PL, Rosenman BA (2003). Developmental biology and human evolution. Annu. Rev. Anthropol. 32: 85–109.

Macintosh AA, Pinhasi R, Stock JT (2014). Divergence in Male and Female Manipulative Behaviors with the Intensification of Metallurgy in Central Europe. PLoS ONE 9(11): e112116. doi:10.1371/journal.pone.0112116.

Marchi D (2004). Cross-sectional geometry of the limb bones of the hominoidea: its relationships with locomotion and posture. PhD thesis, University of Pisa.

Marchi D (2007). Relative strength of the tibia and fibula and locomotor behavior in Hominoids. J. Hum. Evol. 53: 647-655.

Marchi D, Sparacello VS (2006) Cross-sectional geometry of the humerus of a Western Liguria Neolithic sample. Atti del XVI Congresso degli Antropologi Italiani (Genova, 29-31 ottobre 2005) Edicolors Publishing, p. 631-640.

Marchi D, Sparacello VS, Holt BM, Formicola V (2006). Biomechanical Approach to the Reconstruction of Activity Patterns in Neolithic Western Liguria, Italy. Am. J. Phys. Anthropol. 131: 447–455.

Marchi D, Sparacello VS, Shaw CN (2011). *Mobility and Lower Limb Robusticity of a Pastoralist Neolithic Population from North-Western Italy*. In: Pinhasi R,

Stock JT, editors. Human Bioarchaeology of the Transition to Agriculture. Wiley online library.

Megson THG (2005). Structural and Stress Analysis. Second Edition. Elsevier Butterworth-Heinemann, Oxford.

Mercuri AM, Accorsi CA, Bandini Mazzanti M, Bosi G, Cardarelli A, Labate D, Marchesini M, Trevisan Grandi G (2006). Economy and environment of Bronze Age settlements – Terramaras – on the Po Plain (Northern Italy): first results from the archaeobotanical research at the Terramara di Montale. Veget. Hist. Archaeobot. 16: 43–60

Meyer H von (1867). Die architecture der spongiosa. Arch. Anat. Physiol. 34: 615-628.

Natterer F (2001). The mathematics of computerized tomography. SIAM, Philadelphia.

Nunziante L, Gambarotta L, Tralli A (2011). *La trave secondo De Saint Venant*. In: McGraw-Hill Education, editor. Scienza delle costruzioni. McGraw-Hill, Italy.

Ogilvie MD, Hilton CE (2011). Cross Sectional Geometry in the humeri of foragers and farmers from the Prehispanic American Southwest: exploring patterns in the sexual division of labor. Am. J. Phys. Anthropol. 144: 11-21.

Osbahr, DC, Cannon, DL, Speer, KP (2002). Retroversion of the humerus in the throwing shoulder of college baseball pitchers. Am. J. Sports Med. 30: 347–353.

Peroni, R (1979). *From Bronze age to Iron age: economic, historical and social considerations*. In: Ridgway D and Ridgway FR, editors. Italy before the Romans. Academic Press, London.

Pieper HG (1998). Humeral torsion in the throwing arm of handball players. Am. J. Sports Med. 26: 247–253.

Platzer W (2007). Anatomia Umana - Atlante tascabile. Volume 1, Apparato Locomotore. Quarta edizione. Casa Editrice Ambrosiana, Rozzano.

Pulcini L (2014). La necropoli di Olmo di Nogara (Verona). Studio paleobiologico dei resti umani per la ricostruzione dell'organizzazione di una comunità dell'Età del bronzo padana. PhD Thesis, Università di Padova.

Reagan KM, Meister K, Horodyski MB, Werner DW, Carruthers C, Wilk, K (2002). Humeral retroversion and its relationship to glenohumeral rotation in the shoulder of college baseball players. Am. J. Sports Med. 30: 354–360.

Rhodes JA (2004). Humeral torsion and activity related change in the human upper limb and pectoral girdle. PhD thesis, University of Bradford.

Rhodes JA (2006). Adaptation to humeral torsion in Medieval Britain. Am. J. Phys. Anthropol. 130:160-166.

Rhodes JA, Churchill SE (2009). Throwing in the Middle and Upper Paleolithic: inferences from an analysis of humeral retroversion. J. Hum. Evol. 56: 1-10.

Rhodes JA, Knusel CJ (2005). Activity-Related Skeletal Change in Medieval Humeri: Cross-Sectional and Architectural Alterations. Am. J. Phys. Anthropol. 128: 536-546.

Riga A (2008). Robustezza strutturale e marcatori di stress muscoloscheletrico a confronto in un campione dell'Età del Bronzo. MSc thesis, Università di Pisa.

Roux W (1885). Beitrage zur morphologie der funktionellen anpassung. Archiv. Anat. Physiol. Anat. Abt. 9: 120-158.

Ruff CB (2000b). Body size, body shape, and long bone strength in modern humans. J. Hum. Evol. 38: 269–290.

Ruff CB (2002). Long bone articular and diaphyseal structure in Old World monkey and apes. I: locomotor effects. Am J. Phys. Anthropol. 119: 305-342.

Ruff CB (2003). Long bone articular and diaphyseal structure in old world monkeys and apes. II: estimation of body mass. Am. J. Phys. Anthropol. 120:16-37.

Ruff CB (2008). Biomechanical analysis of archaeological human skeletons. In: Katzenberg MA and Saunders SR, editors. Biological Anthropology of the Human skeleton. Second Edition. John Wiley & Sons, New Jersey.

Ruff CB, Hayes WC (1983) Cross-sectional geometry of Pecos pueblo femora and tibiae – a biomechanical investigation: I. method and general patterns of variation. Am J. Phys. Anthropol. 60: 359-381.

Ruff CB, Holt B, Trinkaus E (2006). Who's afraid of the big bad Wolff?: "Wolff's law" and bone functional adaptation. Am J. Phys. Anthropol. 129: 484-498.

Ruff CB, Runestad JA (1992). Primate limb bone structural adaptations. Ann. Rev Anthropol. 21: 407-433.

Ruff CB, Walker A, Trinkaus E (1994) Postcranial robusticity in Homo. III. Ontogeny. Am. J. Phys. Anthropol 93: 35–54.

Salzani L (2005). La Necropoli dell'Età del Bronzo all'Olmo di Nogara. Memorie del Museo Civico di Storia Naturale di Verona - serie sezione scienze dell'uomo, Verona.

Shennan S (1975). The social organization at Branc. Antiquity 49: 279-88.

Shennan SJ (1993). Settlement and social change in Central Europe. J. World Prehistory. 7:121–161.

Sladek V, Berner M, Sosna D, Sailer R (2007). Human Manipulative Behavior in the Central European Late Eneolithic and Early Bronze Age: Humeral Bilateral Asymmetry. Am. J. Phys. Anthropol. 133: 669-81.

Sørensen MLS (1997) Reading Dress: The Construction of Social Categories and Identities in Bronze Age Europe. Journal of European Archaeology. 5: 93-114

Sparacello VS (2015). The bioarchaeology of changes in social stratification, warfare and habitual activities among Iron Age Samnites of Central Italy. PhD thesis, University of New Mexico.

Sparacello VS, D'Ercole V, Coppa A (2014). A bioarchaeological approach to the reconstruction of changes in military organization among Iron Age Samnites (Vestini) from Abruzzo, Central Italy. Am. J. Phys. Anthropol. 156: 305-316.

Sparacello VS, Marchi D (2008). Mobility and Subsistence Economy: A Diachronic Comparison Between Two Groups Settled in the Same Geographical Area (Liguria, Italy). Am. J. Phys. Anthropol. 136: 485–495.

Sparacello VS, Marchi D, Shaw CN (2014). The Importance of Considering Fibular Robusticity When Inferring the Mobility Patterns of Past Populations. KJ Carlson and D Marchi (eds.), Reconstructing Mobility: Environmental, Behavioral and Morphological Determinants. Springer, New York.

Sparacello VS, Pearson OM, Coppa A, Marchi D (2011). Changes in Skeletal Robusticity in an Iron Age Agropastoral Group: The Samnites from the Alfedena Necropolis (Abruzzo, Central Italy). Am. J. Phys. Anthropol. 144: 119-130.

Steele DG, Bramblett CA (2012). The Anatomy and Biology of the Human Skeleton. Ninth Printing. Texas A&M University press, College Station.

Stock JT, O'Neill MT, Ruff CB, Zabecki M, Shackelford L, Rose JC (2011). Body size, skeletal biomechanics, mobility and habitual activity from the Late Palaeolithic to the Mid-Dynastic Nile Valley. Human Bioarchaeology of the Transition to Agricolture. 14: 347-367.

Trinkaus E (1980). Sexual differences in Neanderthal limb bones. J. Human evol. 9: 377-397.

Weiss E (2003). Understanding muscle markers: aggregation and construct validity. Am. J. Phys. Anthropol. 121: 230–240.

White TD, Black MT, Folkens PA (2012). Human Osteology. Third Edition. Elsevier Academic Press, San Diego.

7. Appendices

7.1 *Appendix I – Tombs detailed information*

All the information and tombs images contained in this section are from Salzani (2005) and Pulcini (2014).

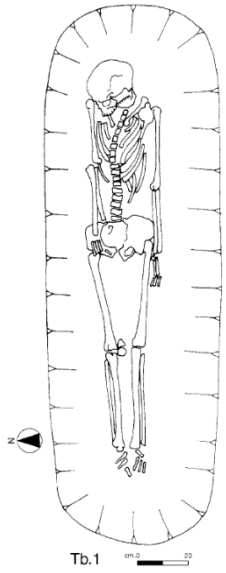

Tomb - Area: 1 - A

Sex: male

Age at death: 30-40

General information: rectangular fossa of 180 x 45 cm. Adult individual laid down with the head reclined on the right shoulder and parallel legs. Oriented in E-W direction. Estimated height 161,7 cm.

Grave goods: none.

Pathologies: none.

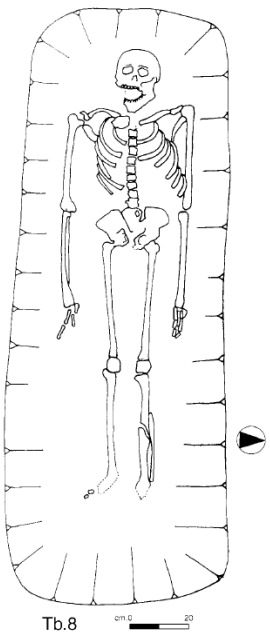

Tomb - Area: 8 - A

Sex: male

Age at death: 40-50

General information: rectangular fossa of 175 x 60 cm. Adult individual laid down supine with parallel legs. Oriented in W-E direction. Estimated height 169,2 cm.

Grave goods: none.

Pathologies: none.

Tomb - Area: 16 - A

Sex: female

Age at death: 55-65

General information: rectangular fossa of 175 x 50 cm. Adult individual laid down supine with the left arm bent on the pelvis and convergent legs. Oriented in E-W direction. Estimated height 155 cm.

Grave goods: two hair ties formed by bronze filaments (A and B).

Pathologies: hidden cleft spine.

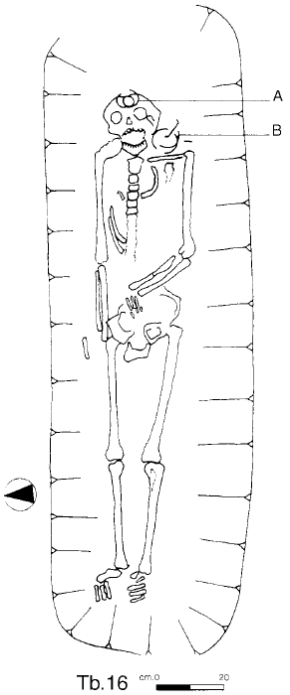

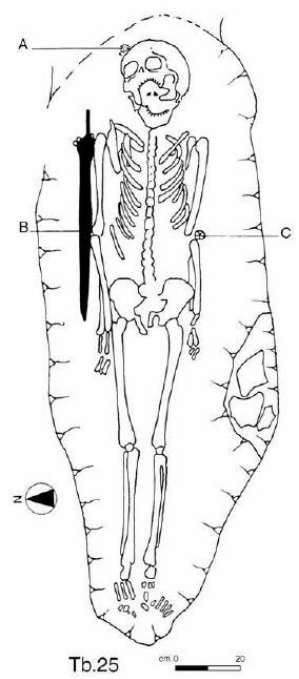

Tomb - Area: 25 - C

Sex: male

Age at death: 45-55

General information: elliptical fossa of 200 x 70 cm. Adult individual laid down supine with back-reclined head and convergent legs. Oriented in E-W direction. Estimated height 160,9 cm.

Grave goods: Three studs (A), one sword (B), a flint pebble (C) and pieces of a broken vase on the side.

Pathologies: none.

Tomb - Area: 28 - C

Sex: male

Age at death: 35-45

General information: rectangular fossa of 180 x 60 cm. Adult individual laid down supine with the head reclined on the right shoulder and convergent legs. Oriented in E-W direction. Estimated height 168,8 cm.

Grave goods: one sword (A).

Pathologies: none.

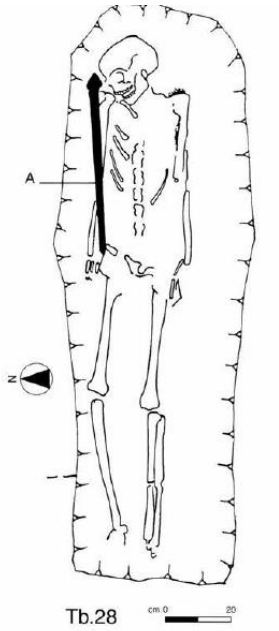

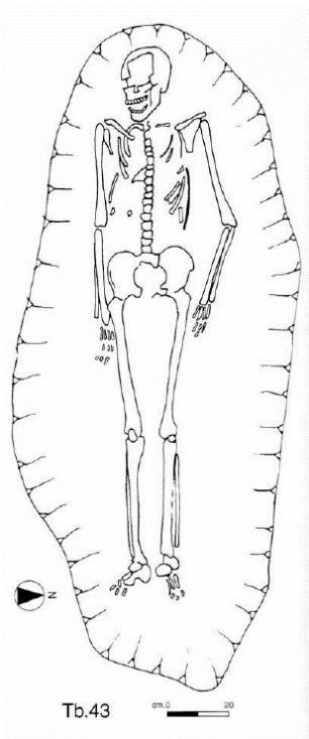

Tomb - Area: 43 - C

Sex: male

Age at death: 35-45

General information: elliptical fossa of 225 x 95 cm. Adult individual laid down supine with the head slightly reclined, the left arm bent and convergent legs. Oriented in W-E direction. Estimated height 182,2 cm.

Grave goods: none.

Pathologies: none.

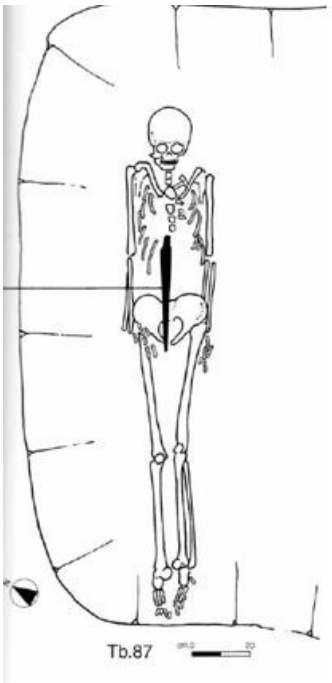

Tomb - Area: 87 - C

Sex: male

Age at death: 35-45

General information: quadrangular fossa of 220 x 210 cm. Adult individual laid down supine with convergent legs and buried together with the individual 88. Oriented in NE-SW direction. Estimated height 167,8 cm.

Grave goods: one sword on the chest.

Pathologies: none.

Tomb - Area: 89 - C

Sex: female

Age at death: 40-50

General information: rectangular fossa of 210 x 85 cm. Adult individual laid down supine with head pointed to the right side and convergent legs. Oriented in NE-SW direction. Estimated height 156,60 cm.

Grave goods: One brooch on the neck (A), two brooches on the chest (B-C) with amber pearls (D-E) and bronze fragments near the skull (F).

Pathologies: none.

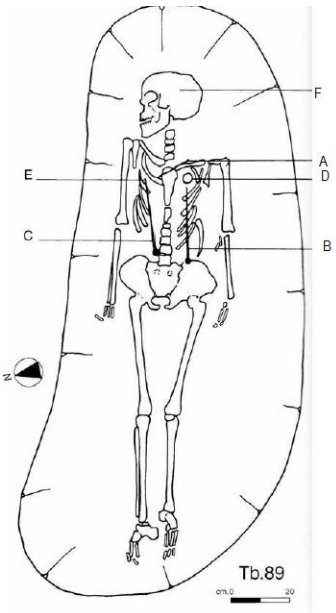

Tomb - Area: 94 - C

Sex: female

Age at death: 35-45

General information: quadrangular fossa of 185 x 80 cm. Adult individual laid down supine with head reclined on the right side, bended shoulders and hands laid on the pelvis. Oriented in E-W direction. Estimated height 158 cm.

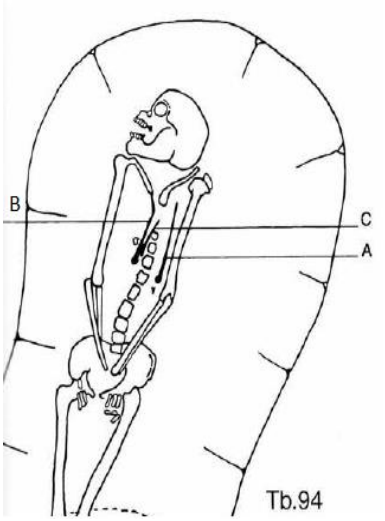

Grave goods: Two brooches on the chest (A-B) and one on the spinal cord (C).

Pathologies: none.

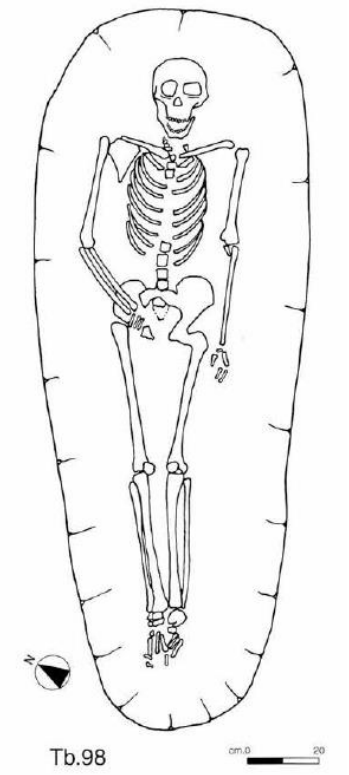

Tomb - Area: 98 - C

Sex: female

Age: 20-25

General information: rectangular fossa of 209 x 78 cm. Adult individual laid down supine with convergent legs and the right arm bent on the pelvis. Oriented in NE-SW direction. Estimated height 160,8 cm.

Grave goods: none.

Pathologies: none.

Tomb - Area: 99 - C

Sex: male

Age: 30-40

General information: rectangular fossa of 230 x 135 cm. Adult individual laid down supine with head reclined on the left side and convergent legs. Oriented in NE-SW direction. Estimated height 159,6 cm.

Grave goods: some studs near the skull (A) and a sword on the pelvis (B).

Pathologies: none.

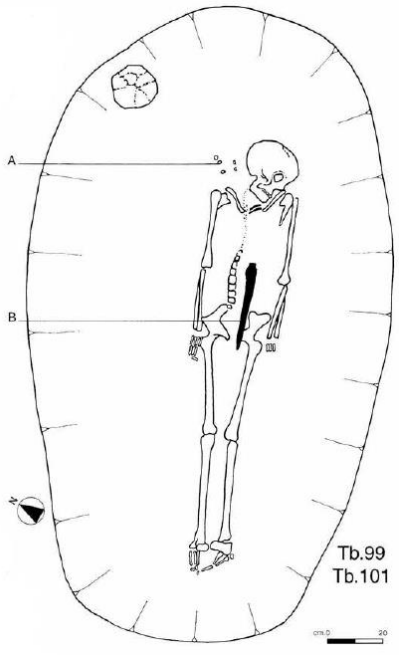

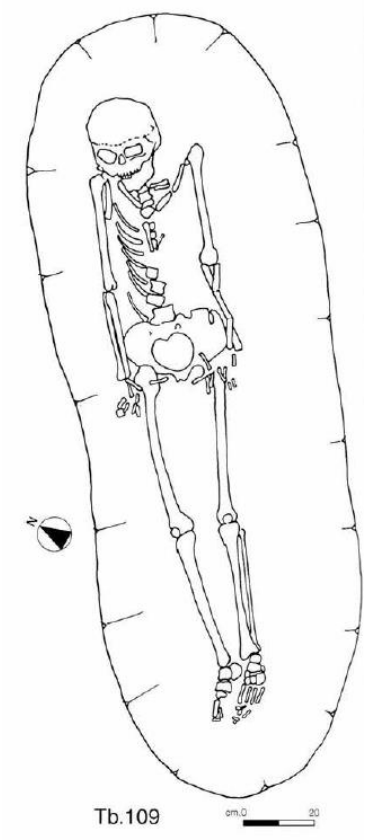

Tomb - Area: 109 - C

Sex: male

Age: 40-50

General information: quadrangular fossa of 230 x 60 cm. Adult individual laid down supine with convergent legs. Oriented in NE-SW direction. Estimated height 173,8 cm.

Grave goods: none.

Pathologies: none.

Tomb - Area: 110 - C

Sex: female

Age: 30-40

General information: rectangular fossa of 200 x 60 cm. Adult individual laid down supine with convergent legs and the skeleton of an infant on the right arm. Oriented in NE-SW direction. Estimated height 154,8 cm.

Grave goods: Two brooches (A-B) and a stud (C) on the chest.

Pathologies: none.

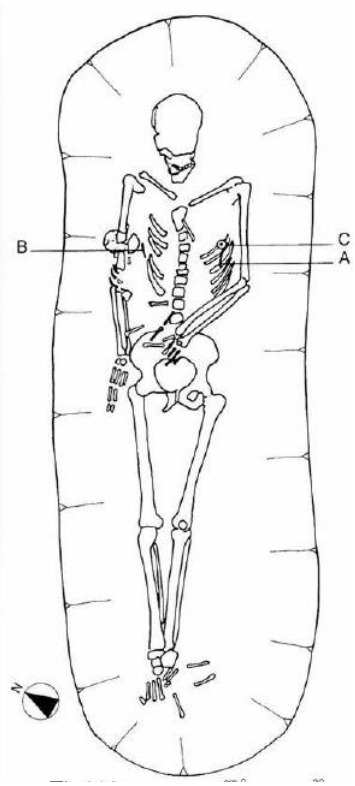

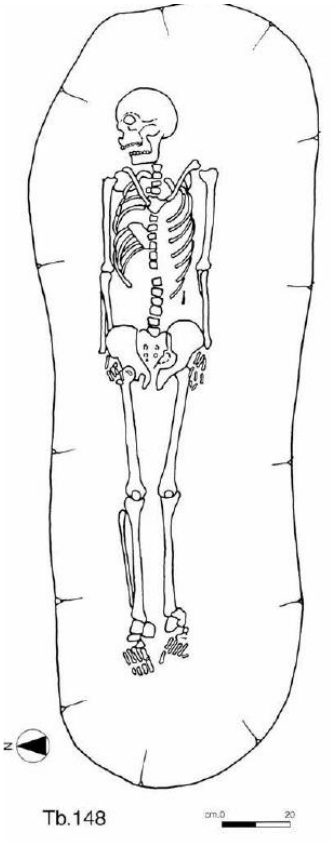

Tomb - Area: 148 - C

Sex: male

Age: 45-55

General information: rectangular fossa of 240 x 80 cm. Adult individual laid down supine with the head pointed in the right side. Oriented in E-W direction. Estimated height 162,5 cm.

Grave goods: none.

Pathologies: none.

Tomb - Area: 159 - C

Sex: female

Age: 40-50

General information: rectangular fossa of 165 x 55 cm. Adult individual laid down supine with the head pointed in the left direction, right arm bent over the pelvis and parallel legs. Oriented in E-W direction. Estimated height 156,1 cm.

Grave goods: none.

Pathologies: none.

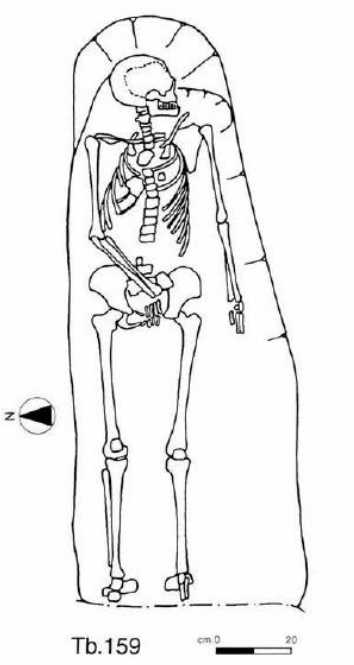

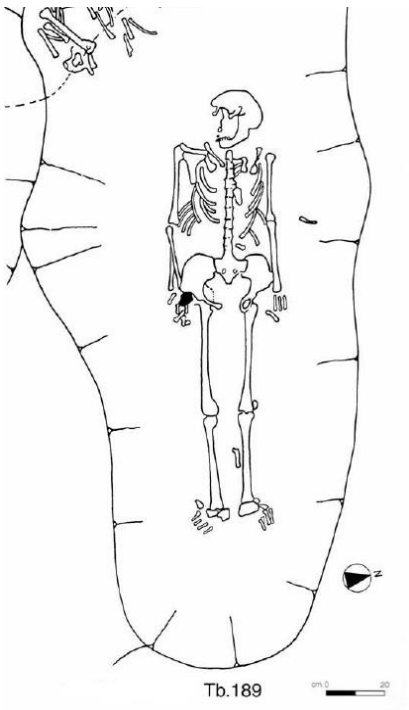

Tomb - Area: 189 - C

Sex: female

Age: 50-60

General information: rectangular fossa of 240 x 90 cm that intersects the tomb 188. Adult individual laid down supine with the head pointed to the right side and parallel legs. Oriented in W-E direction. Estimated height not available.

Grave goods: none.

Pathologies: none.

Tomb - Area: 202 - C

Sex: male

Age: 30-35

General information: rectangular fossa of 255 x 105 cm. Adult individual laid down supine with parallel legs. Oriented in NE-SW direction. Estimated height 162,8 cm.

Grave goods: a sword near the right arm.

Pathologies: none.

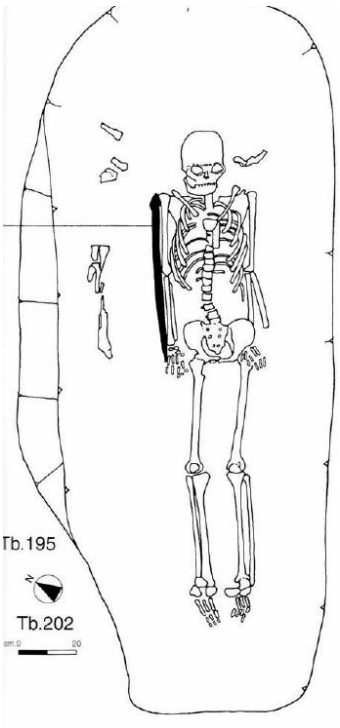

Tomb - Area: 223 - C

Sex: female

Age: 20-25

General information: elliptical fossa of 160 x 70 cm. Adult individual laid down supine, slightly bent in the right direction with head reclined on the right side and the left hand located on the pelvis. Oriented in E-W direction. Estimated height 147 cm.

Grave goods: none.

Pathologies: spondylolysis.

(Map of the tomb not available.)

Tomb - Area: 225 - C

Sex: female

Age: 20-25

General information: rectangular fossa of 180 x 85 cm. Adult individual laid down prone with head pointed to the right side and both hands located under the pelvis. Oriented in NW-SE direction. Estimated height 153,3 cm.

Grave goods: hair tie formed by bronze filaments (A).

Pathologies: none.

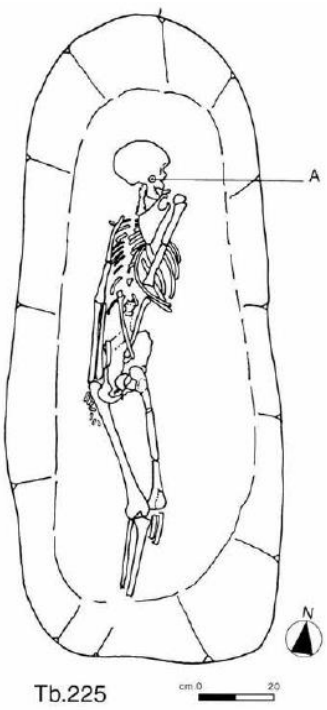

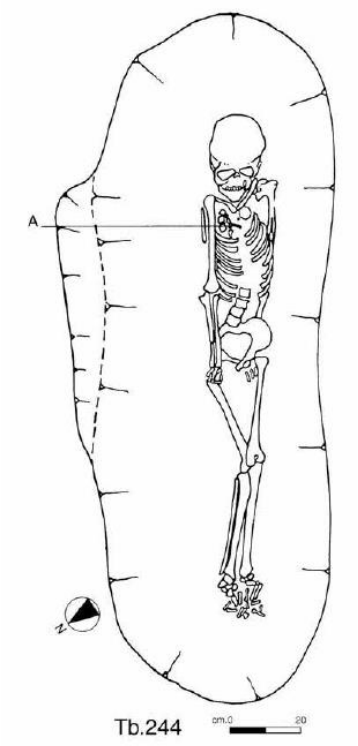

Tomb - Area: 244 - C

Sex: female

Age: 25-30

General information: rectangular fossa of 200 x 65 cm. Adult individual laid down supine with convergent legs. Oriented in SE-NW direction. Estimated height 156 cm.

Grave goods: one brooch made of bone (A).

Pathologies: spondylolysis.

Tomb - Area: 287 - C

Sex: female

Age: 35-45

General information: partially unlimited fossa of approximately 180 x 65 cm. Adult individual laid down supine on the skeleton of the individual 288 and with crossed feet. Oriented in NE-SW direction. Estimated height 149,3 cm.

Grave goods: one brooch under the chin (A), one under the skull (B) and the fragment of another one placed on the skull (C).

Pathologies: none.

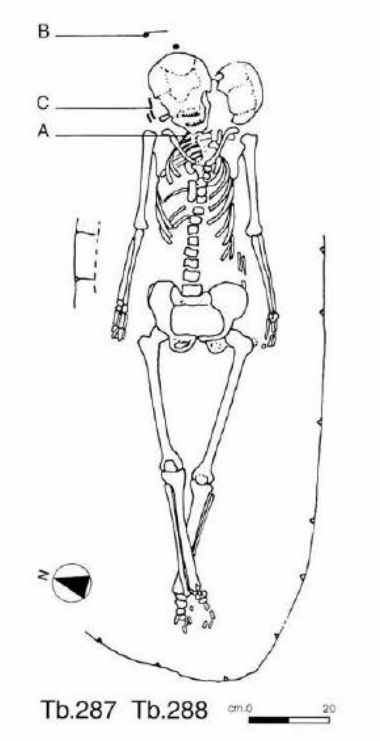

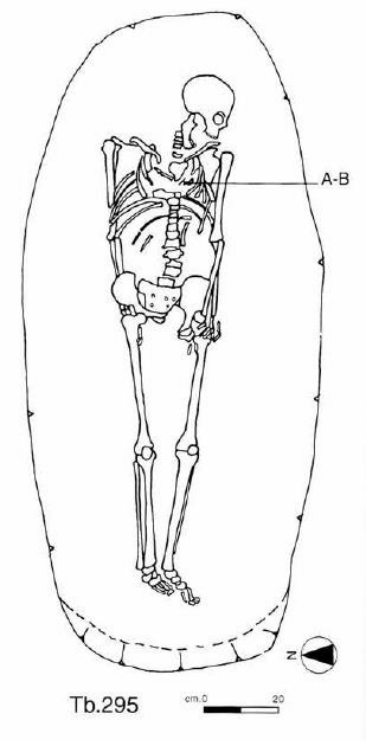

Tomb - Area: 295 - C

Sex: female

Age: 45-55

General information: elliptical fossa of 180 x 80 cm. Adult individual laid down supine with the head reclined on the left shoulder and convergent legs. Oriented in E-W direction. Estimated height 156 cm.

Grave goods: a fragment of a brooch (A) and a pearl (B) on the chest.

Pathologies: none.

Tomb - Area: 297 - C

Sex: female

Age: 50-60

General information: elliptical fossa of 195 x 85 cm that crosses the tomb 304. Adult individual laid down supine with the head pointed to the right direction, the hands placed on the pelvis and parallel legs. Oriented in E-W direction. Estimated height 155,4 cm.

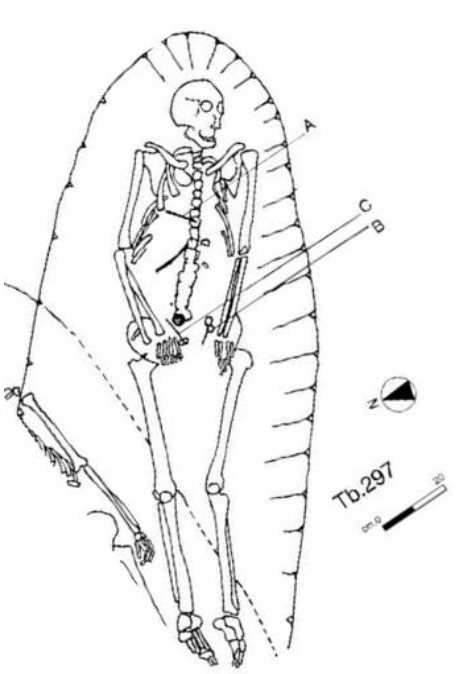

Grave goods: a needle on the chest (A) and two brooches on the pelvis (B-C).

Pathologies: none.

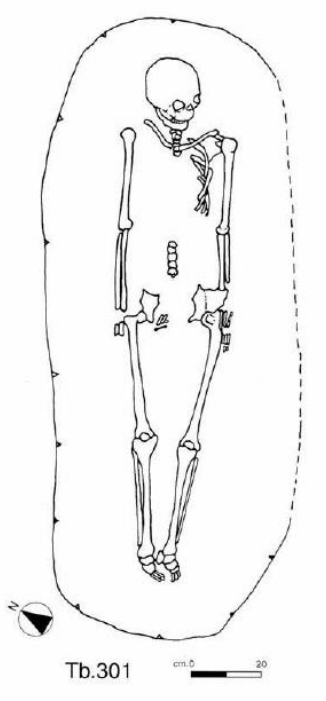

Tomb - Area: 301 - C

Sex: female

Age: 35-45

General information: rectangular fossa of 180 x 70 cm. Adult individual laid down supine with the head slightly pointed to the left direction and convergent legs. Oriented in NE-SW direction. Estimated height 155,5 cm.

Grave goods: none.

Pathologies: none.

Tomb - Area: 316 - C

Sex: female

Age: 50-60

General information: rectangular fossa of 148 x 62 cm. Adult individual laid down supine with the head slightly pointed to the right direction, both arms crossed on the pelvis and convergent legs. Oriented in NE-SW direction. Estimated height 154,6 cm.

Grave goods: one brooch under the left femur (A), another one on the pelvis (B) and some fragments of a needle near the skull (C).

Pathologies: none.

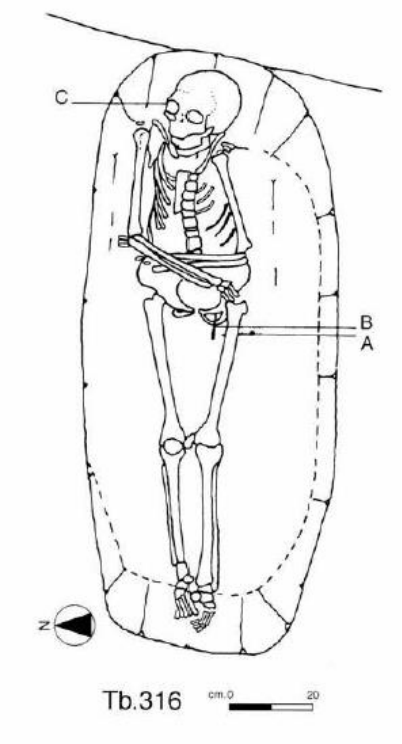

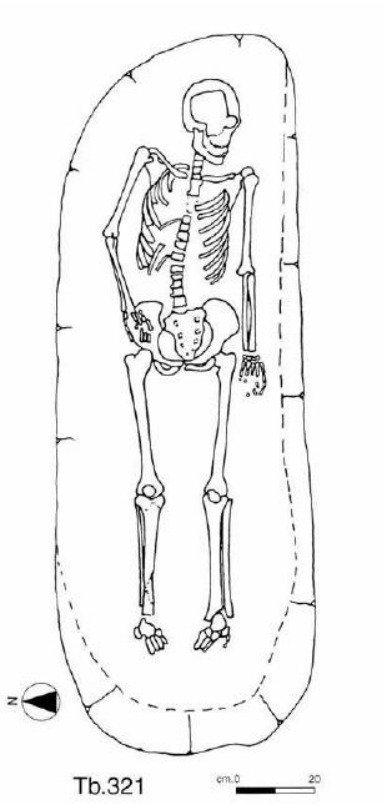

Tomb - Area: 321 - C

Sex: female

Age: 35-45

General information: rectangular fossa of 190 x 65 cm. Adult individual laid down supine with the head slightly pointed to the left direction, the right hand on the pelvis and parallel legs. Oriented in NE-SW direction. Estimated height 150,7 cm.

Grave goods: none.

Pathologies: none.

Tomb - Area: 360 - C

Sex: female

Age: 45-55

General information: rectangular fossa of 175 x 55 cm. Adult individual laid down supine with the head pointed to the right direction and parallel legs. Oriented in N-S direction. Estimated height 152,9 cm.

Grave goods: none.

Pathologies: none.

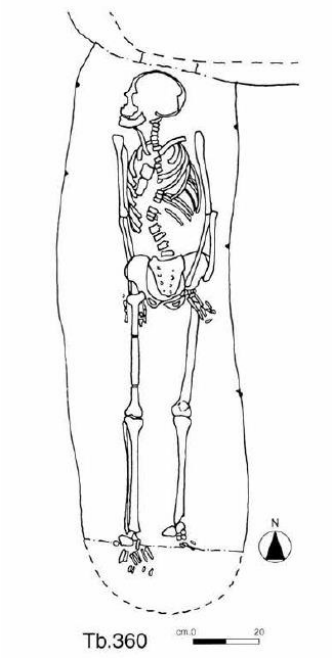

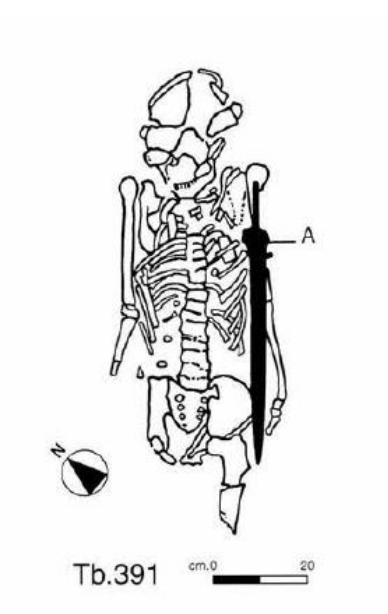

Tomb - Area: 391 - B

Sex: male

Age: 30-40

General information: margins of the fossa non-visible. Adult individual laid down supine with the head reclined on the right shoulder. Oriented in NE-SW direction. Estimated height 158,7 cm.

Grave goods: one sword on the left arm (A).

Pathologies: none.

Tomb - Area: 411 - B

Sex: female

Age: 50-60

General information: rectangular fossa of 290 x 110 cm. Adult individual laid down supine with convergent legs. Oriented in NE-SW direction. Estimated height 158,9 cm.

Grave goods: one bowl behind the skull (A), one hair pin on the left side of the skull (B) and another on the right side (M), two brooches on the chest (D-C) and another on the pelvis (F), a little dagger on the chest (E), an amber pearl on the right forearm (G) and another on the left forearm (H), one fragment of a needle behind the skull (I) and one horn comb oh the chest (L).

Pathologies: none.

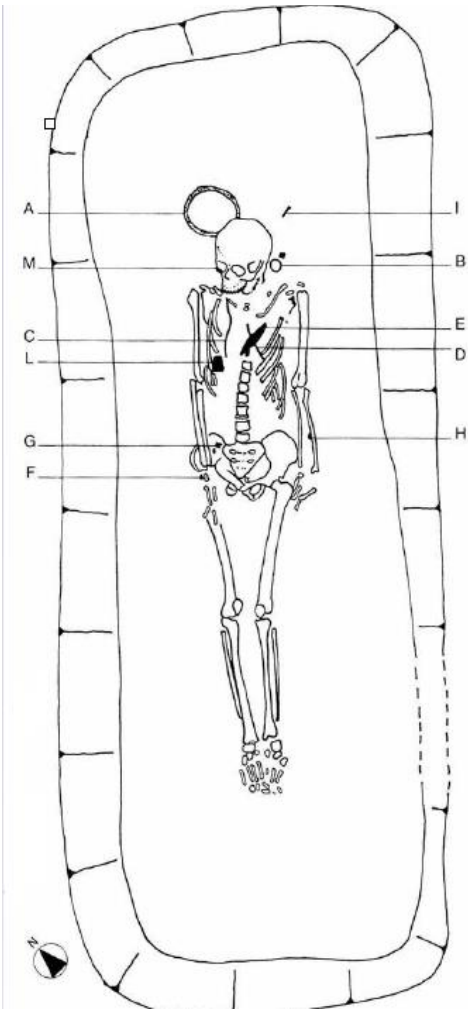

Tomb - Area: 413 - B

Sex: male

Age: 20-25

General information: rectangular fossa of 210 x 80 cm. Adult individual laid down supine with parallel legs. Oriented in NE-SW direction. Estimated height 160,5 cm.

Grave goods: none.

Pathologies: none.

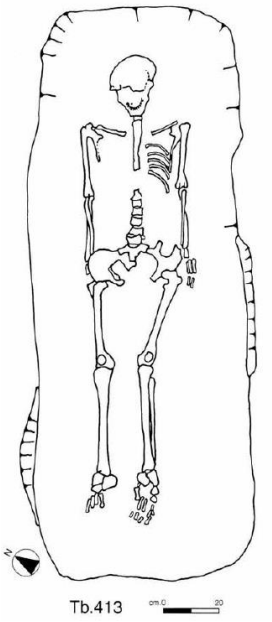

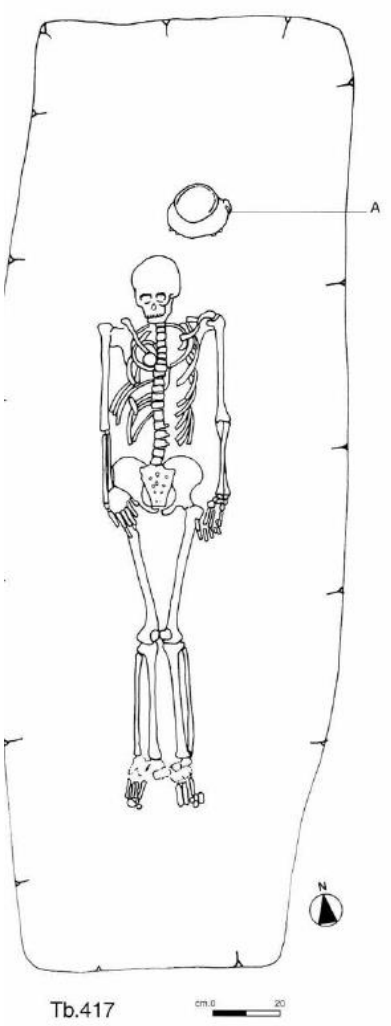

Tomb - Area: 417 - B

Sex: male

Age: 40-50

General information: rectangular fossa of 292 x 110 cm. Adult individual laid down supine with convergent legs. Oriented in NE-SW direction. Estimated height 160,5 cm.

Grave goods: one bowl behind the skull (A).

Pathologies: none.

Tomb - Area: 418 - B

Sex: male

Age: 40-50

General information: margins of the fossa only partially visible. Adult individual laid down supine with the hands on the pelvis and parallel legs. Oriented in NE-SW direction. Estimated height 164,4 cm.

Grave goods: none.

Pathologies: none.

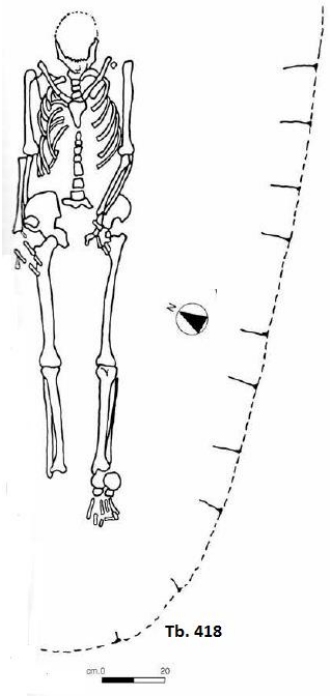

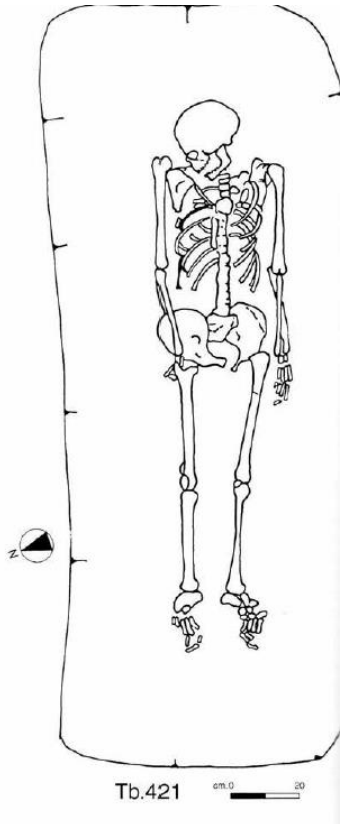

Tomb - Area: 421 - B

Sex: male

Age: 30-35

General information: rectangular fossa of 227 x 95 cm. Adult individual laid down supine with the head reclined on the right shoulder and parallel legs. Oriented in SE-NW direction. Estimated height 173,5 cm.

Grave goods: none.

Pathologies: none.

Tomb - Area: 439 - B

Sex: female

Age: 50-60

General information: rectangular fossa of 210 x 105 cm. Adult individual laid down supine with the head pointed to the left direction and parallel legs. Oriented in SE-NW direction. Estimated height 149,6 cm.

Grave goods: none.

Pathologies: none.

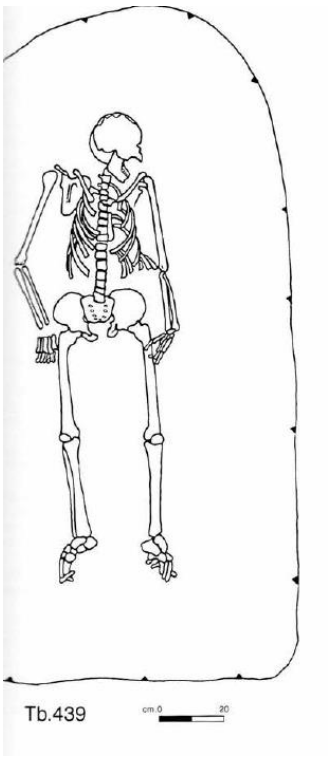

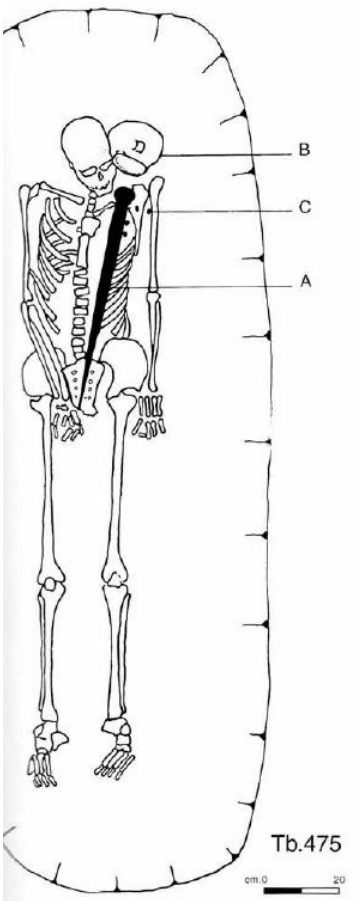

Tomb - Area: 475 - B

Sex: male

Age: 35-45

General information: rectangular fossa of 240 x 85 cm. Adult individual laid down supine with parallel legs. Oriented in SE-NW direction. Estimated height 174,5 cm.

Grave goods: a sword on the chest (A), a bowl on the left side of the skull (B) and a circle of 11 studs on the left side of the chest (C).

Pathologies: hidden cleft spine.

Tomb - Area: 476 - B

Sex: male

Age: >55

General information: rectangular fossa of 240 x 75 cm. Adult individual laid down supine with the head pointed to the left side, both the hands on the pelvis and convergent legs. Oriented in SE-NW direction. Estimated height 165,8 cm.

Grave goods: none.

Pathologies: none.

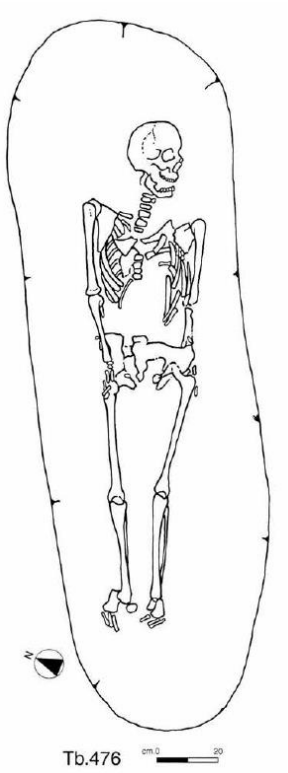

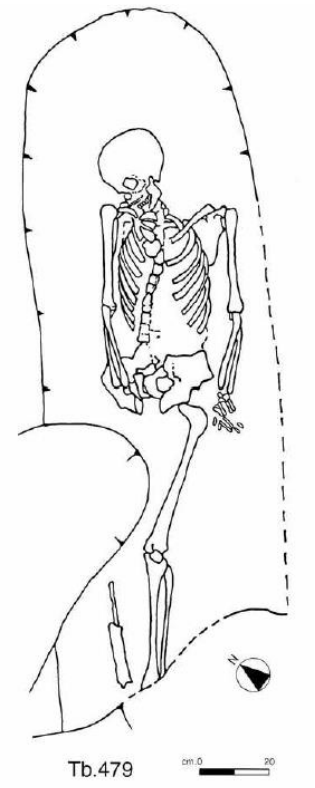

Tomb - Area: 479 - B

Sex: male

Age: 18-21

General information: rectangular fossa of 210 x 70 cm. Young adult individual laid down supine with the head reclined on the right shoulder and convergent legs. Oriented in NE-SW direction. Estimated height 167,9 cm.

Grave goods: none.

Pathologies: none.

Tomb - Area: 484 - B

Sex: male

Age: 40-50

General information: rectangular fossa of 220 x 95 cm. Adult individual laid down supine with the head slightly reclined on the right shoulder and convergent legs. Oriented in NE-SW direction. Estimated height 166,5 cm.

Grave goods: a sword on the left arm.

Pathologies: none.

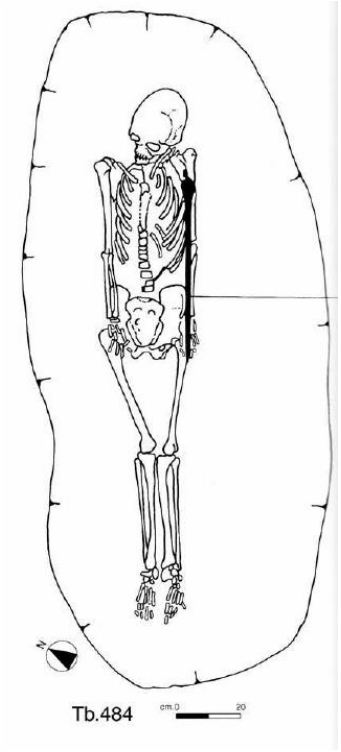

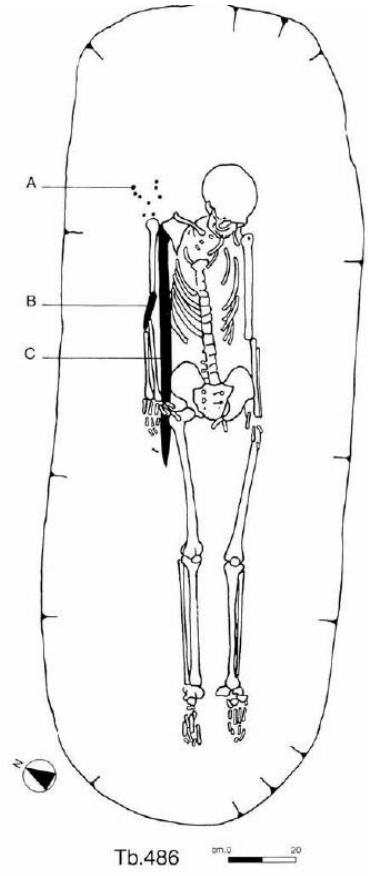

Tomb - Area: 486 - B

Sex: male

Age: 35-45

General information: rectangular fossa of 255 x 80 cm. Adult individual laid down supine with the head reclined on the left shoulder and parallel legs. Oriented in NE-SW direction. Estimated height 168,8 cm.

Grave goods: some studs on the right side of the skull (A), a dagger on the right arm (B) and a sword between the right arm and the body (C).

Pathologies: none.

Tomb - Area: 500 - B

Sex: male

Age: 35-45

General information: rectangular fossa of 230 x 100 cm. Adult individual laid down supine with the right arm on the pelvis and convergent legs. Oriented in NE-SW direction. The head is positioned in a recess located in the NW direction with respect to the fossa. Estimated height 163,7 cm.

Grave goods: a sword (A) and a dagger on the left arm (B).

Pathologies: sinus infection.

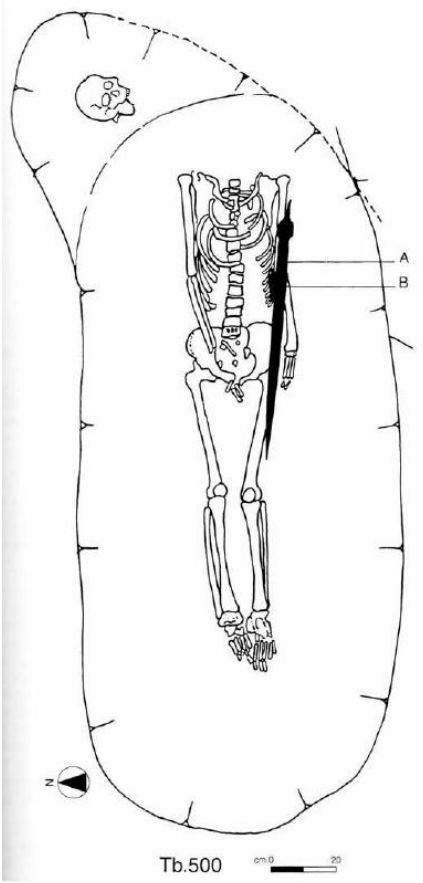

7.1.1 *Raw data*

ID	Side	Sex	Age	BME	CA	Ix	Iy	Imax	Imin	J	I_{max}/I_{min}	I_x/I_y	%CA	HT	Gr. goods
OdN01	L	M	35	56,69	204,71	5944,8	4562,6	5993,3	4514,0	10507,3	1,33	1,30	78,55	32,60	0
OdN01	R	M	35	56,69	230,67	7177,2	5949,1	7552,6	5573,7	13126,3	1,36	1,21	79,58	41,30	0
OdN08	L	M	45	59,97	239,53	7941,8	6074,7	8543,6	5472,9	14016,5	1,56	1,31	80,26	26,20	0
OdN08	R	M	45	59,97	251,50	7666,2	7031,4	8612,9	6084,7	14697,6	1,42	1,09	82,28	22,90	0
OdN16	L	F	50	47,10	189,81	6305,2	6352,3	6412,1	6245,3	12657,4	1,03	0,99	17,02	11,70	1
OdN16	R	F	50	47,10	167,32	4696,4	5135,1	5366,8	4464,7	9831,5	1,20	0,91	63,64	16,30	1
OdN25	L	M	50	58,47	208,85	5712,0	4106,9	5712,5	4106,4	9819,0	1,39	1,39	83,70		1
OdN25	R	M	50	58,47	250,25	7282,8	6181,9	7393,2	6071,5	13464,7	1,22	1,18	85,71		1
OdN28	L	M	40	59,48	220,18	5771,2	5196,7	5949,6	5018,3	10967,9	1,19	1,11	83,10	37,10	1
OdN28	R	M	40	59,48	242,47	7244,3	6508,8	7401,9	6351,2	13753,1	1,17	1,11	81,50	37,70	1
OdN43	L	M	40	76,33	226,77	6844,0	5340,3	6844,0	5340,3	12184,3	1,28	1,28	81,33	9,70	0
OdN43	R	M	40	76,33	232,74	7136,1	5597,3	7142,8	5590,5	12733,4	1,28	1,27	81,86	19,70	0
OdN87	L	M	40	61,60	245,02	7096,5	5175,5	7112,1	5159,9	12272,0	1,38	1,37	88,68	11,40	1
OdN87	R	M	40	61,60	257,50	7245,1	5469,0	7252,0	5462,0	12714,0	1,33	1,32	91,66	25,40	1
OdN89	L	F	45	46,22	204,91	5115,4	4442,9	5201,9	4356,5	9558,4	1,19	1,15	83,04	10,10	1
OdN89	R	F	45	46,22	206,27	5065,8	5118,8	5176,3	5008,3	10184,6	1,03	0,99	80,45	7,40	1
OdN94	L	F	40	52,14	198,31	5696,1	4575,0	5708,2	4563,0	10271,1	1,25	1,25	76,39	13,30	1
OdN94	R	F	40	52,14	209,73	6085,5	5216,8	6169,5	5132,8	11302,3	1,20	1,17	77,17	18,90	1
OdN98	L	F	30	45,17	198,02	4213,7	4092,0	4272,9	4032,8	8305,7	1,06	1,03	86,64	26,80	0
OdN98	R	F	30	45,17	187,53	4273,0	4105,1	4497,8	3880,4	8378,2	1,16	1,04	80,96	28,10	0
OdN99	L	M	35	74,24	214,91	4091,5	4203,3	4237,9	4057,0	8294,9	1,04	0,97	94,55	14,50	1
OdN99	R	M	35	74,24	228,14	4450,5	5107,5	5107,5	4450,5	9558,0	1,15	0,87	93,63		1
OdN109	L	M	45	70,23	257,86	8974,7	7028,7	8976,8	7026,6	16003,4	1,28	1,28	80,22	26,00	0
OdN109	R	M	45	70,23	253,24	9313,5	7095,7	9313,5	7095,7	16409,1	1,31	1,31	77,33	27,80	0
OdN110	L	F	35	62,73	154,08	4508,7	4208,9	4510,9	4206,7	8717,6	1,07	1,07	61,18	24,50	1
OdN110	R	F	35	62,73	186,66	4829,9	3925,0	4843,4	3911,5	8754,9	1,24	1,23	78,79	20,50	1
OdN148	L	M	50	79,42	245,92	6851,0	6178,8	7224,5	5805,2	13029,7	1,24	1,11	85,88	3,10	0
OdN148	R	M	50	79,42	274,13	8421,6	7281,9	9021,9	6681,5	15703,5	1,35	1,16	87,23	3,50	0
OdN159	L	F	45	60,77	220,27	5859,2	5918,5	6386,1	5391,6	11777,7	1,18	0,99	79,77	3,50	0
OdN159	R	F	45	60,77	211,67	5204,5	5528,1	5788,5	4944,1	10732,6	1,17	0,94	80,29	18,60	0
OdN189	L	F	55	71,01	143,56	4651,5	3139,0	4651,5	3139,0	7790,5	1,48	1,48	60,08	23,50	0
OdN189	R	F	55	71,01	158,79	4984,0	3859,4	5062,2	3781,2	8843,4	1,34	1,29	62,90	15,60	0
OdN202	L	M	33	86,57	229,16	7045,5	5554,2	7075,9	5523,7	12599,6	1,28	1,27	80,80	5,70	1
OdN202	R	M	33	86,57	236,62	6508,2	6015,7	6508,5	6015,5	12524,0	1,08	1,08	83,56	2,70	1
OdN223	L	F	23	52,58	162,31	3384,4	3382,3	3554,8	3211,9	6766,7	1,11	1,00	77,69		0
OdN223	R	F	23	52,58	163,37	3041,4	3157,1	3348,4	2850,1	6198,5	1,17	0,96	82,90	30,70	0
OdN225	L	F	23	58,58	186,12	4426,3	3551,8	4449,6	3528,4	7978,0	1,26	1,25	82,35	4,20	0
OdN225	R	F	23	58,58	186,77	4158,4	3988,1	4401,0	3745,5	8146,4	1,18	1,04	81,98	8,80	0
OdN244	L	F	28	64,48	219,25	6125,4	4719,7	6549,5	4295,7	10845,1	1,52	1,30	85,01	15,80	1
OdN244	R	F	28	64,48	210,98	5184,8	4574,9	5666,3	4093,4	9759,7	1,38	1,13	85,37	14,50	1
OdN287	L	F	40	51,97	145,81	3166,0	2450,2	3166,8	2449,4	5616,2	1,29	1,29	77,65	12,70	1
OdN287	R	F	40	51,97	151,20	3207,3	2406,8	3209,9	2404,2	5614,1	1,34	1,33	81,09	29,50	1
OdN295	L	F	50	57,08	152,77	4513,0	3598,9	4521,4	3590,6	8111,9	1,26	1,25	63,02	17,90	1
OdN295	R	F	50	57,08	163,51	4741,7	3575,4	4764,1	3553,0	8317,0	1,34	1,33	68,24	20,60	1

OdN297	L	F	55	62,60	170,00	5406,1	4486,6	5539,2	4353,5	9892,7	1,27	1,20	63,61		1
OdN297	R	F	55	62,60	185,11	5783,9	4903,5	5814,4	4872,9	10687,4	1,19	1,18	68,09	23,10	1
OdN301	L	F	40	64,48	231,31	6377,4	5667,3	6679,2	5365,6	12044,7	1,24	1,13	84,22	15,90	0
OdN301	R	F	40	64,48	230,44	6110,1	5672,6	6244,0	5538,8	11782,7	1,13	1,08	84,87	21,40	0
OdN316	L	F	55	59,35	136,75	4336,7	2935,6	4431,8	2840,4	7272,3	1,56	1,48	59,46	40,50	1
OdN316	R	F	55	59,35	145,91	4409,8	2996,6	4413,6	2992,8	7406,4	1,47	1,47	63,79	35,20	1
OdN321	L	F	40	59,89	214,61	5109,2	4934,6	5492,2	4551,6	10043,8	1,21	1,04	85,55	16,20	0
OdN321	R	F	40	59,89	204,25	4661,2	4330,6	4886,3	4105,6	8991,9	1,19	1,08	86,08	32,30	0
OdN360	L	F	50	64,48	196,11	4828,1	4172,4	5166,7	3833,8	9000,5	1,35	1,16	81,95	9,20	0
OdN360	R	F	50	64,48	194,81	4479,7	3778,8	4639,8	3618,7	8258,5	1,28	1,19	85,93		0
OdN391	L	M	35	64,68	241,53	5959,6	5566,8	6548,6	4977,8	11526,4	1,32	1,07	90,13		1
OdN391	R	M	35	64,68	226,67	6219,3	5521,6	6794,6	4946,3	11740,8	1,37	1,13	83,30	8,70	1
OdN411	L	F	55	40,98	217,44	6762,8	8501,7	8701,1	6563,5	15264,5	1,33	0,80	67,47	7,70	1
OdN411	R	F	55	40,98	185,92	5576,3	5855,9	6612,1	4820,0	11432,1	1,37	0,95	66,90		1
OdN413	L	M	23	66,78	212,39	4999,0	4400,7	5000,9	4398,8	9399,7	1,14	1,14	86,81		0
OdN413	R	M	23	66,78	235,88	5864,5	6020,0	6044,2	5840,4	11884,5	1,03	0,97	85,63		0
OdN417	L	M	45	64,56	243,82	5240,6	6269,5	6340,4	5169,7	11510,1	1,23	0,84	91,11	16,40	1
OdN417	R	M	45	64,56	259,14	6265,4	7235,4	7404,7	6096,2	13500,8	1,21	0,87	89,66	24,20	1
OdN418	L	M	45	71,96	254,19	7404,8	7310,2	8047,3	6667,7	14715,0	1,21	1,01	83,43	11,30	0
OdN418	R	M	45	71,96	270,77	8871,0	7719,5	8955,8	7634,7	16590,5	1,17	1,15	83,24	11,30	0
OdN421	L	M	33	64,56	248,74	6433,1	5892,1	6602,3	5722,9	12325,2	1,15	1,09	89,60	7,70	0
OdN421	R	M	33	64,56	271,83	7524,3	6812,9	7562,0	6775,2	14337,2	1,12	1,10	90,68	12,10	0
OdN439	L	F	55	56,36	155,42	3511,5	2720,7	3661,6	2570,6	6232,2	1,42	1,29	77,06	20,50	0
OdN439	R	F	55	56,36	156,83	3767,0	3000,3	3927,4	2839,9	6767,2	1,38	1,26	74,19	24,30	0
OdN475	L	M	40	87,81	302,68	11570,4	9019,2	11700,2	8889,4	20589,6	1,32	1,28	83,68	7,90	1
OdN475	R	M	40	87,81	313,81	11176,0	9891,4	11465,0	9602,4	21067,4	1,19	1,13	85,63		1
OdN476	L	M	55	83,12	235,49	8723,0	7488,5	9373,4	6838,1	16211,5	1,37	1,16	71,44	8,50	0
OdN476	R	M	55	83,12	248,83	9370,3	8340,4	10156,4	7554,4	17710,8	1,34	1,12	72,51		0
OdN479	L	M	20	90,27	283,75	10376,2	7321,8	10390,1	7307,8	17697,9	1,42	1,42	85,06	28,90	0
OdN479	R	M	20	90,27	274,89	8572,3	6610,3	8748,4	6434,3	15182,6	1,36	1,30	89,17		0
OdN484	L	M	45	86,62	260,98	8425,1	6877,3	8457,8	6844,6	15302,5	1,24	1,23	83,81	21,60	1
OdN484	R	M	45	86,62	264,96	9860,8	7712,6	9865,7	7707,7	17573,4	1,28	1,28	78,56	19,30	1
OdN486	L	M	40	82,26	215,34	6139,5	4918,6	6142,3	4915,8	11058,1	1,25	1,25	80,82		1
OdN486	R	M	40	82,26	231,29	6920,7	5838,3	7118,9	5640,1	12759,0	1,26	1,19	80,68	36,00	1
OdN500	L	M	40	84,60	249,62	7256,0	6030,7	7262,6	6024,2	13286,8	1,21	1,20	86,09		1
OdN500	R	M	40	84,60	260,30	7944,3	6344,7	7944,3	6344,6	14288,9	1,25	1,25	86,81		1

BME = Body mass estimation; CA= cortical area; I_x and I_y = AP (anteroposterior) and ML (mediolateral) second moments of area; I_{max} and I_{min} = maximum and minimum second moments of area; J= polar moment of area; %CA = percentage of cortical area, HT = humeral torsion; Gr. Goods= grave goods (0= none, 1= grave goods).

7.2 Appendix II – Graphs

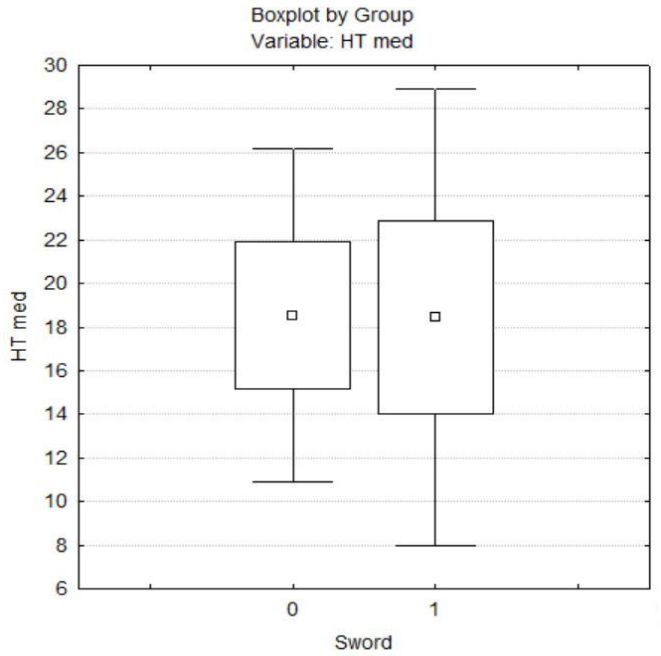

Fig. II.1 - Comparison of mean value of humeral torsion mean value in males buried with and without a sword. Boxes represent Standard error, whiskers represent 0,95 Confidence Interval. 0= no sword, 1= sword

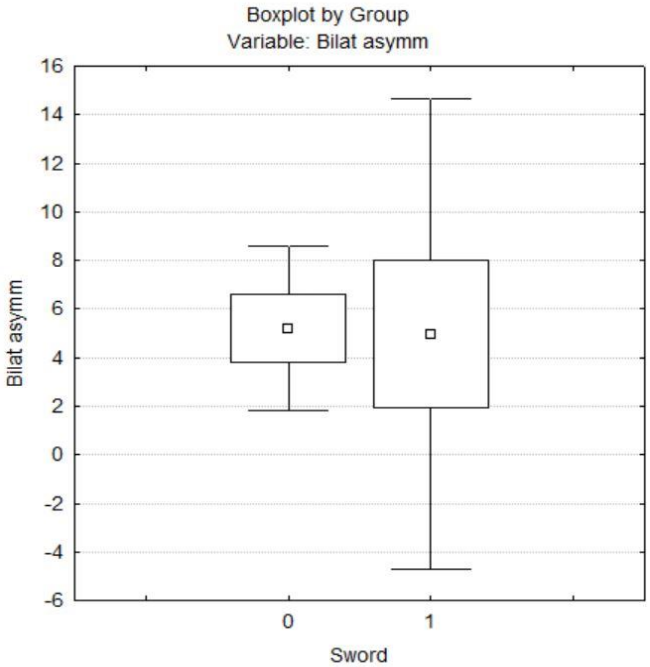

Fig. II.2 - Comparison of mean value of humeral torsion bilateral asymmetry in males buried with and without a sword. Boxes represent Standard Error, whiskers represent 0,95 Confidence Interval. 0= no sword, 1= sword

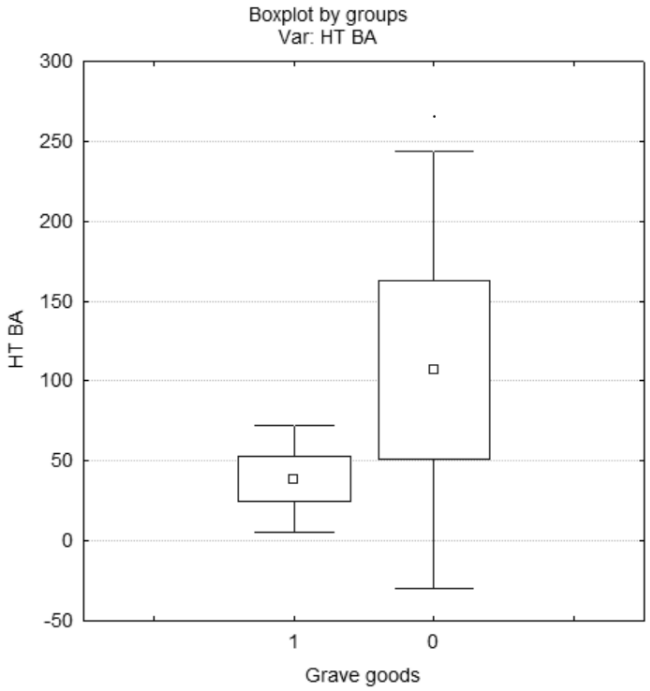

Fig. II.3 - Comparison of mean value of humeral torsion bilateral asymmetry in females buried with and without grave goods. Boxes represent Standard Error, whiskers represent 0,95 Confidence Interval. 0= no grave goods, 1= grave goods

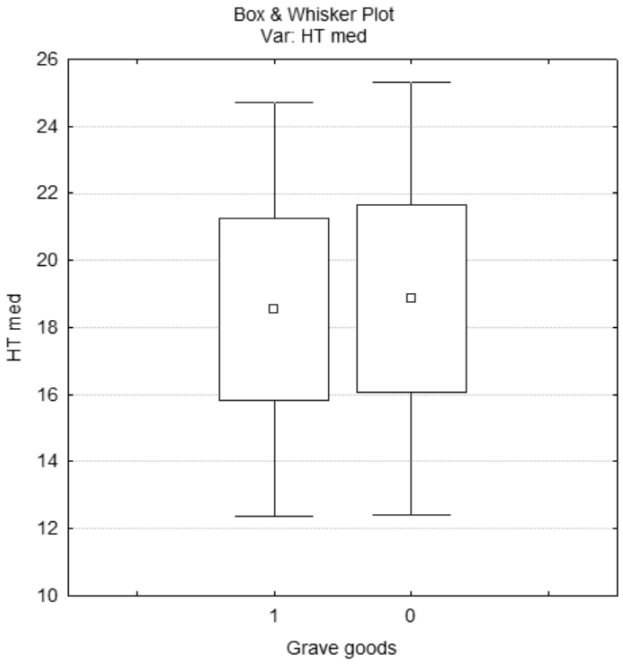

Fig. II.4 - Comparison of mean value of humeral torsion mean value in females buried with and without grave goods. Boxes represent Standard Error, whiskers represent 0,95 Confidence Interval. 0= no grave goods, 1= grave goods.

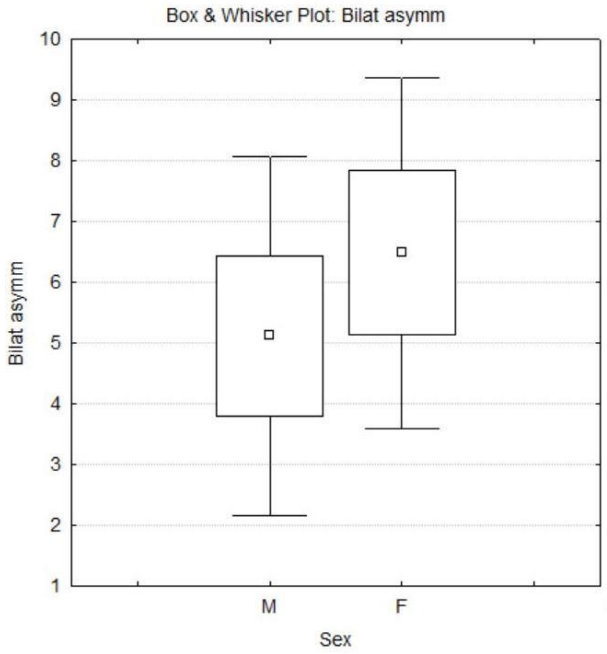

Fig. II.5 - Sexual dimorphism of humeral torsion bilateral asymmetry. Boxes represent Standard Error, whiskers represent 0,95 Confidence Interval.

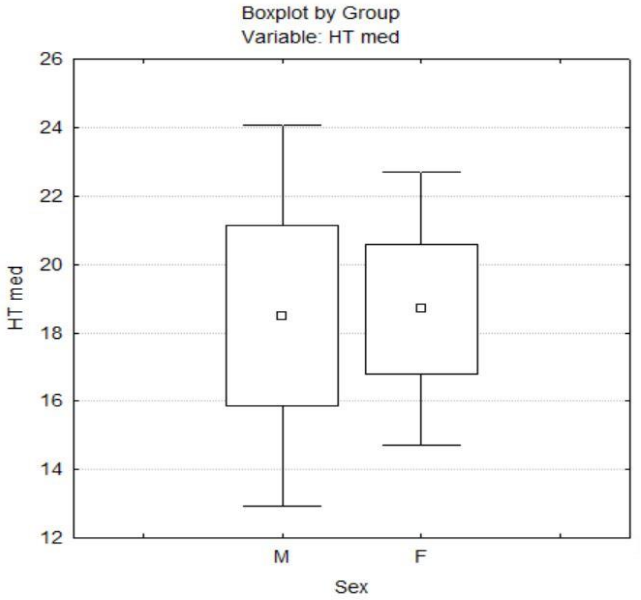

Fig. II.6 - Sexual dimorphism of humeral torsion mean value. Boxes represent Standard Error, whiskers represent 0,95 Confidence Interval.

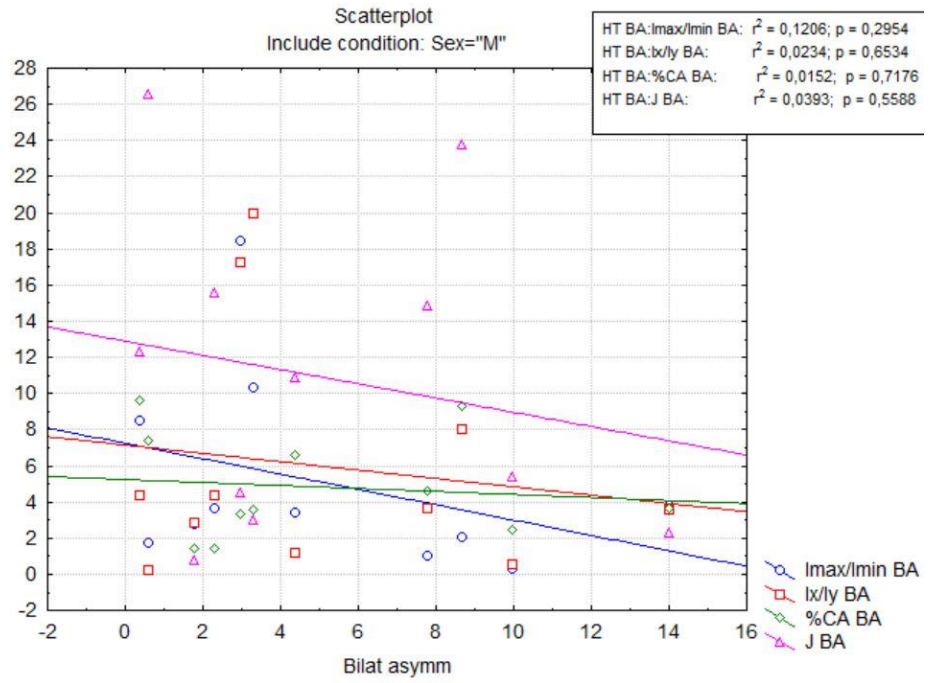

Fig. II.7 - Scatterplot of regression lines for HT and CSG variables bilateral asymmetry: males. BA = Bilateral asymmetry, I_{max}/I_{min} = maximum and minimum second moments of area ratio, I_x/I_y = AP and ML second moments of area ratio, %CA = percentage of cortical area, J = polar moment of area.

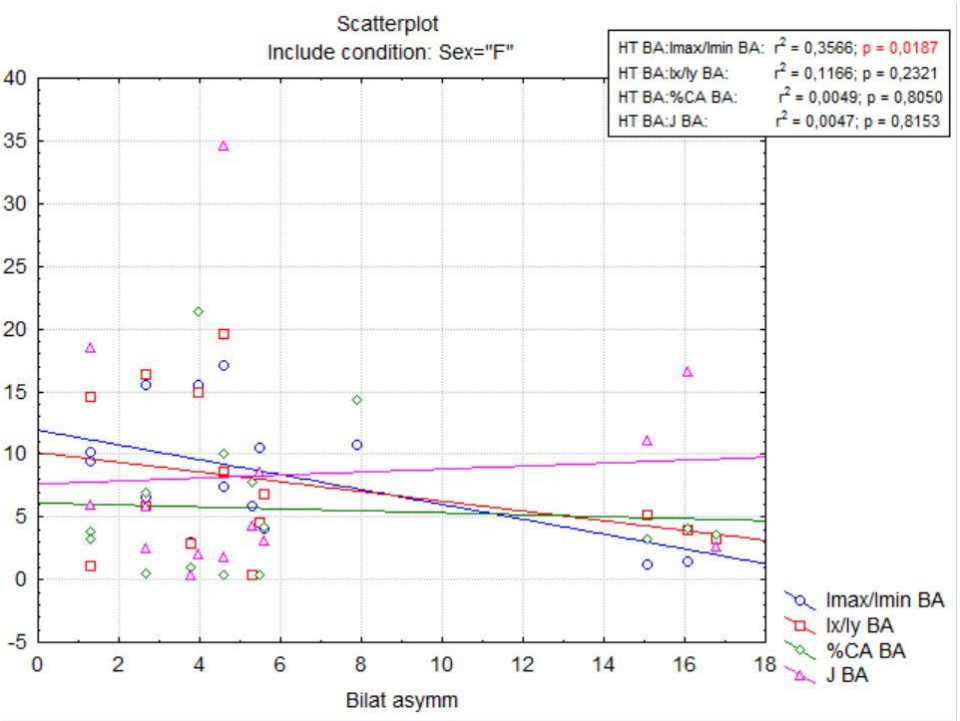

Fig. II.8 - Scatterplot of regression lines for HT and CSG variables bilateral asymmetry: females. BA = Bilateral asymmetry, I_{max}/I_{min} = maximum and minimum second moments of area ratio, I_x/I_y = AP and ML second moments of area ratio, %CA = percentage of cortical area, J = polar moment of area.

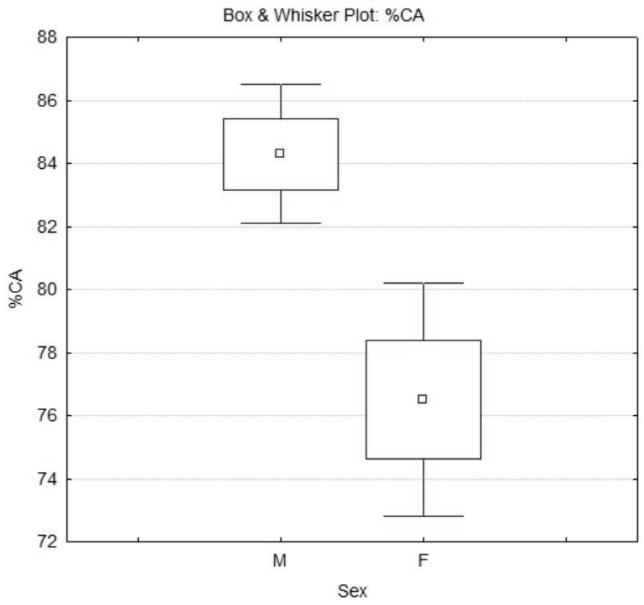

Fig. II.9 - Sexual dimorphism of %CA: right side. Boxes represent Standard Error, bars represent 0,95 Confidence Intervals. %CA = percentage of cortical area.

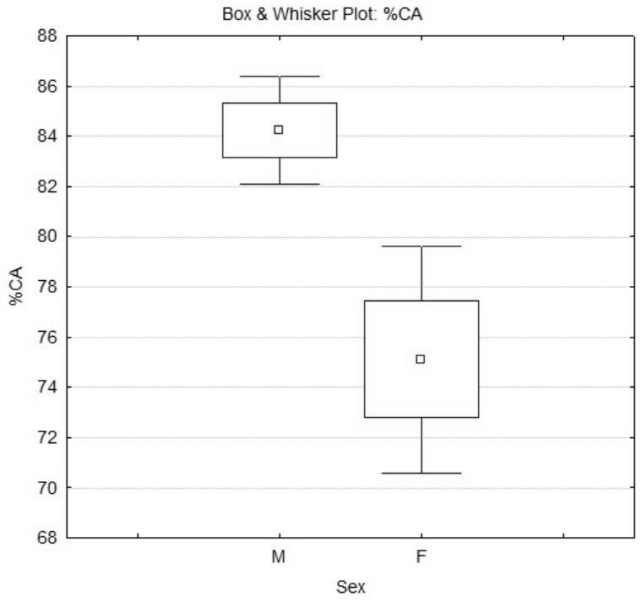

Fig. II.10 - Sexual dimorphism of %CA: left side. Boxes represent Standard Error, bars represent 0,95 Confidence Intervals. %CA = percentage of cortical area.

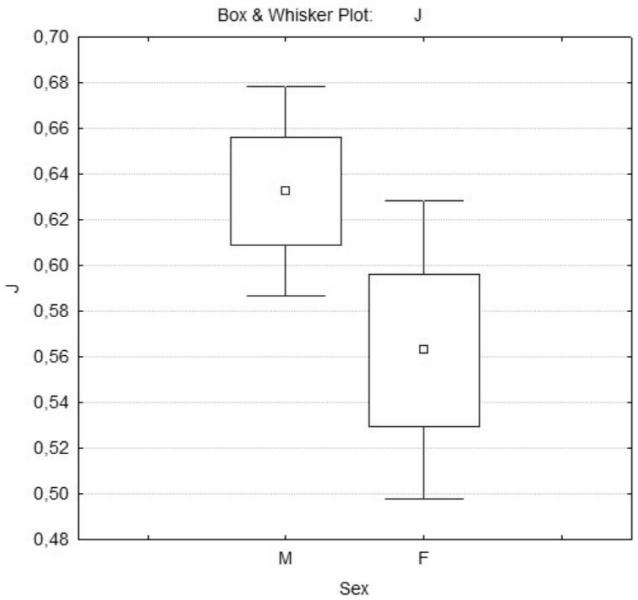

Fig. II.11 - Sexual dimorphism of J: right side. Boxes represent Standard Error, bars represent 0,95 Confidence Intervals. J = polar moment of area.

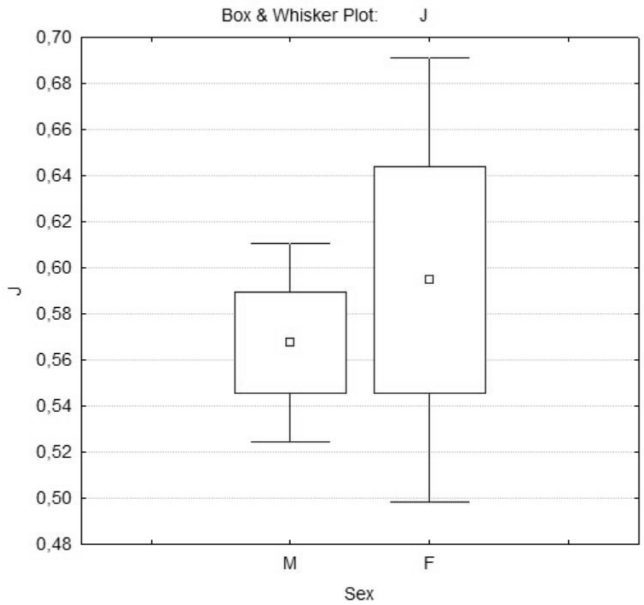

Fig. II.12 - Sexual dimorphism of J: left side. Boxes represent Standard Error, bars represent 0,95 Confidence Intervals. J = polar moment of area.

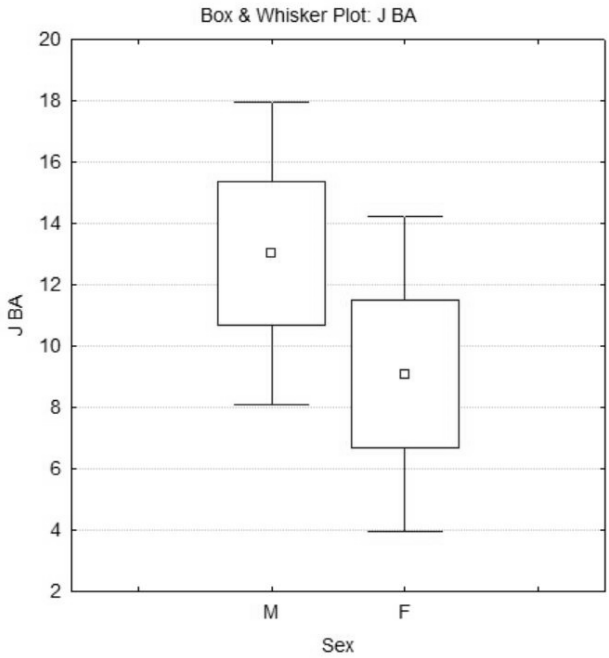

Fig. II.13 - Sexual dimorphism of J bilateral asymmetry. Boxes represent Standard Error, bars represent 0,95 Confidence Intervals. BA = Bilateral asymmetry; J = polar moment of area.

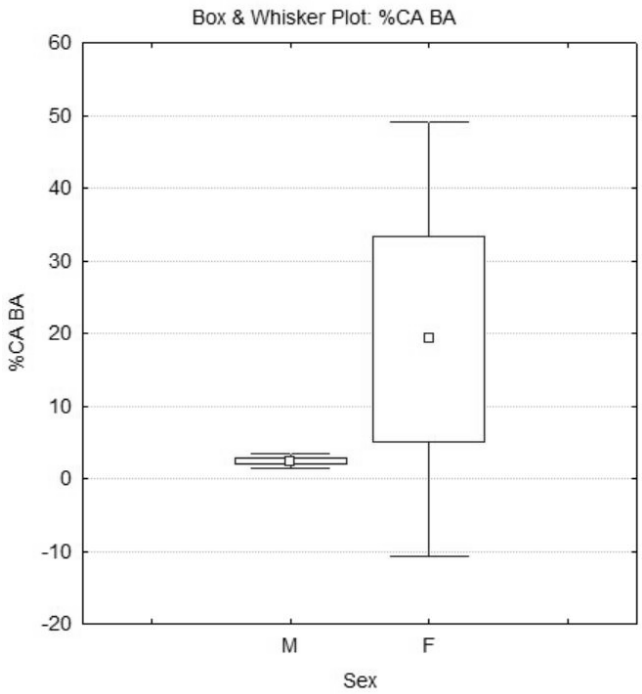

Fig. II.14 - Sexual dimorphism of %CA bilateral asymmetry. Boxes represent Standard Error, bars represent 0,95 Confidence Intervals. BA = Bilateral asymmetry; %CA = percentage of cortical area.

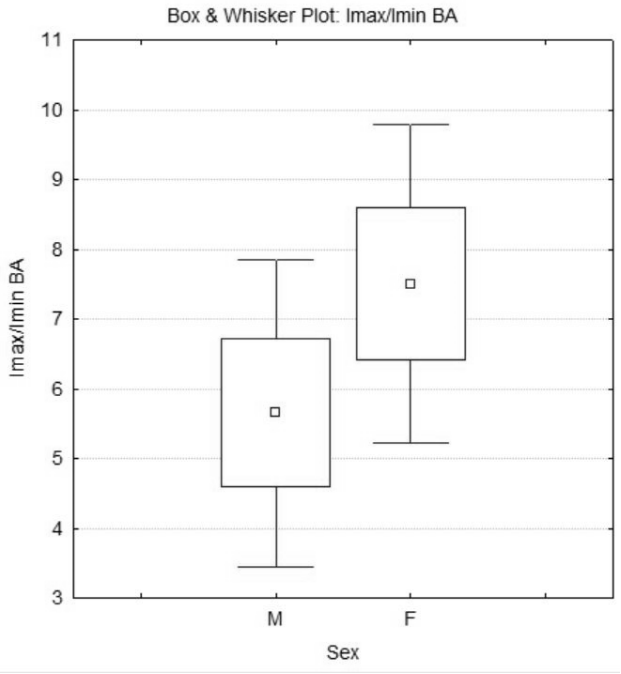

Fig. II.15 - Sexual dimorphism of I_{max}/I_{min} bilateral asymmetry. Boxes represent Standard Error, bars represent 0,95 Confidence Intervals. BA = Bilateral asymmetry; I_{max}/I_{min} = maximum and minimum second moments of area ratio.

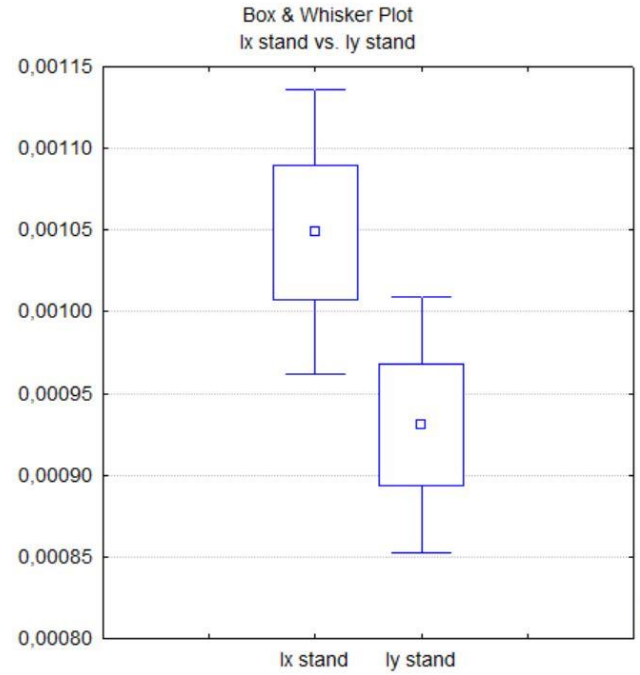

Fig. II.16 - Males right side difference between I_x and I_y. Boxes represent Standard Error, bars represent 0,95 Confidence Intervals. I_x and I_y = AP and ML second moments of area respectively.

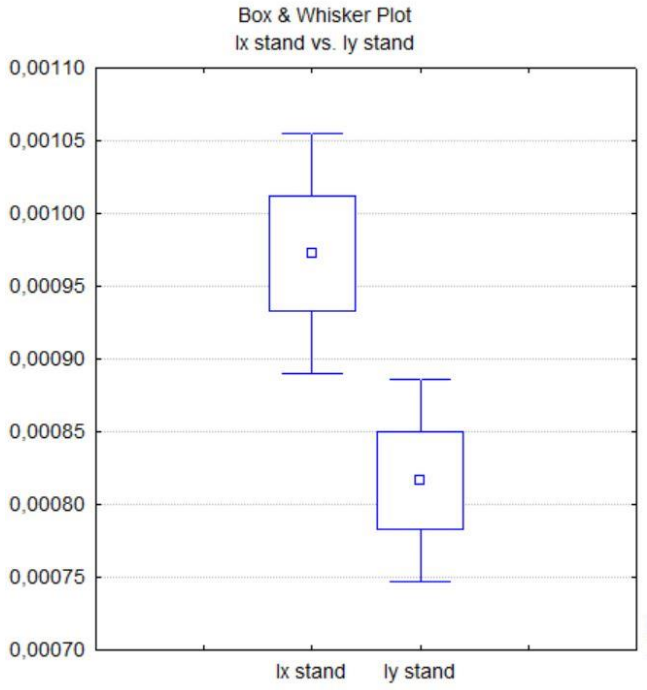

Fig. II.17 - Males left side difference between I_x and I_y. Boxes represent Standard Error, bars represent 0,95 Confidence Intervals. I_x and I_y = AP and ML second moments of area respectively.

Acknowledgments

Many people deserve to be thanked for the contribution they gave to this work. First of all, professor Damiano Marchi for passing down to me the passion for the functional morphology, for being of great inspiration and for his constant and fundamental support, despite my numerous uncertainties. Dr. Vitale Stefano Sparacello, for providing me with the comparison samples and for his precious and essential help with the statistical analysis. Professor Alessandro Canci, for his advices and for granting me the access to the anthropological material necessary for this study. Dr. Sergio Tofanelli and Dr. Marta Colombo, for the support, the insightful comments and the precious advices that they gave to me with patience. Jill Rhodes, for the advices on the humeral torsion measurements. Lisa Savallo, for the willingness with which she shared her experience with me and for always having a word of support. Many thanks also to professor Davide Caramella and Mr. Davide Giustini for having allowed me to do the CTscans and for the help during the process, and to the *Soprintendenza per I beni Archeologici del Veneto*.

Although every academic contribute has been fundamental, emotional support has also been necessary to reach the end of this path, thus many people deserve a mention. A huge thank to Serena, for having always walked by my side, never failing once to believe in me or support me, I am grateful to be able to share this moment and what will come next with you. To my parents and my sister, for their firm support, their unconditional love and for having always supported with pride every choice I made so far. To Eleonora and Valentina - who managed to became my second family in only two years - for every little thing you have done for me and for having believed in me since the beginning; you will always be in my heart. To my

lab mates (Marco, Lisa, Andreas, Lorenzo, Fabio, Claudia), for having shared this experience with me and for the necessary distraction that our chat conversation represented in these last months of work. To my huge family, thank you for your love and for always being there for me. To Veronica, Lucia and Bianca – with whom I shared different moments of my university career -, you were and always be a fundamental part of my life, thank you for having crossed my path. To the entire Filter family (Meb, Livia, Roberto, Antonio, Ivan, Karen, Riccardo, Valentina, Clelia, Giulia and every other customer whose smile I will remember) thank you for your contribution in creating a work environment impossible to forget.

The last thank will never be read, but is still necessary. Thank you grandma, for the immense love you gave to me and that still lives in my heart. This work is for you.